Order Number 9408519

I. Analysis of biological specimens by proton-induced x-ray emission spectroscopy (PIXE). II. Separation and purity of C_{60} and C_{70}

Lowe, Timothy Paul, Ph.D.

The University of Arizona, 1993

U·M·I
300 N. Zeeb Rd.
Ann Arbor, MI 48106

I. ANALYSIS OF BIOLOGICAL SPECIMENS BY PROTON-INDUCED X-RAY EMISSION SPECTROSCOPY (PIXE)

II. SEPARATION AND PURITY OF C_{60} AND C_{70}

by

Timothy Paul Lowe

A Dissertation Submitted to the Faculty of the

DEPARTMENT OF CHEMISTRY

In Partial Fulfillment of the Requirements
For the Degree of

DOCTOR OF PHILOSOPHY
WITH A MAJOR IN CHEMISTRY

In the Graduate College

UNIVERSITY OF ARIZONA

1 9 9 3

THE UNIVERSITY OF ARIZONA
GRADUATE COLLEGE

As members of the Final Examination Committee, we certify that we have read the dissertation prepared by Timothy Paul Lowe

entitled I. Analysis of Biological Specimens by Proton-Induced X-Ray Emission Spectroscopy (PIXE).

II. Separation and Purity of C_{60} and C_{70}.

and recommend that it be accepted as fulfilling the dissertation requirement for the Degree of Doctor of Philosophy/Chemistry

Quintus Fernando	8/17/93 Date
Jeanne E Pemberton	17 Aug 93 Date
[illegible]	8/17/93 Date
S K Vemulapalli	8/17/93 Date
John V. Rund	8/17/93 Date

Final approval and acceptance of this dissertation is contingent upon the candidate's submission of the final copy of the dissertation to the Graduate College.

I hereby certify that I have read this dissertation prepared under my direction and recommend that it be accepted as fulfilling the dissertation requirement.

Quintus Fernando
Dissertation Director

8/17/93
Date

STATEMENT BY THE AUTHOR

This dissertation has been submitted in partial fulfillment of requirements for an advanced degree at The University of Arizona and is deposited in the University Library to be made available to borrowers under the rules of the Library.

Brief quotations from this dissertation are allowable without special permission, provided that accurate acknowledgment of source is made. Requests for permission for extended quotation from or reproduction of this manuscript in whole or in part may be granted by the head of the major department or the Dean of the Graduate College when in his or her judgment the proposed use of the material is in the interests of scholarship. In all other instances, however, permission must be obtained from the author.

SIGNED: 

ACKNOWLEDGEMENT

I wish to thank my research director, Dr. Quintus Fernando, for the support and direction which made my educational experience at the University of Arizona possible. Without the help of Dr. John A. Leavitt, Dr. Larry McIntyre Jr. and Don A. Ashbaugh of the Department of Physics, the PIXE project would have been impossible. Since the PIXE project is an on-going endeavor, the participation of the PIXE group including Quan Chen, Irianto Setiarahardjo and Julie Li Qiu was, and is, essential for the continuation of PIXE at the University of Arizona. The help of Dr. Michael F. Burke and David D. Johnson was inexpendable in the process of developing and understanding the research concerning the separation of fullerenes. For her understanding and the emotional support she extended to me during the writing of this dissertation, I would like to thank my friend Molly Ryan. Finally, I would like to thank the members of the Fernando research group for sharing their thoughts and ideas, and for providing an environment which exemplifies the spirit of scientific investigation.

TABLE OF CONTENTS

TABLE OF CONTENTS, Continued

TABLE OF CONTENTS, Continued

LIST OF FIGURES

PART I.

LIST OF FIGURES, Continued

PART II.

LIST OF TABLES

PART I.

PART II.

ABSTRACT

Proton induced x-ray emission spectroscopy (PIXE) is a rapid and sensitive analytical technique for the non-destructive simultaneous determination of elemental concentrations above atomic number 11 (sodium) and is the only analytical technique that can determine 20-30 elements nondestructively in a single small sample (≈5 mg) with detection limits of 1-5 ppm (dry weight). Part I of this dissertation outlines work done on the optimization of instrumental parameters and sample preparation for the analysis of biological tissue. Cultured rabbit renal slices were used as the biological system to demonstrate the use of PIXE analysis. The renal slices were exposed to $HgCl_2$, $CdCl_2$, $K_2Cr_2O_7$, or $NaAsO_2$ alone or in a mixture. The analysis of biological samples by PIXE provides information on inter-elemental interactions in tissue and body fluids. A computer program for spectrum processing and quantitation, which decomposes overlapped peaks, corrects for thick target matrix effects and calculates results without resorting to the use of standards, is explored.

In part II of this dissertation, a convenient method of removing solvent from a benzene extract of graphitic soot containing fullerenes using sublimation, is outlined. Separation of macroscopic quantities of the fullerenes C_{60} and C_{70} has been accomplished using a combination of selective precipitation of C_{60} and chromatography. C_{60} is selectively crystallized by freezing and thawing a benzene solution of mixed fullerenes, then using the C_{70} enriched supernatant as starting material in the chromatographic separation of C_{60} and C_{70}. In the separation scheme, a bed of modified silica sorbent is charged with the fullerene mixture and the fullerenes are eluted using a hexanes/THF mobile phase. The methods of UV-Visible and infrared spectroscopy, as well as high performance liquid chromatography (HPLC) are evaluated for their ability to determine the purity of a C_{60} or C_{70} sample.

I. ANALYSIS OF BIOLOGICAL SPECIMENS BY PROTON-INDUCED X-RAY EMISSION SPECTROSCOPY (PIXE)

ANALYSIS OF BIOLOGICAL SPECIMENS BY PROTON-INDUCED X-RAY EMISSION SPECTROSCOPY (PIXE)

INTRODUCTION

Ph.D candidates in the Fernando Group typically explore several problems in analytical chemistry before selecting a project as the main topic of their dissertation research. After working on solubility measurements of organic compounds and reactions of rare earth oxides in supercritical carbon dioxide, and the destruction of pollutants by electrolysis in brines, the acquisition of a commercial energy-dispersive x-ray emission (EDXRF) instrument in 1989 inspired the development of a proton-induced x-ray emission (PIXE) instrument based on the x-ray detection system found in the EDXRF instrument, thereby reviving PIXE research begun by the Fernando group ten years earlier[1].

With able help from the Department of Physics, the EDXRF instrument was converted for PIXE, while maintaining the EDXRF capabilities of the commercial unit with minimal conversion requirements. The benefits of the ability to easily convert between EDXRF and PIXE will be demonstrated later in this dissertation.

After initial characterization of the system and development of sample preparation protocols, analysis of rabbit renal slices was undertaken in collaboration with the Department of Toxicology. To date, over 4000 rabbit kidney slice samples have been analyzed, and the results have given new insight into the uptake of toxic metals in biological tissue.

This section of the dissertation is dedicated to the description of the PIXE instrument, the theoretical and practical aspects of PIXE analysis of biological tissue, and the preparation of biological samples for analysis by PIXE. The second dissertation topic, "Separation and Purity of C_{60} and C_{70}", will be introduced separately.

THEORY OF PIXE

Since its introduction by Johansson, et al. in 1970[2], elemental analysis by PIXE has been shown to be a powerful, multielemental analysis technique of high sensitivity[3].

Analysis of samples by PIXE involves bombardment of a target with accelerated protons in the MeV range of energy, which ionize inner-shell electrons of the elements in the sample; the subsequent rapid decay of the induced excited electronic state produces x-rays (or Auger electrons) whose energies are characteristic of the elements present in the sample. The process of generation of x-rays is demonstrated schematically in **Figure 1.** The emitted x-ray photons from the sample can be detected by a lithium-drifted solid-state silicon crystal, or Si(Li) detector. The electronic signals generated by the x-ray photons in the Si(Li) detector are sorted by a multichannel analyzer according to their energies. The x-ray emission spectrum is then built from a plot of "counted" x-ray photons versus their energies and is stored on a computer disk for spectrum processing and quantitation. The advantages and disadvantages of PIXE analysis are outlined in **Table I.**

In the PIXE spectrum, the number of detected x-ray counts at the energy corresponding to a particular element is directly proportional to the concentration of that

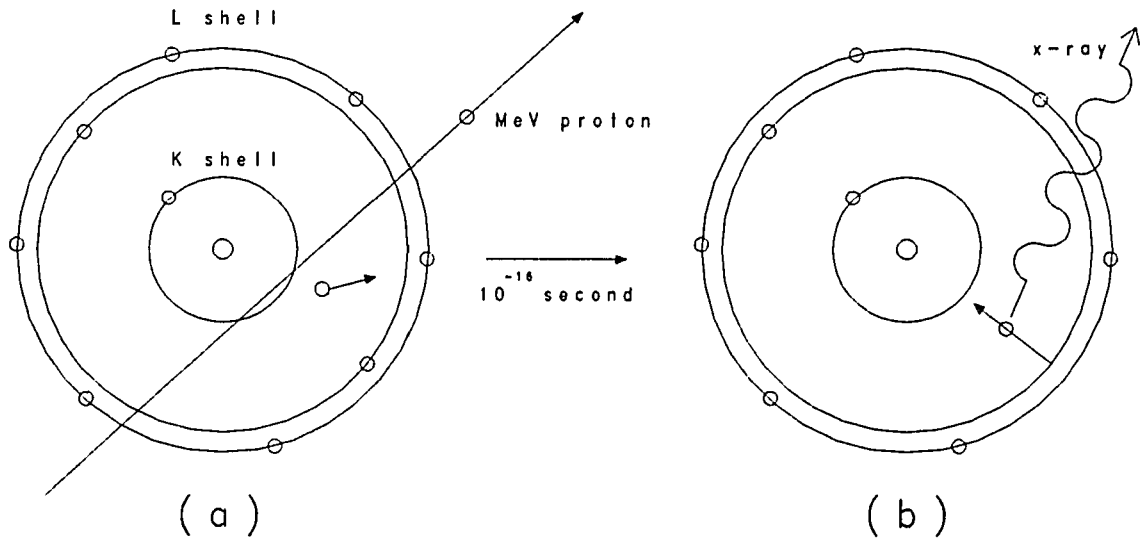

Figure 1. Diagram of proton-induced x-ray emission. (a) A high energy proton ejects an electron, and (b) an x-ray is emitted as the vacancy is filled from an outer electron shell.

ADVANTAGES
Simultaneous multielemental quantitation
High sensitivity
Small sample size requirements
Short analysis times
Often non-destructive
Mono-energetic excitation
Possibility of automation
Micro-PIXE can image elemental concentrations
DISADVANTAGES
Limited sampling depth (ca. 10 μm)
Elements below atomic number 11 (Na) are not detected
Oxidation state information is not obtained
Computer-based processing is required for quantitation
The beam source is generally expensive and complex
Matrix effects in thick samples cause problems

Table I. Advantages and Disadvantages of the PIXE Technique.

element in the sample. With the use of tables of excitation cross sections for protons of a defined energy which impinge on a particular element, along with x-ray fluorescence yields of elements ionized by the proton beam, elemental concentrations are calculated from the x-ray spectrum by computer. The corrections for complex spectral overlaps and matrix corrections have also been calculated for specimens of intermediate and of infinite (relative) thickness. Computer software designed to model or remove the spectral background, decompose overlapped spectral peaks, identify spectral artifacts such as silicon escape peaks, and to correct for matrix effects in the case of thick target analysis has been developed specifically for application to PIXE analysis.

At the University of Arizona, the GUPIX software package is used to process PIXE spectra. The GUPIX program uses a combination of instrumental parameters and the use of a standard reference to calculate elemental concentrations of a sample from PIXE data.

Several hundred laboratories in the United States can perform PIXE analysis[4], but at present there is no commercially available instrumentation for PIXE.

Production of proton beams in the MeV range used in PIXE requires expensive hardware; fortunately, Van de Graaff generators, acquired by the "atom smashing" nuclear physics

research community in the 1950-1970's, have been abandoned in favor of higher energy accelerators, and are now available for analytical uses such as Rutherford backscattering spectroscopy (RBS) and PIXE. The advent of relatively inexpensive small tandem accelerators[5] also makes PIXE analysis a financially viable alternative to other elemental analytical techniques.

Other PIXE configurations. An extension of the PIXE technique, micro-PIXE, is undergoing rapid development, and can be compared to the electron microprobe[6]. A micro-PIXE instrument is currently under construction in our laboratory for the imaging of elements of interest in biological specimens. Micro-PIXE utilizes an electro-magnetic lens to focus the proton beam to diameters as small as 1 μm and can scan the beam over a ca. 1 mm square area, allowing elemental imaging of samples as small as a single cell. An advantage that micro-PIXE offers over the electron microprobe is the realization of higher sensitivities, although the resolution of the micro-PIXE technique is lower, due to the difficulty of focussing protons, which are more massive than electrons.

Another derivation of the PIXE technique is external-beam PIXE[7], in which the proton beam is extracted from the end of the beam line through a thin window into air,

allowing analysis of objects such as wet biological samples, paintings or archaeological artifacts, or other samples which are too large to fit into the evacuated PIXE target chamber or which cannot withstand analysis in vacuo. Although a significant drop in beam range and analytical sensitivity is encountered in the external-PIXE technique in air, use of a helium atmosphere (i.e. in a bag around the specimen and external beam) attenuates the proton beam and emitted x-rays to a much smaller extent; the range of a 2 MeV proton beam in air is 7 cm and in helium is 27 cm[8].

Comparison to other methods of analysis. In contrast to X-ray fluorescence spectroscopy (XRF), which uses x-ray bombardment of the sample to stimulate x-ray emission, PIXE uses a 1-3 MeV proton beam for sample excitation. The high x-ray production cross sections for charged particle beams and low background in the x-ray spectrum result in the low detection limits of elements of atomic number greater than 11 (sodium) and is an important advantage of the PIXE technique over XRF, which must employ a filter in front of the x-ray tube to separate x-ray excitation emissions from x-rays generated by the sample. The mono-energetic protons used in PIXE analysis also allow quantitation using fundamental parameters, a benefit shared with Rutherford backscattering spectroscopy. The simultaneous quantitation

of a large number of elements in a sample makes PIXE an attractive analytical tool that has been exploited for many diverse applications[4]. In contrast, XRF requires several instrumental conditions to cover the entire range of elements. The advantages of PIXE over XRF are somewhat offset by the limited depth of analysis in PIXE; proton beams used in PIXE penetrate the sample to a depth of several tens of microns, and x-rays can penetrate to depths of several centimeters. PIXE, therefore, is limited to analysis of the near-surface region of thick samples. See Appendix B for an experimental comparison of these two x-ray emission techniques.

Atomic emission spectroscopy (AES) is another method of analysis that offers simultaneous multielemental quantitation. While AES offers higher sensitivity than PIXE (AES has detection limits in the ppb range for many elements under favorable conditions), the complexity of the ultraviolet-visible emission spectrum from outer shell electronic transitions makes quantitation of mixtures difficult, due to overlapped spectral peaks. The x-ray emission spectrum found in PIXE is much simpler, due to the limited number of inner electron shell transitions, which makes quantitation easier by PIXE. AES requires samples to be in solution, which usually requires dilution of a digested or soluble solid, thereby increasing the detection

limit and introducing a possible source of contamination; the ability of PIXE to analyze very small (<1 mg) solid samples non-destructively, precludes the use of AES in the analysis of small, irreplaceable samples.

The importance of sample preparation for PIXE. The ease of sample preparation for PIXE analysis is one of its important advantages. Many thin solid samples can be analyzed without pretreatment, and solutions can be analyzed on an appropriate backing material after evaporation of the solvent. In addition, the technique is relatively non-destructive (although living tissue will not survive the radiation!), and samples can be reused for other determinations after PIXE analysis is complete. Although lower detection limits can be obtained with thin (less than about 10 μm thick) samples, thicker samples can be analyzed quantitatively by PIXE if the matrix is well characterized, but with a concomitant increase in detection limits.

Sample preparation is the key to obtaining meaningful information from PIXE analysis. For reasons relating to background reduction and minimizing matrix effects, thin (less than a few tens of microns) samples are required for highest sensitivity. Preparation of thin sample targets with a homogeneous distribution of elements in the sample is something of an art, and each sample type (i.e. solution,

tissue specimen, inorganic solid, etc.) requires the development of a separate sample preparation protocol. The development of a procedure to sandwich microtomed tissue has allowed the analysis of rabbit kidney slices with a high degree of reproducibility[9].

PIXE offers a powerful method of elemental analysis for biological specimens. Several reviews that have been published within the last few years on the application of PIXE to the analysis of biological samples[10,11] indicate the maturity of the field. Although PIXE offers certain real advantages over other methods of tracė (ppm) analysis, it is not an "ultimate" method of elemental analysis and in many cases, alternative analytical techniques used in the analysis of biomedical specimens can be employed to complement or replace PIXE in order to obtain more specific information[12]. It is anticipated, however, that PIXE will eventually find its rightful place in the arsenal of analytical tools available to the trace-element analyst.

A BRIEF HISTORY OF THE PIXE TECHNIQUE

The observation of x-rays produced by ion bombardment was first reported in 1912 by Chadwick, who used alpha particles (helium ions) from radioactive sources for excitation[13]. Although the superiority of the use of protons over electrons for x-ray excitation had previously been established[14], development of electron microprobe analysis (EMPA) preceded PIXE by several years. PIXE was demonstrated in its present configuration that employs a proton beam and Si(Li) detector, by Johansson, et al. in 1970[2]. Si(Li) detectors were developed as early as 1961, when Bailey and Mayer used a Si(Li) detector with a resolution of 47 keV for the detection of 663 keV gamma rays from a cesium radioactive source[15]. Since then, refinements in the production of Si(Li) detectors have improved resolution to around 150 eV. The resolution of a Si(Li) detector has been defined as the width at half maximum of the Mn K_α characteristic peak at 5.9 keV, measured at 1000 counts/second[16]. The Mn K_α radiation emission energy has been established as the standard for the measurement of x-ray resolution; our system has yet to be calibrated with a Mn source.

Although bent crystals were used in wavelength dispersive x-ray fluorescence spectroscopy (WDXRF) in the early applications of XRF, the Si(Li) detector has been used

exclusively in PIXE because of the requirements for high x-ray detection efficiency and multichannel detection of x-rays[17]. New x-ray detectors, which do not require cooling to liquid nitrogen temperatures, are under development.

Originally referred to as particle-induced x-ray emission, PIXE has come to stand for proton-induced x-ray emission, because the optimization of the technique requires the use of protons in the MeV energy range for efficient excitation of x-rays from a sample. The use of protons has therefore become standard practice in the PIXE technique.

THE PIXE INSTRUMENT

A diagram of the PIXE instrument constructed in the Department of Physics at The University of Arizona is shown in **Figure 2.** Hydrogen is ionized in the Penning source in the high voltage terminal of the Van de Graaff generator, and the H_2^+ is accelerated across a 4 MV potential. The ions proceed down a beam line evacuated to 10^{-6} torr, and are bent by a large magnet whose field is kept stable. A pair of control slits down stream from the magnet are used to monitor the beam position and vary the acceleration potential so that a beam of constant energy is sent down the beam line. A quadrupole magnet allows some degree of beam focussing or defocussing to aid in the control of the beam profile which reaches the defining slit chamber. Two sets of four slits in the defining slit chamber configure the beam which passes through a 7.6 μm thick Kapton (polyimide) window and strikes the target mounted on the sample wheel in the target chamber. A diagram of the target chamber is shown in **Figure 3.** The Kapton window at the end of the beam line has several purposes: (1) The kapton foil maintains the high vacuum in the beam line, since the sample chamber must be periodically opened for changing the samples, and is kept at higher pressure than the beam line during spectrum acquisition. (2) The kapton is coated with a thin layer of cobalt, which serves as a beam-resistant element for the

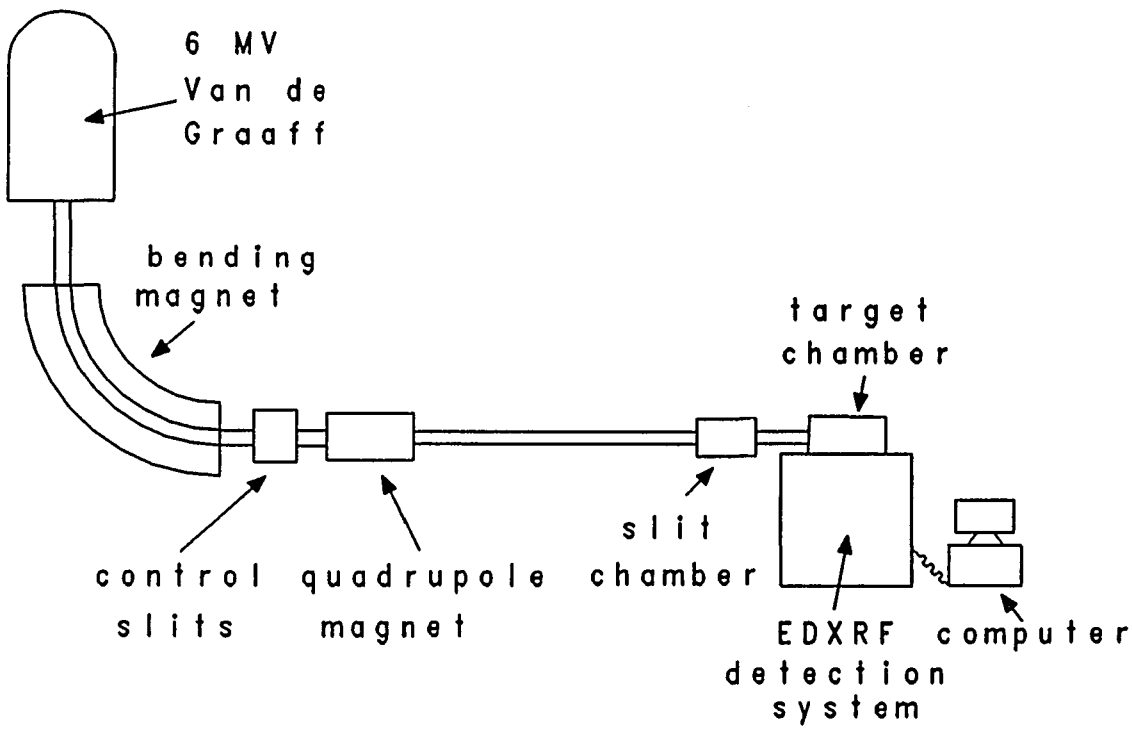

Figure 2. Diagram of the PIXE Instrument (not to scale).

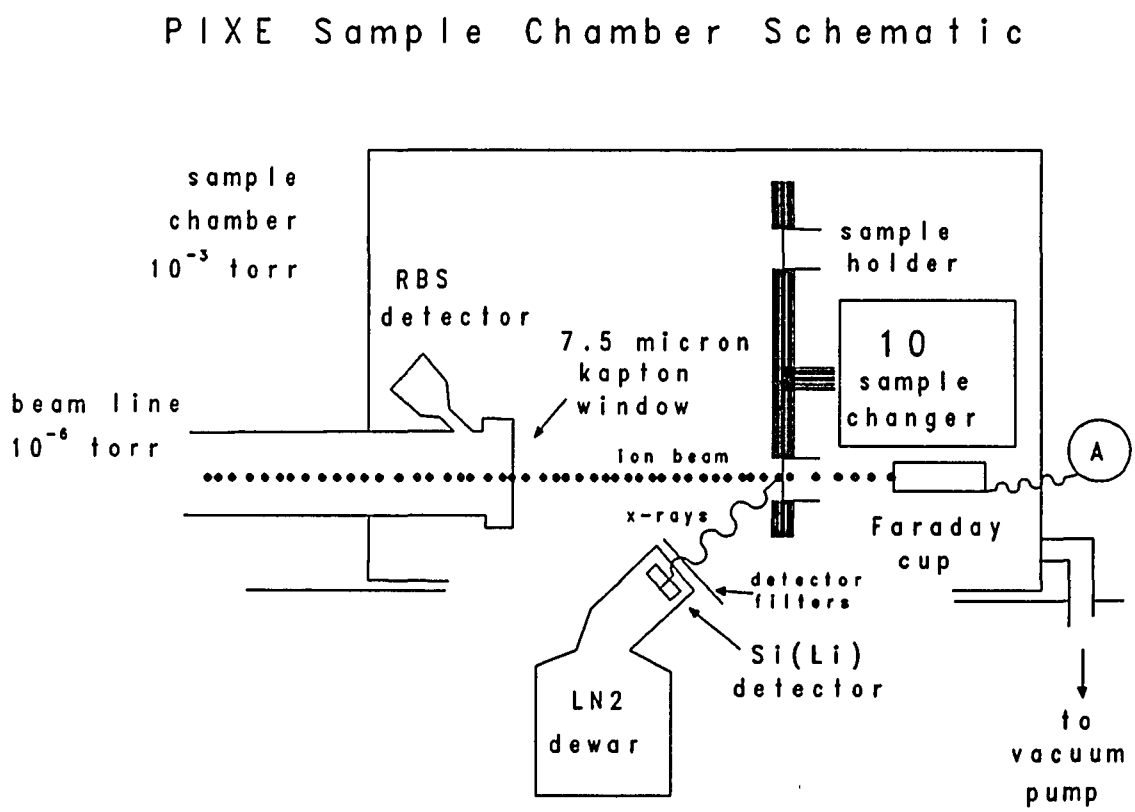

Figure 3. Diagram of the PIXE Sample Chamber.

Rutherford backscattering spectroscopic (RBS) detection of protons. The RBS spectrum is used in the determination of the number of particles (and therefore, total integrated charge) which passes through the window. (3) The ion beam is initially composed of 4 MeV H_2^+, which decomposes into 2 MeV protons during passage down the beam line or by passing through the window. (4) Insulating samples can become charged during analysis and the discharge of the sample can create x-ray background in the PIXE spectrum. The passage of the beam through the Kapton window provides a shower of electrons which counteracts the charging of the sample (see below). The 2 MeV protons in the beam experience an energy loss of 60 keV as the particles pass through the window which results in a 1840 keV proton beam at the sample surface[18].

The EDXRF instrument whose detection system is used in acquisition of PIXE spectra is a TRACOR model 5000 instrument (Tracor X-Ray, Mountain View, CA) and is equipped with a horizontal ten-position sample changer; a gear train for transferring the sample wheel to a vertical position was designed by Dr. J. A. Leavitt of the University of Arizona, Department of Physics. The aluminum sample wheel is protected from scattered protons and other excitation sources by a thick kapton shield to avoid spurious x-ray contributions to the spectra. The X-rays produced in the

sample are detected by a Si(Li) detector placed at a 45° angle below the target on the upstream side of the target. The distance from sample to detector was measured at 4.5 cm. Mylar and/or aluminum filters are placed over the detector to reduce the low energy x-ray contributions to the spectra. The filters are necessary to reduce the dead time of the detection system and optimize the detection of low atomic number (Z>15) elements. An unsuppressed Faraday cup is positioned to intercept the beam when no target is in place, allowing approximate tuning of the beam using an ammeter to monitor the beam current. The sample chamber replaces the turret used in the EDXRF instrument, and is connected to the beam line by a flexible bellows. Although helium flush operation is available, the sample chamber is routinely kept at approximately 10^{-3} torr for spectrum acquisition, in order to reduce the attenuation of low energy x-rays by ambient air. The control of detection parameters, atmosphere and file management is done by the EDXRF system.

Beam considerations. The field of the bending magnet must be stable in order to provide a beam of uniform energy. Calibration of the magnetic field and therefore the beam energy is performed using known nuclear reactions. Three nuclear reactions were used for calibration of the magnetic field produced by the analyzing magnet at the University of

Arizona. The $^{24}Mg(\alpha,\gamma)^{28}Si$ resonances at 2.4374, 2.868 and 3.200 MeV, as well as the $^{14}N(\alpha,\alpha)^{14}N$ resonance at 3.576 MeV and the $^{16}O(\alpha,\alpha)^{16}O$ resonance at 5.058 MeV were used to calibrate the beam energy with an uncertainty of ± 0.08% and an energy spread of 2 keV[19]. The 1.374 MeV (p,γ)-resonance for fluorine was used in Sweden, with an accuracy better than ±10 keV[20]. To control the beam energy, a set of slits connected to electronic feed back circuitry monitors the position of the beam as it exits the magnet, and controls the accelerating voltage so that the beam is constrained to pass between the slits.

The beam cross-section must be uniform, because "hot spots", or areas of high intensity will cause nonuniform excitation of the sample and could potentially damage the sample. To obtain a uniform beam intensity profile, the beam can be diffused by use of electro-magnetic defocussing lenses placed at a distance of 5 meters from the final collimating slits. This results in a more uniform beam intensity but also results in a substantial loss of intensity. Alternatively, a thin carbon foil can be placed in the beam a meter or two upstream from the final collimating slits to scatter the particles in the beam and give a more uniform beam intensity. The beam must be collimated to define the size of the sampling area on the target. Collimation is usually accomplished by using a set

of adjustable slits, which can be moved to vary the dimensions of the beam.

The choice of material used in the construction of the components of the PIXE instrument is important in order to avoid excessive γ-radiation and x-ray contamination of the spectrum. Because of its high resistance to the eroding effects of the beam and low γ-radiation production cross-section, tantalum is usually the material of choice for slit jaws, and graphite is often used near the detector area for apertures and collimators in order to reduce unwanted x-ray lines in the PIXE spectrum.

Effects of the beam on the sample. As the proton beam strikes the target, heat, x-rays, secondary electrons are generated, and the beam deposits electrical charge, which is built up on insulating targets. This charge can attain kV ranges of potential, and can be discharged to surrounding conductive objects, thereby increasing the background in the x-ray spectrum. The charging of the target can be reduced by coating insulating samples with a conductor, such as carbon[21], or by placing a carbon foil in the beam near the target in order to spray the target with electrons to neutralize the charge on the target[22], or by installing an electron gun to spray the target with a negative ion stream[23]. Similar to the use of a carbon foil, the cobalt-

treated Kapton exit window in the University of Arizona instrument is close enough to the target to provide a spray of electrons which neutralize the charging effects. Use of a helium atmosphere will also reduce target charging by providing an ionized path along which the target can discharge. Target heating is often a problem in PIXE analysis of organic samples, but reduction of the beam current or use of a helium atmosphere are effective in allowing the sample to dissipate heat. In our work with rabbit kidney sections, proton beams with currents of around 30 nA, and diameters of about 6 mm, can impinge on the dried tissue section for 10 minutes in vacuum with only minor discoloration of the tissue.

Chamber geometry. The beam-sample-detector geometry is an important factor in target chamber design. Two designs are commonly employed: the target is at 45° to the beam and the detector is at 90° to the beam; or the target is normal to the beam with the detector at 135° to the beam (45° from the sample plane). The latter configuration, which detects x-rays from the upstream side of the target, has an advantage which results in a two-fold decrease in electron bremsstrahlung background, but the advantage is occasionally more than offset by the greater sample-detector distance required[24], especially when very low concentrations of

analytes are being determined[25]. The PIXE system used in the determination of elements in rabbit renal slices has a sample-detector distance of ca. 4.5 cm; The micro-PIXE beam line under development at the University of Arizona has a shorter sample-detector path, so a lower detection limit for elements in a sample will be realized when operating in a macro-PIXE mode.

The Si(Li) detector. A diagram of a Si(Li) detector is shown in **Figure 4.** X-rays enter the silicon crystal through the thin gold layer electrode and ionize the silicon, producing electron-hole pairs, which are collected using a bias voltage of 600-1000 volts across the front and back of the silicon crystal. The number of electron-hole pairs created is directly proportional to the energy of the incident x-ray photon. Lithium is drifted into the crystal to increase its resistance. The detector and first-stage signal amplifier are maintained at liquid nitrogen temperature (-196° C) to prevent the lithium from diffusing out of the silicon crystal and to reduce electrical noise. Each detector is unique, due to differences in lithium concentration profiles, silicon crystal imperfections and electrode layer thickness. These parameters define the efficiency of detection of x-rays and the resolution of x-ray lines. The efficiency of the Si(Li) detector in use at

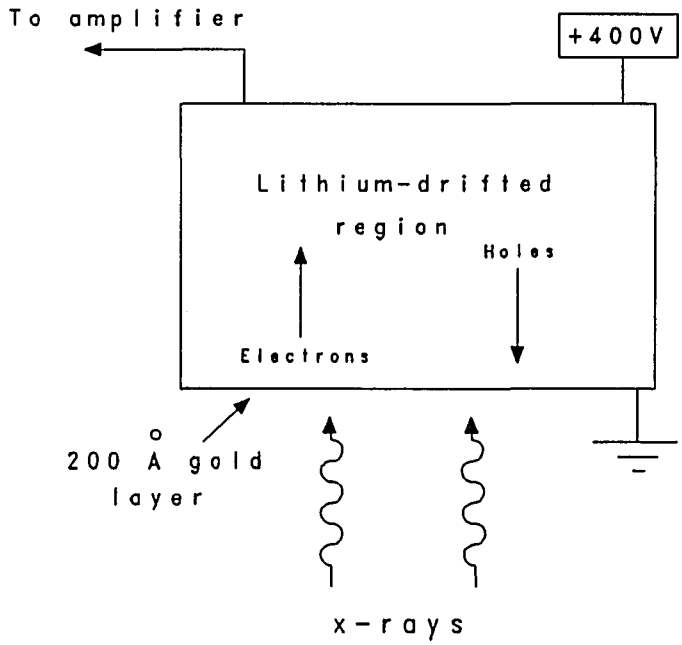

Figure 4. Diagram of the Si(Li) Detector.

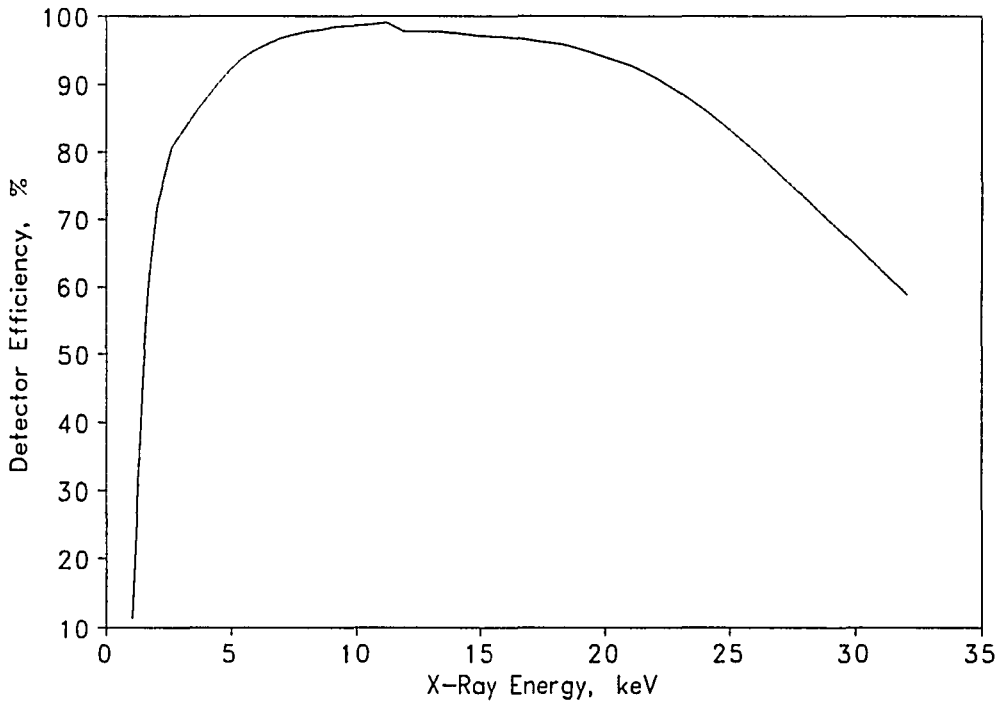

Figure 5. Efficiency of a Si(Li) Detector. The decrease in efficiency near 12 keV is due to the absorption x-rays by the gold electrode in the Si(Li) detector.

the University of Arizona is shown in **Figure 5.**

The detector is mounted behind a thin beryllium window which retains the vacuum around the detector, while allowing x-rays of greater than about 500 eV to pass through and reach the detector. Transmission through the window defines the lower energy limit of detected x-rays. If analysis of elements with atomic number less than 11 is desired, the window can be removed, although precautions to maintain vacuum around the detector must be taken.

If there is a large amount of low energy background or if large amounts of low atomic number material are present in the sample (as is common in the case of biological samples which often contain high concentrations of sodium, potassium, chloride ions, etc.), a filter to reduce transmission of low-energy x-rays (in addition to the permanent Be detector window) and attenuate the low energy end of the spectrum, is employed. **Figure 6** shows the percent of x-ray intensity which can pass through two different detector filter combinations. The attenuating filter is generally constructed of mylar, although many combinations of filter composition and thickness have been used. The aluminum and mylar combination filter which effectively removes the x-ray emission of elements lower than atomic number 20 (calcium) was used in the analysis of rabbit kidney slices at the University of Arizona. Use of a

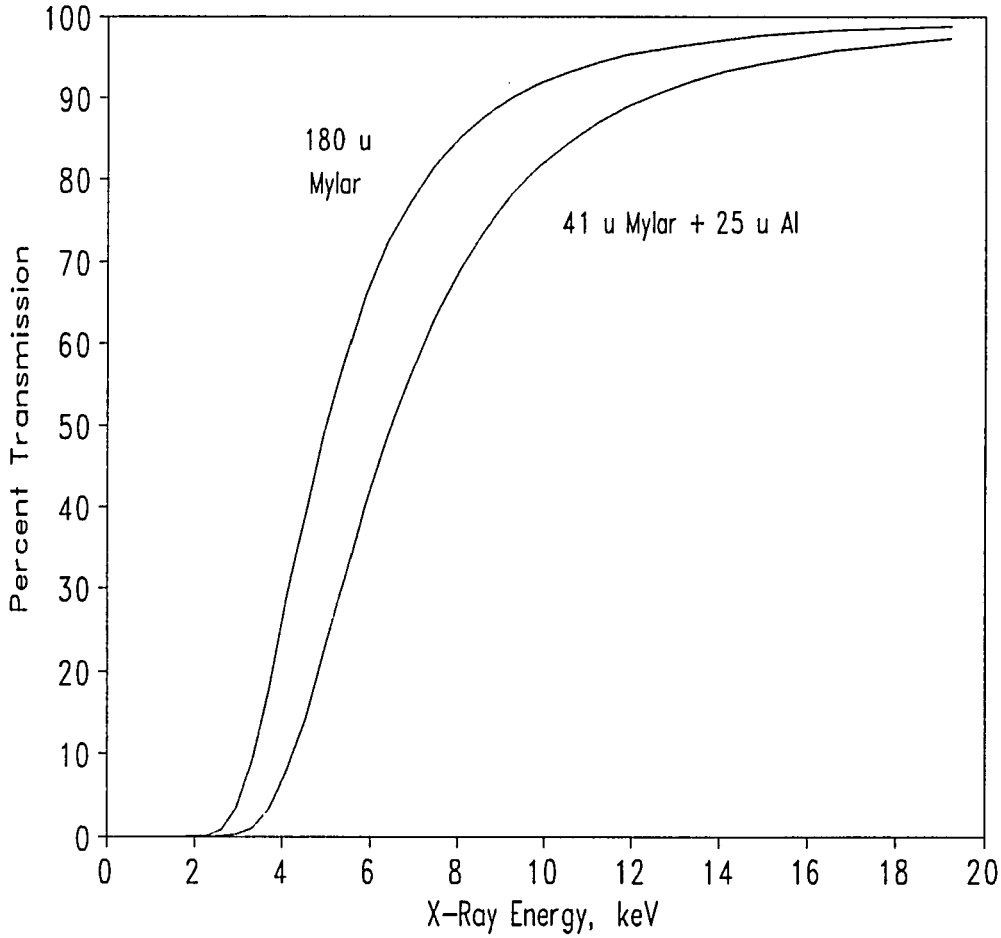

Figure 6. Percent Transmission of X-Rays by 180 μm Mylar and by a Combination of 41 μm Mylar and 25 μm Aluminum.

filter reduces the detection system dead time and so also reduces the overall rate at which x-rays are counted, resulting in a more efficient detection of higher atomic number elements. In addition, the filter removes the contribution of backscattered protons, which can enter the detector (see the section below on the PIXE spectral background).

Charge integration. The concentration of an element in the sample is directly proportional to its peak area in the spectrum, which in turn depends on the number of protons which strike the sample. Ideally, the current generated by the beam could be integrated using a Faraday cup designed to trap the charged particles after passing through an ideally thin sample; this method of monitoring the charge deposited on the target has been commonly employed elsewhere for reasonably thin samples. The Faraday cup in the University of Arizona system is not equipped for suppression of secondary electrons which can escape the cup, and most samples which are analyzed are not thin enough to allow the beam to pass through without attenuation. In other systems, this problem has been overcome by employing a rotating vane which periodically intercepts the beam or by coupling a current integrator directly to the electrically insulated sample holder in the analysis of thick specimens. At the

University of Arizona, an elegant method similar to that reported by Mitchell, et al.[26] for integrated charge measurement using protons backscattered from the beam line exit window has been employed. A surface barrier detector, located upstream of the window (**Figure 3**), measures the number of protons backscattered from a thin layer of cobalt which was vacuum evaporated onto the 7.6 μm kapton from which the window was constructed. The areal density (atoms per cm^2) of cobalt on the kapton had been accurately determined previously by RBS. From the number of protons backscattered from the cobalt on the kapton window, the number of particles passing through the window can be calculated by use of the backscattering equation if the beam energy, detector solid angle and Rutherford cross section for protons on cobalt are known. Provided that the beam is smaller in area than the sample, the total number of protons hitting the sample is known from the intensity of the cobalt peak. In practice, one RBS spectrum is recorded concurrently with each PIXE spectrum, and the charge deposited is calculated from **Equation (1):**

$$Q = \frac{LT_{PIXE}}{LT_{RBS}} \frac{N_{Co}}{500} \qquad (1)$$

where:

Q	is the charge deposited;
LT_{PIXE}	is the livetime of the PIXE spectrum;
LT_{RBS}	is the livetime of the RBS spectrum, calculated from the frequency of a 60 Hz synthetic pulse fed into the RBS detection system;
N_{Co}	is the number of counts in the cobalt peak in the RBS spectrum;
500	is the RBS factor for conversion of cobalt peak counts to μCoulombs.

Signal processing. The electronic processing of the signals produced in the Si(Li) detector begins with a FET preamplifier located close to the detector. The electrical pulses are amplified, then shaped by a pulse processor, before conversion from an analog voltage signal to a digital representation by an analog-to-digital converter (ADC). The conversion is accomplished by timing the duration of the analog pulse using a digital clock; the duration of a pulse is proportional to the energy of the original x-ray photon which generated the signal in the detector[27]. The resulting digital value is then stored either in a multichannel analyzer or in a block of computer memory which is divided into channels, each channel representing an x-ray energy range in the spectrum. In order to prevent another x-ray induced signal from entering the detection circuit while it is busy processing the last signal, the detector is deactivated while each pulse is processed. The time during which the detector is off is called dead time.

The possibility exists for two x-ray photons to enter the detector within a sufficiently short period of time so as to be interpreted as a single photon. These pile-up peaks in the spectrum can masquerade as x-ray lines of a different element and complicate the spectrum. A common method of pile-up peak reduction (and the one in use in the current system) is to use an electronic pile-up rejector[28], which puts the pre-amplifier signal through a fast amplifier and looks at the pulse profile for small anomalies which indicates the presence of two closely spaced signals. If anomalies are found, the pile-up rejector issues a veto signal to the main amplifier, which rejects the signal. The electronic pile-up rejector significantly reduces, but does not eliminate, pile-up peaks in the spectrum.
Alternatively, the beam can be deflected from the target momentarily, using a pair of conducting plates, while pulse processing is accomplished[29,30]. Complete removal of pile-up signals is not realized by this "on-demand" beam deflection system because of the time delay in switching the deflection voltages on and off; other advantages, however, such as less signal distortion and less sample irradiation, are realized using beam deflection pile-up rejection[31].

THE PIXE SPECTRUM

The PIXE spectrum consists of a plot of counted x-ray photons versus energy. Characteristic x-ray emission lines from elements in the target are superimposed on a background which arises from several sources. **Figure 7** is a PIXE spectrum of a thin copper film deposited on a carbon substrate, and shows background and instrumental features found in PIXE spectra. Although the energy width of characteristic x-ray emission lines is small, instrumental considerations broaden the lines to yield peaks in the spectrum which are basically Gaussian in shape. Peak overlap, and background in the spectrum require the use of computer-based spectrum processing to obtain accurate information from PIXE spectra.

Production of x-rays. In PIXE, ionization of inner-shell electrons occurs primarily by Columbic interaction of accelerated protons with atoms in the sample. Whether the initial ionization of an atom occurs by the action of a proton beam (PIXE) or x-rays (XRF), de-excitation occurs rapidly (10^{-16} second), either by emission of characteristic x-rays or Auger electrons or both. Auger electrons are ejected from the atom from outer shells as the inner shell vacancy is filled. The probability of generation of an x-ray, rather than the emission of an Auger electron, is the

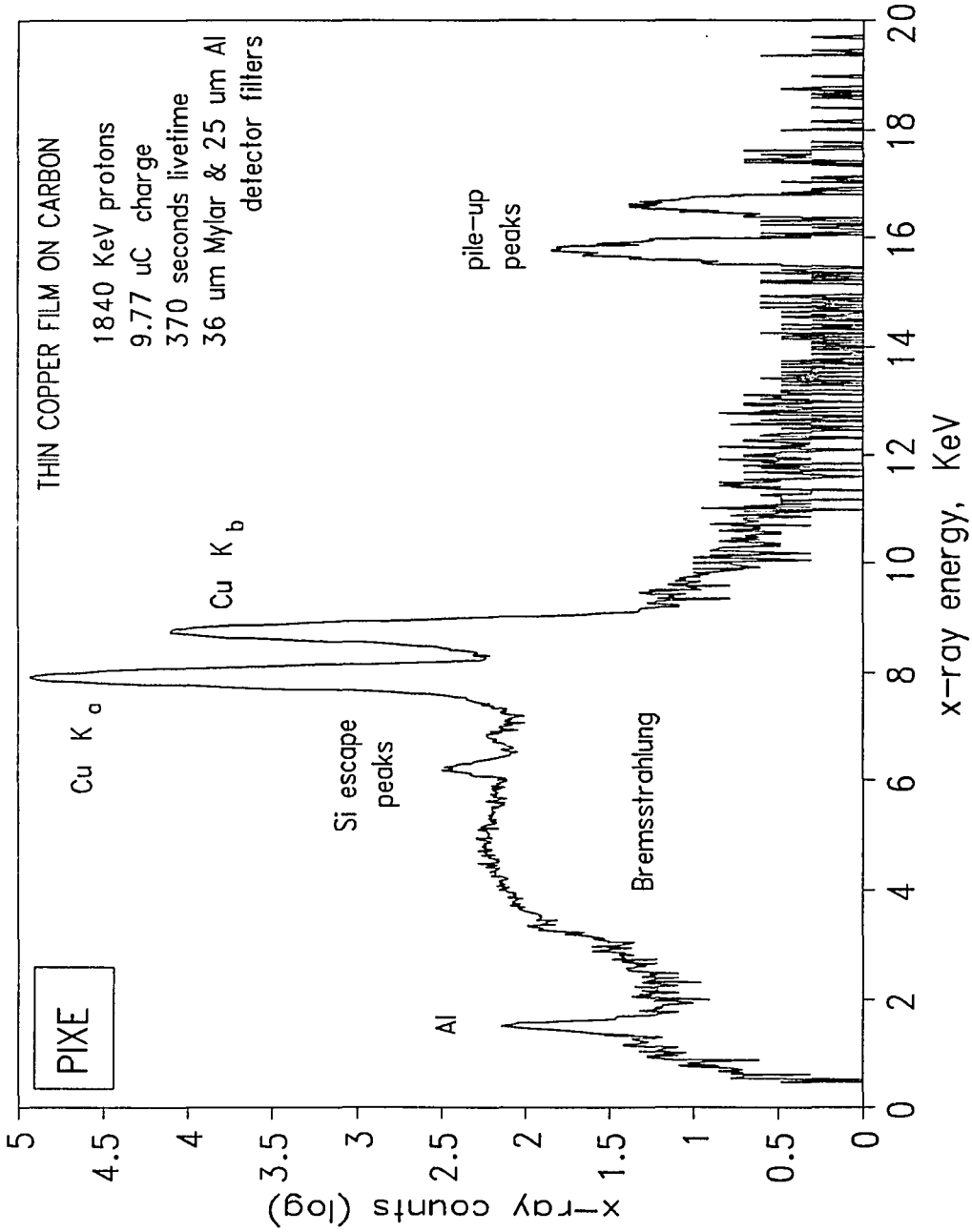

Figure 7. PIXE spectrum of a thin copper film on a carbon substrate.

fluorescence yield, ω. Bambynek, et al. calculated fluorescence yields for K and L electron shells to a high degree of accuracy[32], and showed that the fluorescence yield increases with atomic number.

A highly simplified energy level diagram of electronic transitions and the resulting x-ray emissions is shown in **Figure 8**. The K series of x-rays occurs when a K shell electron vacancy is filled, the L series when a L shell electron is filled, and so on. Each shell above the K shell is composed of increasing numbers of sub-shells of different energies, and consequently there are many more L transitions than K transitions, and even more M transitions. In the simplified energy level diagram none of these sub-shells are shown. Not all transitions are allowed; selection rules limit them. The Si(Li) detection system often cannot resolve closely spaced (<150 eV) x-ray emissions, and overlapped transitions appear in the spectrum as a single peak. The intensities of some x-ray emissions are so weak that they can be ignored for practical purposes. The useful range of x-ray energies in PIXE is approximately 1-30 keV. The relative intensities of x-ray emissions for a single element, i.e. K_α vs. K_β, were calculated by Scofield[33], and agree closely with experimental data. Knowledge of these relative intensities of x-ray emissions is useful in decomposing spectral overlaps in the spectrum.

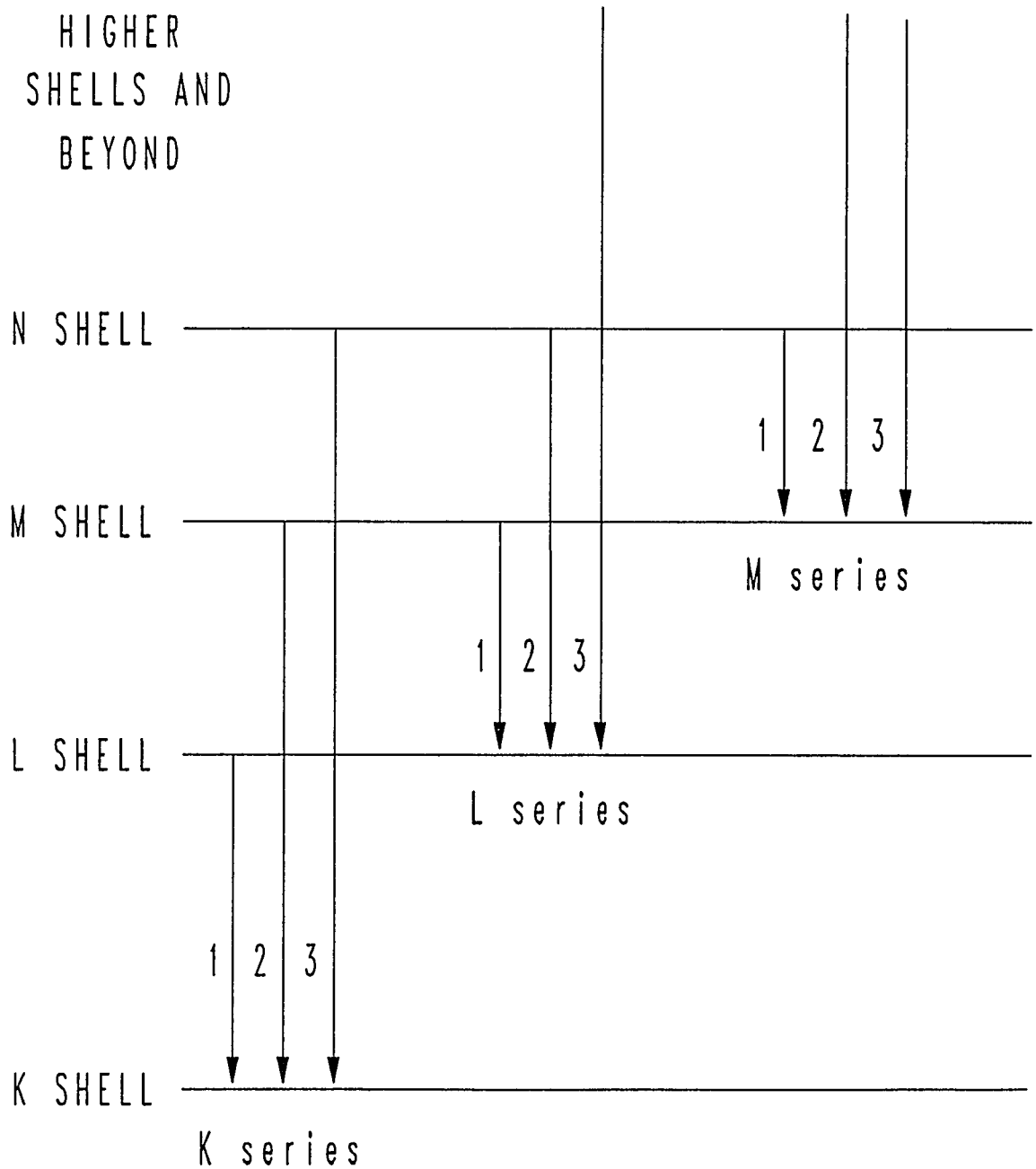

Figure 8. Simplified atomic level diagram showing possible electronic transitions which result in x-ray emission. 1 refers to α transitions, 2 to ß transitions, 3 to γ transitions.

Spectral peak shapes. While characteristic x-ray emission lines have an intrinsic width of less than 1 eV, the detection system introduces a statistical counting uncertainty which broadens the signal, yielding a Gaussian peak shape in the PIXE spectrum. The major contributor to the x-ray counting uncertainty is the distribution of charges induced in the Si(Li) detector by x-rays entering the active area of the detector. Other contributors to peak broadening include inefficiencies in charge collection in the detector and random noise in the pulse processing and amplification system. The peak shape of characteristic lines in the PIXE spectrum is primarily Gaussian, although tailing is observed, especially in intense spectra.

The low energy tailing of peaks in the PIXE spectrum arises from processes such as loss of x-ray photon induced Auger and photo-electrons in the detector to the Si(Li) crystal surface "dead layer", and loss of charge, both to regions of weak charge-collection fields and imperfections within the detector. In addition, x-ray Auger satellites, from atoms whose L shells are ionized while another proton induced S shell event (yielding a K_α or K_β x-ray photon, reduced by a small amount of energy) is occurring, are detected. Compton scattering of photons above about 15 keV also contributes to tailing of high energy peaks[34]. Low

energy peak tailing is therefore due to nuances in detector construction and other photon energy-dependent processes. Tailing is not an important contributor to peak area, but will cause errors during quantitation of an element whose peak is overlapping the tail of a stronger peak.

An instrumental contribution to the PIXE spectrum is the silicon escape peak. The escape peak is due to the escape of Si K_α x-rays following penetration of the Si(Li) detector by proton induced x-ray photons. The escape peak is found at 1.742 KeV lower energy than the parent peak, which is the energy of the parent peak less the energy of the lost Si K_α x-ray. Si escape peaks are generally less than 1% of the area of the parent peak.

PIXE spectrum background. One of the advantages of the PIXE technique is its ability to detect trace levels of elements in a sample. In a typical PIXE system, detection limits of less than 1 ppm (μg/g) for thin organic samples are attainable[35]. The high sensitivity of the PIXE technique is largely due to the low background in the spectrum. Much of the background in PIXE spectra is due to bremmstrahlung (braking radiation) from the deceleration of beam protons and energetic secondary electrons (produced by the beam) as they pass through the sample.[3] Secondary electron bremsstrahlung, resulting from the numerous proton beam-

electron interactions in the sample, contributes to the background at the low energy end of the spectrum, and falls off rapidly with increasing energy. PIXE spectra of 7.5 μm Kapton backing material obtained with two different detector filters are shown in **Figure 9**. Aside from the K_α and K_β lines of calcium, the spectrum represents the background obtained from a relatively pure backing material. The effect of using a detector filter is also demonstrated in the figure; the secondary electron bremmstrahlung is attenuated below around 3 keV and the x-ray emissions at 6.9 and 7.3 keV from iron (a trace impurity) are seen clearly once the background is removed by the use of the 180 μm Mylar detector filter. The spectrum in **Figure 9** obtained without a detector filter shows a continuum of background whose intensity is constant at approximately 30 counts. This background is eliminated by using the thin mylar detector filter, and therefore cannot arise from x-rays, since the higher energy x-rays would not be effectively attenuated by the thin detector filter. Since there were no detected x-rays above about 8.5 keV when the Mylar detector filter was used, the background is likely due to protons backscattered from the target, which can penetrate the thin beryllium detector window and gold electrode layer on the Si(Li) crystal and enter the active area of the detector.

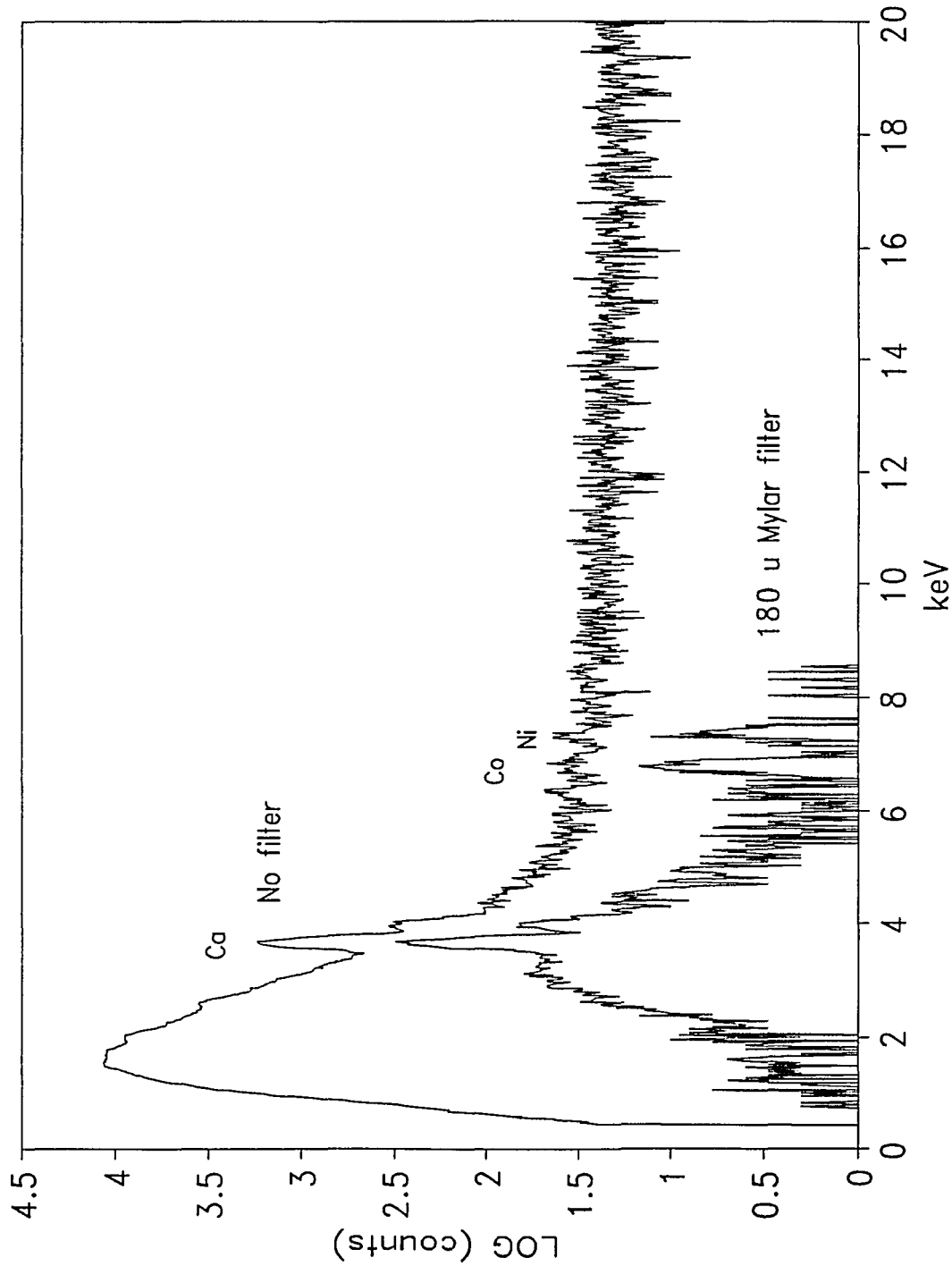

Figure 9. PIXE spectra of 7.5 μm Kapton backing material.

Another possible contribution to background at the high energy end of the PIXE spectrum is γ-radiation produced in nuclear reactions in the sample, if low atomic number elements are present in the sample and the beam energy is sufficiently high. γ-radiation produces x-ray background due to Compton scatter in the detector, which is a process by which γ-rays lose energy upon interacting with electrons. To reduce the γ-radiation background it is therefore desirable to use a low beam energy for analysis, but maintain the energy high enough to produce a reasonably high characteristic x-ray yield. Proton beams of 1-3 MeV are therefore best suited for PIXE[3], and since proton beams with under 2 MeV energy are used in the University of Arizona PIXE laboratory, γ-radiation background has not been observed.

Thick, insulating targets which stop the beam are prone to charging effects and attain kV potentials. Arcing from the target to a nearby conductor generates a continuum of x-rays in the spectrum, and therefore, some method of discharging targets which are insulators or are mounted on insulating materials must be employed. The Kapton window at the end of the beam line in the present system is effective in providing a spray of electron that neutralize charging effects.

SPECTRUM PROCESSING

Spectrum processing software

The GUPIX PIXE spectrum processing program in use at The University of Arizona was developed at the University of Guelph at Guelph, Ontario, Canada by J. L. Campbell, J. A. Maxwell and W. J. Teesdale. The need for computer-assisted spectral analysis is clear, given the complexity of PIXE spectra due to the need for thick sample matrix correction, corrections for inter-elemental interactions and the common occurrence of overlapped peaks. The GUPIX program uses a Marquardt non-linear least-squares fitting routine[36] which fits a model spectrum to the experimental spectrum and uses the fitted parameters to derive the concentration of elements present in the sample. The fit of the model to the experimental spectrum is evaluated with a chi-squared test in an iterative fashion, and the parameters of the fitted spectrum are varied to improve the value of chi-squared with each iteration. **Figure 10** is a flow chart outlining the steps carried out by the GUPIX software.

Spectrum files. PIXE spectra are stored by the EDXRF detection system using a format developed by TRACOR for use by the TRACOR spectrum processing software. Because the spectrum stored by the EDXRF detection system is stored in a

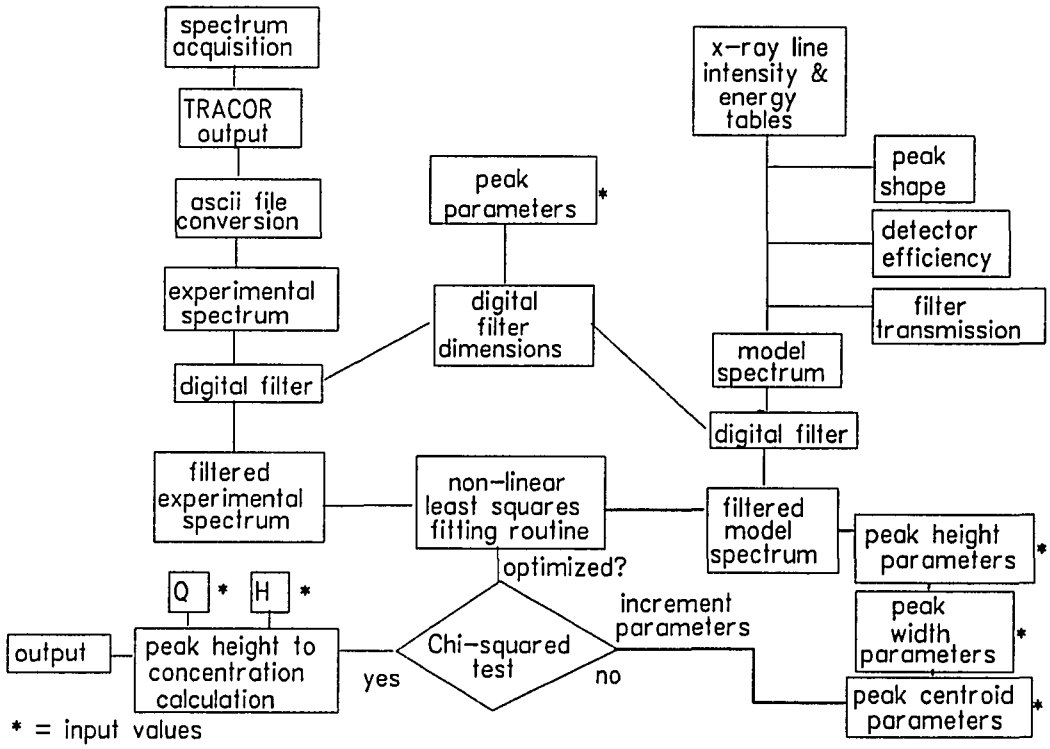

Figure 10. Flow of operation of the GUPIX program.

format unacceptable by the GUPIX program, the spectrum must first be translated into an ascii file readable by the GUPIX program. D. Ashbaugh of the University of Arizona Department of Physics developed a simple program for accomplishing the conversion. The spectrum file consists of 1024 numbers, each representing the number of counts registered by the detection system during spectrum acquisition.

The PIXE background spectrum. The background in PIXE spectra arises from many complex phenomena, and agreement on a general approach to modelling it does not yet exist. A way of circumventing the background modelling problem, by removal of the background with a digital filter, was developed for electron probe micro-analysis. Although other spectrum processing programs which analytically model the background exist, the GUPIX program uses the digital filter to obviate the problem. The digital filter (**Figure 11**) consists of a zero-area "top hat" function that, when applied channel-by-channel across the spectrum, has the effect of removing the gently sloping components of a spectrum, while leaving the typically

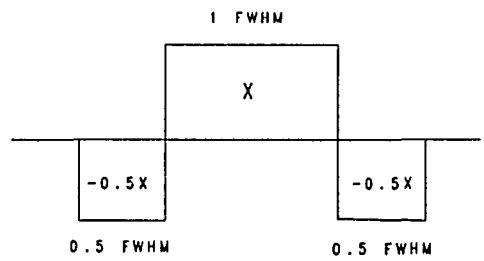

Figure 11. Digital Filter.

Gaussian peaks produced by characteristic x-rays in a Si(Li) detector intact. The optimal dimensions of the digital filter have been found to be 1 full width at half maximum (FWHM) of a typical x-ray emission peak for the positive lobe of the filter and 1/2 FWHM for each negative lobe[37]. The dimensions of the filter are calculated from the input parameters which define peak width (**Equation (8)**). The filtering operation is analogous to taking the second derivative of the spectrum, and the assumption is made that the continuum background is roughly linear in the region of the peak. The filtered spectrum obtained by the use of this filter is demonstrated in **Figure 12.**

The model spectrum. The model pulse-height spectrum is assembled from a list of calculated x-ray detector response factors for x-ray lines of each element in the spectrum and the modelled peak shape determined for the detection system. The model peaks are placed at the channels corresponding to the energy of the element to be looked for, and the spectrum filtered using the same digital filter as was used on the experimental spectrum. The height of each peak is varied in the non-linear least-squares fitting routine until the synthetic spectrum is optimally fit to the experimental data as determined by the value of chi-squared, a parameter reflecting the degree of similarity between the two spectra.

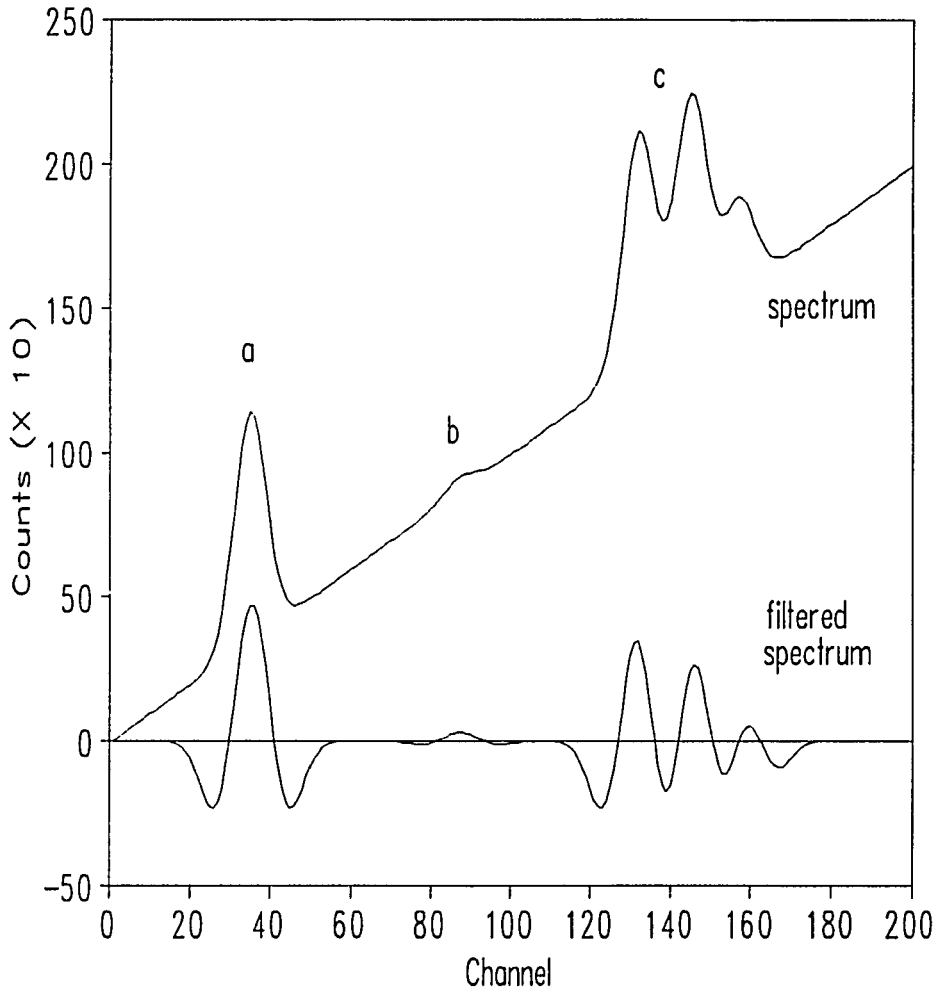

Figure 12. Demonstration of the spectrum resulting from the use of the "top hat" digital filter on a synthetic spectrum. a, a single peak; b, a small peak near the detection limit; c, three overlapped peaks.

The peak height parameters are then converted to elemental concentrations using a value determined for the instrumental calibration by standardization with a known sample. The concentrations are reported along with an associated statistical error and limit of detection for each element.

The elemental line spectrum. The GUPIX program calculates a model spectrum consisting of lines describing the relative peak heights of all x-ray lines for each element expected to be present in the sample, corrected for detector efficiency, filter attenuation and matrix effects. The individual elemental contributions are then summed to form a peak height spectrum.

The expected detector response factors are calculated from a table of the relative intensities of the various x-ray lines corresponding to the elements expected to be present in the sample, corrected for any detector filters used in the analysis and the detector efficiency, as shown in **Equation (2):**

$$R'_{nm} = cR_{nm}T_{nm}(ab)\,\varepsilon^{I}_{nm} \qquad (2)$$

where,

- R'_{nm} is the corrected line intensity of the m^{th} line of the n^{th} element;
- c is the normalization constant to set the most intense line of the element n to unit area;
- R_{nm} is the relative line intensity taken from data tables[38];
- $T_{nm}(ab)$ is the attenuation factor due to the use of

detector filters;

ϵ_{nm} is the intrinsic detector efficiency

The heights of each line, relative to the principal (analytical) line must be corrected for width, since the model spectrum requires peak heights, and the relative intensity is a ratio of areas. The factor for converting area (intensity) to height is σ_j/σ_l, where σ is the standard deviation of the Gaussian (peak width), j is the less intense line (i.e. K_β), and l is the principal line (i.e. K_α). R'_{nm} is multiplied by this factor to yield line heights.

This is a simplified process for obtaining the expected peak heights, and works well for thin targets. If the beam is attenuated by thick samples, then another factor, f, which deals with matrix corrections, must be multiplied in the right side of **Equation (2)**:

$$f = \int_{E_0}^{E_f} \frac{\sigma_Z(E)\, T_Z^{nm}(E)}{S(E)}\, dE \qquad (3)$$

where,

$\sigma_Z(E)$ is the ionization cross-section at beam energy E for the element with atomic number Z

$T^{nm}_Z(E)$ is a term describing the transmission of x-rays of the $\underline{m}^{th}$ line of the $\underline{n}^{th}$ element through the matrix element with atomic number Z

S(E) is the matrix stopping power at beam energy E

If the target is infinitely thick, the upper limit of integration is zero, since the beam is stopped by the target. The identity of the matrix must be known for this correction, although if the concentration of elements in the matrix is unknown, their concentrations can be varied each iteration of the least-squares fitting program until an approximate match to the experimental spectrum is obtained.

Detector efficiency, which defines the peak height observed for a given x-ray photon energy, is related to the detector's physical properties. Using the non-linear least-squares fitting routine requires absolute knowledge of the detector efficiency, which depends on the physical dimensions of the Si(Li) crystal and detector-sample positioning. The efficiency is modelled using **Equation (4)**.

$$\varepsilon = \frac{\Omega}{4\pi} \left(\exp\left[-\sum_{i=1}^{3} \mu_i d_i\right]\right) f_{esc} \left[1-\exp\left(-\mu_{Si} D\right)\right] \qquad (4)$$

where,

- Ω is the detector solid angle, as a fraction of 4π, which includes the diameter of the detector and sample-detector distance
- μ_i is the mass attenuation coefficient for filter element i
- d_i is the thickness of materials in front of the detector crystal, including the thickness of the beryllium window which maintains the vacuum in the detector, and the thickness of the gold surface barrier electrode
- f_{esc} is the factor correcting for losses due to the Si escape peak
- D is the thickness of the detector crystal.

These parameters are supplied by the manufacturer of the Si(Li) detector, although several empirical methods exist for determining them[4].

Modelling of PIXE spectral peak shapes. At this point, the model spectrum is only a list of corrected x-ray detector response factors for the various K, L and/or M lines of each element to be analyzed, normalized to the principal analytical line. The peak shapes are defined by the detection and pulse processor electronics, and are modelled using theoretical and experimental considerations. Once the peak shape reference has been established, it is multiplied into the above determined response factors to form the completed model spectrum.

The peak shape is modelled after the experimental output of the Si(Li) detector, which is basically Gaussian in shape, but which contains low energy tailing components due to several phenomena (see the section on spectral peak shapes) which must be added to the basic Gaussian count distribution. The Gaussian component, G_i, of the peak shape, related to channel number i is given by **Equation (5):**

$$G_i = H_g \exp\left[\frac{-(i-c)^2}{2\sigma^2}\right] \qquad (5)$$

where:

H_g is the height of the peak;
c is the channel number of the peak centroid;

σ is the standard deviation of the peak.

One last peak shape feature modelled by the GUPIX program is the silicon escape peak (designated E_i) which is found at 1.752 keV (Si K_α=1.742 keV, nominally) lower in energy than the characteristic peak. The GUPIX program models the Si escape peak as a Gaussian shaped peak whose intensity is taken as a fraction of the parent peak using a parameterization developed by Johansson[39].

The peak shape related to channel i, F_i, is then described as in **Equation (6)**:

$$F_i = G_i + xS_i + yST_i + zD_i + E_i \qquad (6)$$

where x,y and z are the numbers of each tailing type used to describe peak tailing

The relative line intensities and peak shape were calculated by the above equations, so for each element, the spectrum is:

$$F_n = \sum_n A_n F(i)_n \qquad (7)$$

where:

F_n is the spectrum, including peak shape and heights normalized to the analytical line;

A_n is the height parameter which is varied in the fitting routine;

$F(i)_n$ is the calculated peak shape.

The only parameter to be determined in the least-squares fitting routine is the value of A_n, the height of the principal x-ray line for each element, n.

The complete model spectrum is then the sum of all elemental spectra.

Spectrum fitting. It would appear that the modelling of PIXE spectra would require many parameters, but the GUPIX program treats many of the response factor and peak shape and centroid parameters as constants, so the characteristics of each spectrum are described by five parameters which are first input, then varied in the least-squares fit to optimize peak position and width. In addition to these five parameters, one parameter for each element determined is varied to determine concentrations of the analytes. These parameters are described below.

The GUPIX program simplifies the description of the peak centroid positions by determining the peak centroid channel, c_i, for each element i to be fitted using three parameters, A_1, A_2 and A_3, and a table of elemental x-ray line energies, E, as in **Equation (8)**:

$$c_i = A_1 + A_2 E_i + A_3 E_i^2 \qquad (8)$$

The detection system generally places measured photon energy counts linearly into the channels of the spectrum, so only

A_1 and A_2 should be needed, although slight non-linearity which may arise is dealt with using the small A_3 term.

The width, characterized by σ, of all peaks in the spectrum are represented by two parameters A_4 and A_5:

$$\sigma(E) = \sqrt{A_4 + A_5 * E} \qquad (9)$$

The other parameters in the fitting routine are the principal peak height for each element in the spectrum, A_6 through A_N.

The parameters A_1 through A_N are optimized using the non-linear least-squares fitting routine, and the other coefficients in the equations for peak shape, response factors, matrix effects, detector efficiency, escape peaks, etc. are all assumed to be functions of the fit parameters A_1 - A_N. So, after all the constant parameters defining instrumental characteristics and initial values for A_1 - A_5 have been entered, the GUPIX program builds and optimizes a fitted spectrum, varying the parameters A_1 - A_N.

Fit optimization. The initial model spectrum is first filtered using the same digital filter as used on the experimental spectrum, then optimized repetitively by the non-linear least-squares fitting program, and evaluates the

fit each loop, using the parameter chi-squared. Chi-squared is calculated as in **Equation (10)**:

$$\chi^2 = \frac{1}{d} \sum \frac{[Y_{mod}(x) - Y(x)]^2}{\sigma_x^2} \qquad \textbf{(10)}$$

where:

$\underline{d}$	is the number of degrees of freedom (the number of channels in the spectrum reduced by the number of parameters being determined)
$Y_{mod}(x)$	is the counts in the x^{th} channel in the model spectrum
$Y(x)$	is the counts in the x^{th} channel in the experimental spectrum
σ_x	is the standard deviation of $Y(x)$, given by the square root of $Y(x)$

Use of the non-linear fitting routine allows wide variation in the system parameters, which a linear fitting routine would hold constant, thereby allowing the best fit, regardless of whether the calibration of the instrument has drifted over time or not. In practice, use of the digital filter for removing the background requires fitting of a model spectrum to the "curvature" of the filtered experimental spectrum, since the filtering is analogous to double differentiation of the original spectrum, and chi-squared is therefore often optimized at values less than 1.

Error analysis. The only explicit source of error entered into the program is the statistical counting error in each channel, σ_x in **Equation (10)**, which leads to the assumption that the data base and modelling routines are free of error.

To make the error assessment more realistic, the GUPIX program assigns an uncertainty to the detector filter thickness, calculates the corresponding uncertainty in the filter transmission term (**Equation (2)**) for each channel of the spectrum and adds this to the $\sqrt{n}$ error for n counts in that channel. This has the effect of weighting the spectral regions least affected by the filter more heavily in the fit than the regions more strongly attenuated by the filter, which would be expected to have larger uncertainties. Other peak fitting programs use innovative approaches to error estimation such as including the error in attenuation coefficients in thick samples or using peak background intensity estimations and calculating error as $(I_p+2I_b)^{1/2}$; instrumental error in the present system is generally estimated experimentally for each sample type by acquiring spectra from repetitive runs on a single sample, and calculating the standard deviation of the reported concentrations. However, the error calculated by the GUPIX program does give an indication of the minimum error expected. Error calculated by the GUPIX program for the elements analyzed in a renal slice study in which arsenic was the toxicant is shown in **Figure 13.** The dependence of the error on the intensity of the x-ray peak can be seen as a trend in the figure, with variation in the trend, demonstrated by Cl, Ar, and Sc, due to overlap of the peak

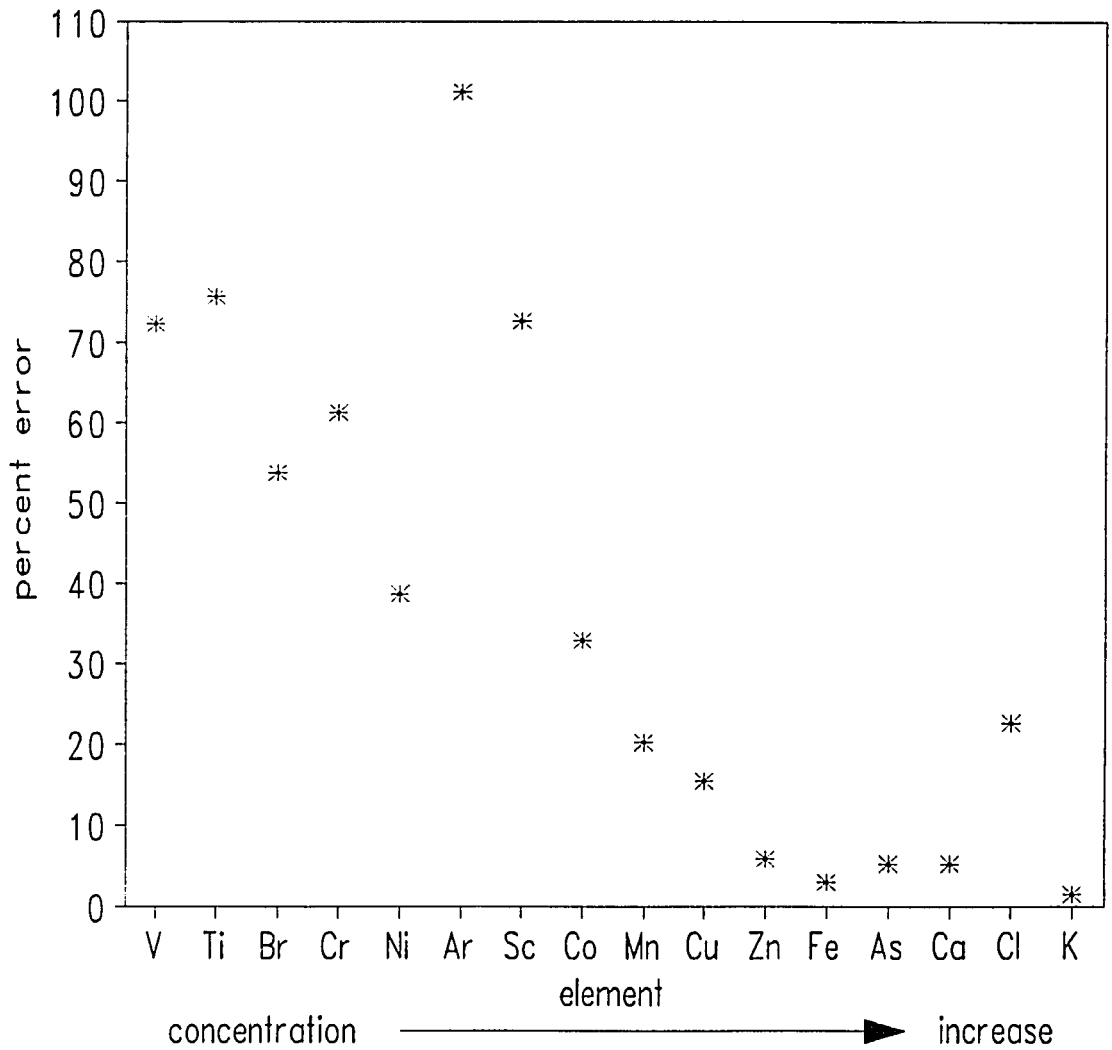

Figure 13. Error as calculated by the GUPIX program for renal slices.

with other peaks or bremmstrahlung background. The low errors for K, Ca, Fe, Zn and As are the result of the relatively high concentrations of these elements in renal slices.

Limits of detection. The limit of detection (LOD) for each element is reported by the GUPIX program in terms of statistical counts and in concentration units. Detection limits are generally calculated from the background counts under the analytical peak for an element in the spectrum. To calculate the counts corresponding to the LOD, the GUPIX program uses LOD = $3\sigma_B$, where σ_B is the square root of the counts in the background. The background width is taken as 1 FWHM, centered on the analytical peak, and the counts are calculated from the original, unfiltered, spectral data iteratively by summing counts in the data spectrum minus counts in the fitted spectrum over the 1 FWHM range, and if the counts in any channel of the computed background exceeds the average background by 1σ, the counts in that channel are reduced to the average value, and the process repeated until the "smoothed" background no longer changes. To this calculated background is added contributions from overlapped peaks, then the square root of this background in taken as σ_B. A factor of 1% of the overlap area is added to σ_B, to account for systematic errors. Then $3\sigma_B$ is the reported

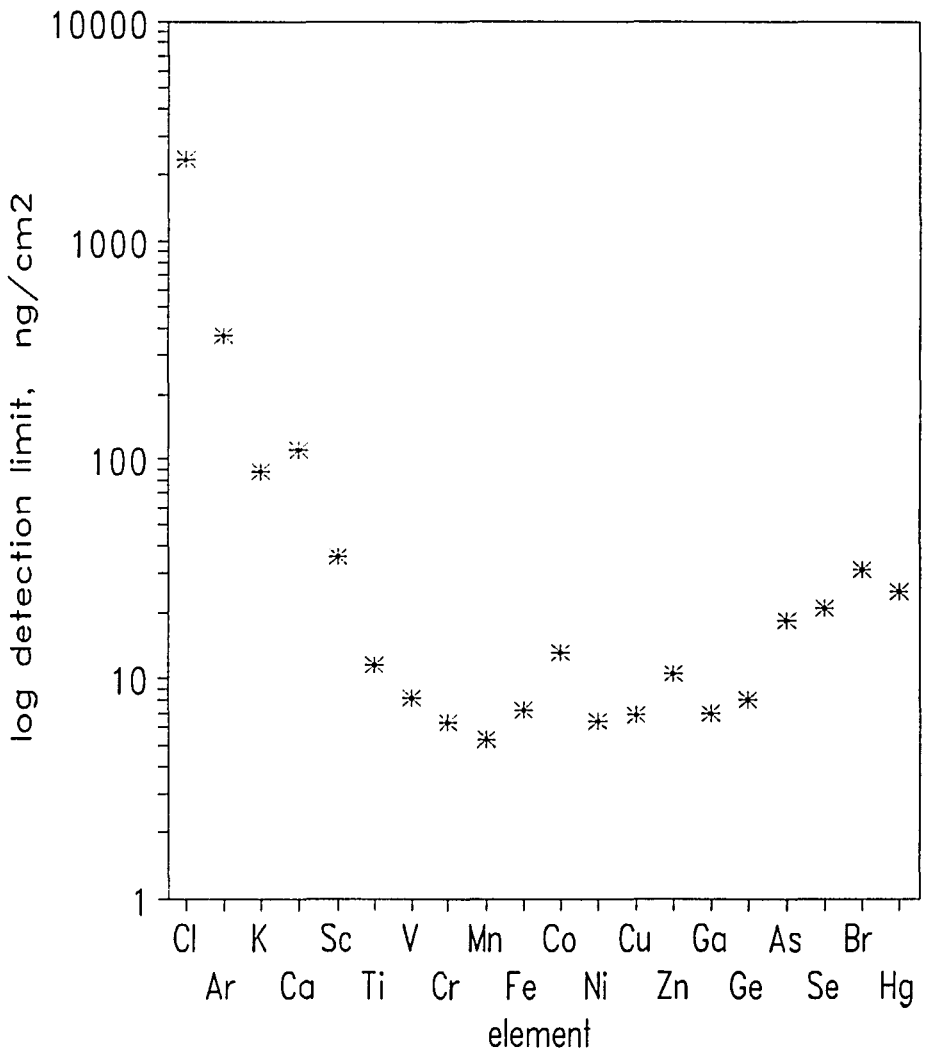

Figure 14. Detection Limits for elements in renal slices as calculated by the GUPIX program.

counts LOD, and $3\sigma_B/Q*H*Y_{lt}*T$ (see **Equation 11**) is the concentration LOD. Detection limits calculated by the GUPIX program for a kidney slice experiment in which As was the toxicant are shown in **Figure 14**. The detection limit curve follows expected trends; since there is higher background at the low energy end of the spectrum, detection limits for the low Z elements are higher than for the elements whose x-ray emission lines fall in the higher energy range of the spectrum. Variations in the trend for Co and Fe are due to consistent overlap of their emission peaks in the renal slice analyses.

Accuracy of the PIXE technique. The accuracy of the PIXE technique is usually determined by the analysis of standard materials. NIST standard bovine liver or orchard leaves have been powdered and attached to a thin backing with a polystyrene glue. The results of earlier experiments showed that the accuracy of the technique was of the order of 10%[1], which is the value that is generally agreed upon for the accuracy of PIXE. The results of the analysis of NIST standard reference material 1571, orchard leaves, with a comparison to the NIST certified values is shown in **Table II**. The sample was prepared by first grinding a small amount of the material in a polystyrene vial with a ball pestle using a Wig-L-Bug shaker. A thin film of the powder was then attached to 7.5 μm Kapton by use of a solution of

	Orchard Leaves ppm	+/-[a]	NIST Value ppm	+/-
Cr	2.31	0.8	2.6	0.03
Mn	-	-	91	4
Fe	300*		300	20
Co	0.51	2.1	(0.2)	
Ni	2.56	1.0	1.3	0.2
Cu	10.8	0.8	12	1
Zn	24.4	1.3	25	3
Ga	ND		(0.08)	
As	ND		10	2
Se	ND		0.08	0.01
Br	10.8	2.3	(10)	
Rb	17.7	3.1	12	1
Sr	35.9	4.9	37	1
Cd L	-	-	0.11	1
Sb L	ND		2.9	0.3
I L	ND		(0.17)	
Cs L	ND		(0.04)	
Ba L	39.5	5.1	(44)	
Pb L	39.0	5.4	45	3
Bi L	ND		(0.1)	

Table II. Results of the PIXE analysis of orchard leaves, SRM 1571. 86.4 uC charge was deposited, and a 180 μm Mylar detector filter was used in the analysis. a; statistical error. * PIXE results were calculated relative to the NIST certified value for Fe. NIST values in parentheses were determined by only one method. ND: none detected.. The instrumental conditions were similar to those in **Table I.**

cellulose acetate dissolved in glacial acetic acid, and was analyzed by PIXE. The low atomic weight elements were not detected due to the use of a 180 μm Mylar detector filter. Overlaps of the manganese K x-ray lines with x-ray lines of chromium and iron, and overlaps of the L x-ray lines of cadmium with the K lines of calcium and potassium caused erroneous results for those elements. Use of a 180 μm detector filter precluded the accurate analysis of elements with atomic number below 22. The study confirms the accuracy of the technique when optimized.

PRACTICAL APPLICATION OF THE GUPIX PROGRAM

The GUPIX program is an ab initio calculation of trace element concentrations in a sample, and therefore requires detailed knowledge of the instrumental properties. **Table III** defines the parameters input into the GUPIX program, classified as calibration and individual spectrum parameters. **Table IV** lists typical values used in the GUPIX program during the analysis of kidney slice samples. A typical GUPIX output report, which includes initial and final values of the input parameters and all other pertinent values calculated by the program is included in **Appendix A.**

Conversion of peak intensities into concentrations

Standardization of the PIXE instrument is accomplished by the GUPIX program using **Equation (11):**

$$Y_{(Z,M)} = Y_{1t}(Z,M) \cdot C_Z Q \cdot fq \cdot \Omega \cdot \varepsilon \cdot T \qquad \textbf{(11)}$$

where;

- $Y_{(Z,M)}$ is the intensity of the element Z in the matrix M
- Y_{1t} is the theoretical x-ray yield per μCoulomb per unit concentration per steradian
- C_Z is the actual concentration of Z in M
- Ω is the detector front face solid angle
- Q is the measured charge deposited on the sample
- fq converts Q to μCoulombs if Q is measured in a different system of units
- ϵ is the detector efficiency
- T is the transmission through any detector filters

INSTRUMENT CALIBRATION PARAMETERS	
ALPHA	the beam-to-target normal angle
THETA	the detector-to-target normal angle
$A(1)+A(2)\cdot$peak energy(keV) $+A(3)\cdot(\text{peak energy})^2$	three parameters used as shown to calculate the peak centroid
$[A(4)+A(5)\cdot(\text{peak energy})]^{1/2}$	two factors to calculate peak width (channels)
detector ID	parameters used to calculate detector efficiency
Be window thickness	
Au electrode thickness	
Si crystal thickness	
target-detector distance	
lower energy cutoff (keV)	
pulse deadtime (μseconds)	
Si escape peak energy (keV)	

INDIVIDUAL SPECTRUM PARAMETERS	
spectrum file name	ascii file containing the PIXE spectrum, as a list of counts in each channel
NCHAN	channel offset to locate the fit region in the spectrum
NST	number of the first channel
NSP	number of the last channel
proton beam incident energy	if the target is thin, then incident energy = exit energy. Also can input target thickness in mg/cm^2
proton beam exit energy	
matrix composition	thick target matrix composition
detector filters (Z, thickness)	parameters used to calculate attenuation of x-rays by detector filters
μcoulombs of charge deposited	charge from exposure to the beam
H	standardization value obtained from standards
elements to be fitted	a list of elements expected to be present in the sample

Table III. GUPIX Parameters.

NCHAN	1
NST	1
NSP	1024
ALPHA	0°
THETA	45°
proton energy:	
incident	1840 keV
exit	1840 keV (thin targets)

spectrum energy scale

	20 keV	40 keV
A(1)	4	2
A(2)	50	25
A(3)	0	0
A(4)	7	3
A(5)	2	1

detector:	
Be window	0.00203 cm
Au electrode	2.0×10^{-6} cm
Si crystal	0.47 cm
target-detector distance	4.50 cm
lower energy cutoff	3.00 keV
pulse deadtime	25.0 μseconds
Si escape peak energy	1.752 keV
detector filters: (for kidney slices)	25.0 μm aluminum 43.0 μm mylar
charge	depends on the sample, often 10-30 μCoulombs
elements analyzed	depends on the sample
H	varies due to minor changes in the system, usually 0.006 ± 0.001

Table IV. Typical values used in the GUPIX program.

The standardization constant, **H**, is the factors Ω and fq combined, and is determined by analysis of a standard with known concentration and using **equation 11** to calculate **H**. Using **equation 11** to calculate concentrations of analytes incorporates both theoretical treatment of peak intensities and use of a standard to calibrate the instrument, through the use of the constant, H. The units reported by the GUPIX program are then related to the units used in the standard, which is most often a thin film measured in mg/cm^2 or ng/cm^2. The reported units for thick samples are related to the matrix composition, and therefore are in parts per million (ppm).

APPLICATIONS OF PIXE IN BIOLOGICAL SAMPLE ANALYSIS

PIXE is well suited to the analysis of biological specimens which can be prepared as thin films. In particular, PIXE offers rapid, simultaneous multielemental analysis of (1) animal tissue, which can be conveniently prepared as microtomed slices, (2) body fluids, which can be evaporated on a suitable thin backing material, (3) ashed, homogenized or digested material, which can be analyzed either as a powder spread on an appropriate backing or dissolved and treated as a liquid sample and (4) self-supporting specimens such as air and water particulate filters, hair, insect wings or leaves, which can be analyzed directly. The small sample size requirements also make PIXE an attractive method for the analysis of limited quantities of sample, such as biopsies or small volumes of body fluids. Thick samples like bone, teeth and pelletized samples can also be analyzed, with a concomitant increase in detection limits. PIXE is recognized to be a superior multielemental method for the determination of trace elements, with detection limits in the range required for the analysis of trace metals that are present in biological systems[12]. PIXE is capable of assessing inter-element interactions in a single sample from an organism. PIXE's ability to sample small areas also facilitates point-by-point analyses of

specimens rich in spatial information, such as tree rings or hair. One limitation of the technique is its shallow sampling depth. The penetration of protons in the MeV range of energy is typically limited to a depth of several tens of microns.

SAMPLE PREPARATION

Sample preparation techniques. Sample preparation is the key to obtaining meaningful information from PIXE analysis. X-ray emission methods of analysis provide information about many types of samples without pre-treatment, but, since biological specimens are particularly susceptible to variations in near-surface composition, the preparation of duplicate samples becomes quite difficult. Since the lowest detection limits obtainable are required for quantitation of the low levels of trace elements found in biological systems, the instrumental conditions must be optimized, and sample preparation techniques must be rigorously controlled to provide meaningful results. Thin sample films make the best targets for PIXE; if analysis of the bulk composition of a specimen is required, homogenates or digestions of a large sample mass can be spread thinly as a powder or evaporated on a suitable backing material.

Sample types: Thin films. Solutions and suspensions (homogenates made in a blender or by sonication) are conveniently prepared for PIXE analysis; a small amount (2-20 μL) is evaporated on a backing material. An advantage in the analysis of liquids is the improvement in accuracy that is obtained by the addition of an internal standard. The hydrophobic nature of most plastic films can cause problems.

Redistribution of the constituents in the sample while drying, or inhomogeneous distribution of the sample on the backing or formation of crystals or precipitates which are thick enough to attenuate the proton beam, can all occur while preparing and drying a liquid sample. Highly concentrated solutions, suspensions and liquids such as blood are prone to deform on backing materials while drying. Many methods for obtaining even distributions of solution residues have been developed. Biological suspensions and solutions have been deposited onto rotating substrates by nebulizing the sample[40], or by using a battery of capillary tubes to deposit a sample onto a backing, followed by freeze-drying to prevent differential migration of the constituents[41], or by rotating a backing material at 18,000 RPM during rapid deposition of an aqueous-ethanol solution[42]. To obtain an even distribution of solution residues, lecithin, insulin, liposomes or EDTA have been used as conditioning additives to reduce crystal size in residues[43].

Blood and related protein rich fluids often adhere poorly to a backing. Use of Nucleopore filter material aids in the adherence of solution residues, although mylar, which is more hydrophobic, contributes 40% less background bremmstrahlung to the spectrum since it is thinner than the Nucleopore filter[44]. In order to render the surface of the

backing film more hydrophilic, treatment with NaOH and a dilute solution of polyvinylpyrrolidone, a surfactant, has been successful[45].

Bulk tissue can be sliced with a microtome after freezing or imbedding the sample, yielding slices 100 μm or less. Tissue prepared in this way has been placed on a backing material and freeze-dried to produce thin targets for PIXE analysis. Much of the research done for this dissertation involved the development of sample preparation techniques for the analysis of raw, unfrozen tissue (see the section on preparation of tissue samples below). The use of unpreserved tissue was necessary due to the need for live cells in the metals uptake study carried out by A. J. Gandolfi and his group in the Department of Toxicology at the University of Arizona. The challenge was to prepare rabbit renal slices in a reproducible manner for analysis by PIXE.

Sample types: thick targets. PIXE penetrates to a limited depth in typical samples; and a thick target therefore, is one in which the beam is stopped, often less than 10 μm inside the target. The characteristic x-rays generated in thick targets are attenuated as they pass out of the matrix of the sample, and the calculated x-ray yields must be corrected for these matrix effects. Utilizing tables of x-

ray absorption coefficients, computer programs can correct for matrix absorption effects, provided information on the composition of the matrix is available.

PIXE has two advantages over XRF in thick target analysis: (1) the process of stopping a proton beam (PIXE) produces less background radiation than the stopping of x-rays (XRF), and (2) since the range of protons in matter is shorter than the range of x-rays, a smaller sample depth is analyzed by PIXE than XRF, so matrix corrections are more intensive for XRF[46].

Thick samples produce more background in the x-ray spectrum, resulting in a lower signal-to-noise ratio than for thin targets and therefore, higher detection limits. Nevertheless, thick samples have been extensively analyzed by PIXE. Samples of human teeth have been analyzed for fluoride distribution by PIXE[47]; the external-beam PIXE technique has been applied in air for the analysis of drill cores[46] and thick tissue samples.[48]

Preconcentration techniques. Many analyses in the literature involve determination of elemental concentrations which are near to or lower than the detection limit of the PIXE technique. Detection limits can often be improved by reducing the mass of the sample, thereby increasing the concentration of analytes in the sample. Tissue samples are

often reduced in mass by lyophilization (freeze-drying), resulting in a reduction in mass by a factor of about five[49], and/or ashing before mounting the powder or the dissolved ashed sample onto a backing or sandwich made of thin plastic film[50], but the throughput of the analytical technique is improved if the sample preparation does not include a digestion step.

Ashing, either by wet methods which employ strong acids or bases and heating in an oven or microwave[51], or by dry methods which oxidize organic material, results in a higher degree of sample mass reduction than lyophilization, and has been commonly used for analysis of biological samples by PIXE. Even though ashing and digestions of biological material often result in mass reductions by factors of 5 to 20, the expected improvement in detection limits is often limited to a factor of 2 or 3 when the sample is dry ashed; the proportionately higher concentrations of low atomic weight elements in the digested sample results in a significant increase in the spectral background[52,53]. Ashing often results in the loss of volatile analytes, and contamination from reagents and sample handling is also possible. The benefits in sensitivity using digestion should be weighed against the possibility of loss of volatile elements, contamination and the expenditure of time required for the preparation of samples[54].

Techniques which give low parts-per-billion (ppb, mass concentration) detection limits for elements in aqueous solution include (1) vacuum evaporation of a 30 mL water sample onto a thin porous film which is analyzed directly[55], (2) use of thin ion-exchange media to adsorb ions in solution, followed by the analysis of the ion-exchange membrane directly[56], (3) the use of a complexing agent such as 8-hydroxyquinoline, which complexes the ions in solution and is extracted into activated carbon and analyzed as a pellet[55], and (4) the analysis of coprecipitated solids, where the ions in solution are coprecipitated with a precipitant such as iron hydroxide, and the solids are pressed into a pellet and analyzed[57]. The application of these analytical techniques must be carefully tested before they can be used routinely for biological solutions, because the high concentration of salts or proteins found in this type of sample often interfere with the sample preparation.

Preparation of tissue samples. When a large mass of tissue sample is available, there is little advantage in analysis of microtome slices; the homogenization or digestion of a larger sample will undoubtably yield results which are more representative of the overall composition of the sample[59]. The ability of PIXE to analyze very small samples, however,

is a real advantage when limited-size samples such as liver biopsies or synovial fluid are to be analyzed, or when experiments provide only one microtomed slice or an epitaxially grown cell specimen for multielemental analysis. In addition, if spatial information is required, the beam size can be reduced and spot-by-spot analysis can be undertaken.

We have found that there are significant advantages of analyzing tissue in thin, desiccated sections sandwiched between two pieces of thin mylar as shown in **Figure 15.** The sandwiched tissue was dried by making a small hole in the sandwiching mylar film and storing the assembled sample in a desiccator overnight. In this study, the lowered detection limits obtained by digestion of the sample were more than offset by the time required for digestion and the possibility of contamination of the sample. The small sample size also prohibited a high degree of preconcentration of analytes. In a search for a fast method for homogenizing small tissue samples, various chemical and enzymatic digestion agents were added to rabbit kidney slices and the samples sonicated. The addition of even 0.5 mL of reagent or solvent to a 0.1 g kidney section resulted in a dilution of the sample; even if all the material was redeposited and evaporated on a backing, the resulting sample target is similar to the original section, although a

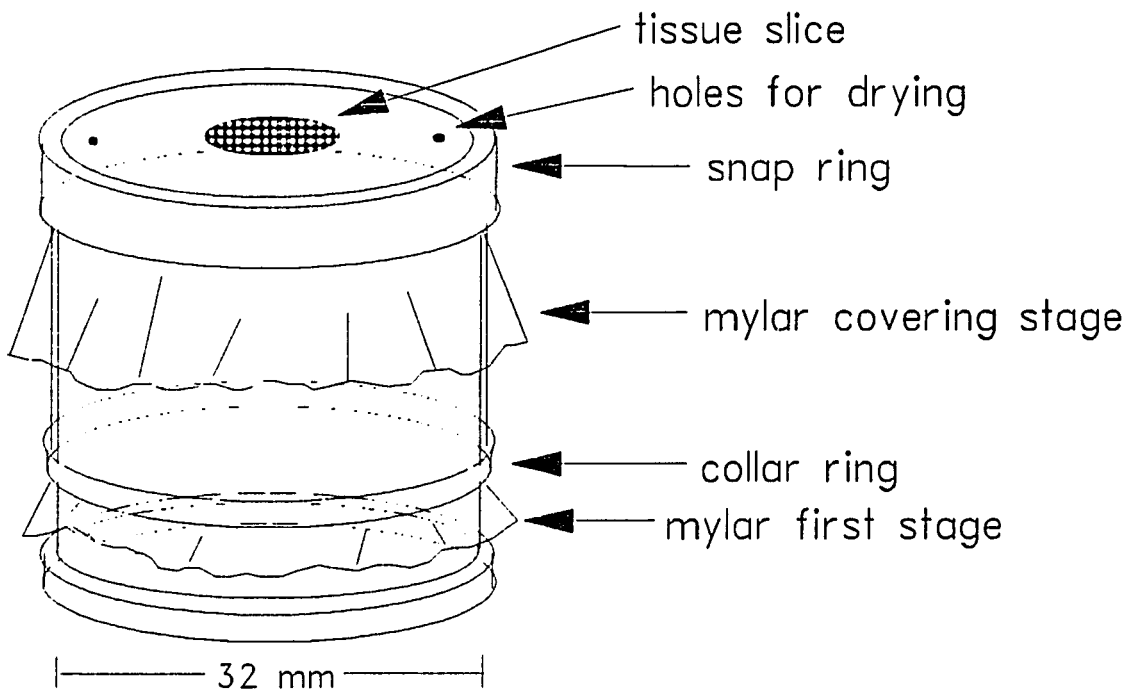

Figure 15. Sandwich assembly for mounting tissue slices.

more homogenous target could be produced in this manner. Possible advantages of homogenization include the ability to employ an internal standard and to obtain results which reflect the bulk composition of the sample. A single tissue slice prepared as a sandwich is relatively easy to prepare and analyze. Care must be taken in quantitation, however, because the use of internal standards is precluded by this method of sample preparation, and use of the instrumental fundamental parameters is required. The reproducability in the analysis of similar specimens was also found to be aided by drying the tissue slice after sandwiching; the surface uniformity and retention of original sample area obtained by sandwiching are factors that improve reproducability. A PIXE spectrum of a rabbit kidney slice prepared by the mylar sandwich technique is shown in **Figure 16**. Jundt, et al.[58] compared the preparation of tissue by 1) slicing frozen tissue, 2) slicing tissue while embedded in paraffin and 3) preparing tissue as a homogenate. The slices or homogenate were placed on a Formvar (polystyrene) backing material and were desiccated. They found that the frozen sections were easiest to prepare, forming films as thin as 100 $\mu g/cm^2$, and fewer analytes were lost than in the preparation of paraffin-embedded or homogenized specimens. In the study metal uptake by rabbit kidney slices, the microtomed slices were not frozen before sandwiching, since the study required

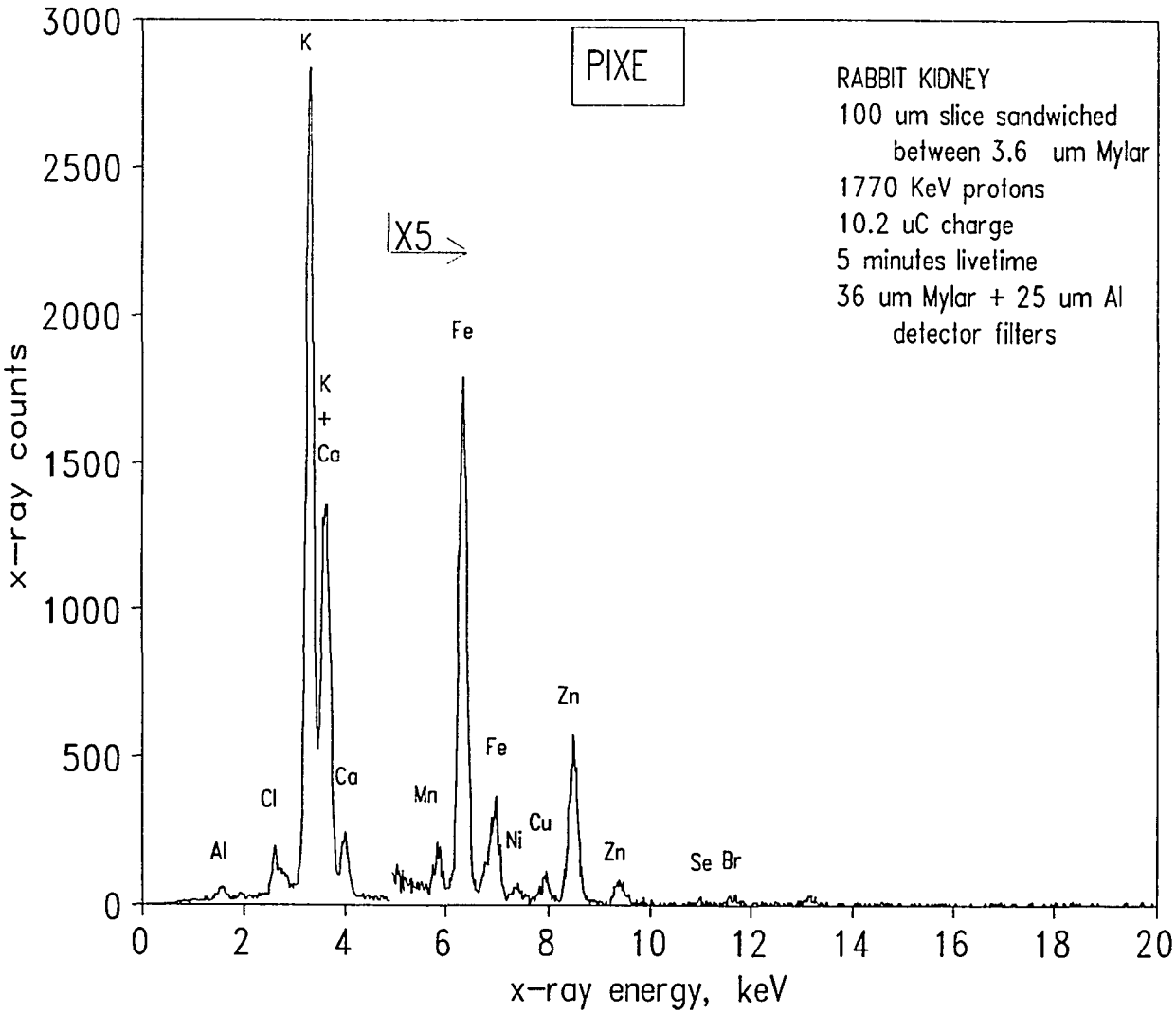

Figure 16. PIXE spectrum of a rabbit renal slice.

in vitro measurement of metal uptake by the kidney cells. It was found, however, that the technique of mounting the raw tissue slice produced reproducible results, and that if the prepared sandwiched tissue slices were frozen overnight prior to drying, the samples were more homogeneous than if the sandwiched slices were dried without first freezing them.

Backing materials. Thin specimens for PIXE analysis require an appropriate support. The support ideal would be a thin film composed of low atomic number elements that is sufficiently pure and thin that it does not contribute x-rays to the emission spectrum. Many proprietary backing materials are available to the PIXE analyst, who must decide which material would be most practical to use in an analysis. Reviews of the available backing materials are given by Campbell[59] or Russell[60]. Although they are good electrical insulators, thin plastic films are desirable supports for samples, since they are made of light elements and will not contribute much background bremmstrahlung to the spectrum. Plastic films also contain only small amounts of contaminating elements which are detected by PIXE. The thinnest backings are formed by dropping a solution of a polymer onto the surface of pure water and then picked up from the water with a frame. Thin films give

a low background, but are fragile, and should be used when the maximum sensitivity is required. Formvar (Shawinigan Products, Corp.) polystyrene film is quite pure and shows little spectral background contribution, but is so fragile that a drop of concentrated solution can disrupt the film when it dries. Formvar also does not conduct heat well, and therefore low beam currents must be used. Formvar has been successfully used in the analysis of tissue sections[58], and is one of the more common thin-film supports used in PIXE analysis. Carbon foils, available commercially on glass plates, are floated off the glass in water and picked up on a frame. They are stronger and dissipate heat well and are beam-resistant. Carbon foils, however, are expensive, and like Formvar, require careful preparation and handling.

If some background (and higher detection limits) can be tolerated, then a host of thicker polymer films are available. These films are made of polyamide, polyester, polycarbonate or polypropylene, and are sold under various tradenames. The films are available in thicknesses varying from 1.5-7.6 μm, and contain varying amounts of contaminants, mostly Ca, Fe, Cu and Zn[61]. They are durable, and generally withstand the effects of the proton beam well. Currently, Kapton (polyamide, DuPont) and mylar (polyester, DuPont) are the most commonly used commercially available support because they are free of contamination and

can be made into durable, thin supports. Polycarbonate films like Kimfol (Kimberly-Clark) are considered a desirable backing material[62], because they are thin and free of high levels of contaminants. In all cases where a backing film is used, a blank spectrum should be taken of the backing material alone, to subtract the elemental contributions from the film. **Table V** summarizes a few of the properties of some of the available polymer films.

Adhesives for mounting tissue sections. Samples on thin film backings (especially the more hydrophobic plastic film backings) often separate from the backing or crack while drying, or while under vacuum during analysis. Therefore, it is sometimes necessary to secure the sample to the backing using a wetting agent or an adhesive, or to use a covering film which sandwiches the sample and prevents it from shifting. Several researchers have used a low molecular weight polystyrene in toluene (100:1) as a glue for the fixation of powdered lyophilized or ashed samples to a backing[63] and blood serum to 6 μm polyester backings[64]. Zapon, a commercially available glue, has also been used for this purpose[65]. The direct analysis of powders is less preferable to the analysis of a solution residue, because of particle size effects and inhomogeneity of the powder film.

	mg/cm^2	ADVANTAGES	DISADVANTAGES
Kapton (polyimide)	1.08	high beam resistance low contamination	low transmission of low-energy x-rays
mylar	0.88-1.06	fair beam resistance inexpensive	contaminants at 5-500 ppm.
Formvar	0.01-0.15	thin high purity	fragile, poor heat conductor
carbon	0.02-0.04	good heat conductor low background	variable purity expensive
Nucleopore (8μ pores)		liquid samples adhere well	relatively thick
polycarbonate (Kimfol)	0.24	thin	poor chemical resistance

Table V. Properties of some available backing materials.

In our preparations of kidney tissue sections, we have tried several wetting agents, including ethylene glycol, Triton X-100 (a non-ionic surfactant, Kodak) and glycerol. When ethylene glycol was used, the tissue slices fell off the mylar backing material. A large amount of Triton X-100 was required to be effective. The use of glycerol with the kidney slices resulted in a non-uniform surface texture and sample thickness. The use of adhesives and other reagents in sample preparation is a recognized source of contamination.

ANALYSIS OF RENAL TISSUE SLICES

Experimental. Microtomed rabbit kidney sections were prepared by coring the organ with a 6 mm corer, followed by production of 250 μm sections with a precision microtome. The slices were incubated in a buffered solution for varying periods of time, while being exposed to 10^{-6} - 10^{-3} M concentrations of Cr, As, Cd and/or Hg. Experiments varying the concentrations of the four metals individually and in combination were conducted. After incubation, each slice was removed from the incubator, rinsed briefly in distilled, deionized water, and was placed on a 3.6 μm mylar film stretched across a 32 mm double open-ended XRF sample cup (Chemplex Industries, Tuckahoe, New York, NY). The XRF sample cups were designed with a retaining collar which conveniently held the first stage of the mylar sandwich while the kidney slice was positioned. A second piece of mylar film was placed over the slice, and a snap-on retaining ring pulled the entire assembly taut. Two small holes were then made near the edge of the mylar in order to allow the slice to dry, and the sample was desiccated overnight under vacuum. The desiccated samples were found to be 2-5 μm thick, measured from five typical desiccated kidney samples. (The differences in thickness of the sample

reflect the uncertainties observed in the quantitation of trace elements in the tissue).

The prepared samples were attached to the 10 place sample assembly in batches of 8, with a standard consisting of 0.941 ng/cm^2 (areal density, from RBS) copper on a carbon substrate in position 1, and a heat resistant quartz glass with a mark for centering the sample wheel in position 10. The copper standard was analyzed before and after each set of samples.

Proton beam currents of 100-200 nA were used to deposit 5-18 μCoulombs of charge on approximately a 4 mm x 4 mm area of the Kidney slices during livetimes of 5 minutes.

Assessment of the charge deposited on the sample was calculated from the intensity of the cobalt peak in the RBS spectrum obtained from a surface barrier detector positioned to measure protons back-scattered from the cobalt-coated Kapton window through which the beam was passed into the target chamber.

The PIXE spectrum for each run was stored on computer disk for off-line spectrum processing and quantitation using the GUPIX spectrum processing software. A RBS spectrum was acquired and stored on disk for each PIXE analysis in order to calculate the total charge deposited on each sample.

After the completion of each set of samples, visual inspection was carried out on each sample, and notations concerning the effect of the beam, such as cracking, discoloration and off center sample positioning were noted in the sample logbook. Results of the GUPIX program were reported as areal concentrations in units of ng/cm^2, without uncertainties or limits of detection, with the understanding that these important results would be summarized in a more general fashion in a separate report.

Quality assurance of the PIXE system for the analysis of tissue slices was conducted by repetitive measurement of a single sample for each set of ca. 40 samples in each experiment. Detection limits and instrumental uncertainties were calculated by the GUPIX program (**Figures 12 and 13**) and the overall precision of the technique was determined from measurement of replicate samples prepared in the same manner from the same tissue specimen. Accuracy of the technique was measured by using thin metal film standards whose thickness had been measured to within 3% by RBS.

Kidney slice results. Results of the analysis of 35 rabbit kidney slice controls from 9 experiments are shown in **Table VI**. A detector filter consisting of 25 μm aluminum and 32 μm mylar was used in the analysis to attenuate the intense low Z element x-rays. The % transmission of x-rays

	avg conc. ± ng/cm^2	ng/cm^2	conc. ppm	% STD DEV (overall)	Statistical error,%	<-ng/cm^2-> Limit of Detection	blank conc.
K	24376	3116	4193	12.8	0.60	79.0	<45
Ca	3571	476	614	13.3	1.87	133	1805
Cr	12.3	9.14	2.12	74.1	60.67	4.40	<2.4
Mn	28.1	2.98	8.83	10.6	9.12	4.17	<1.8
Fe	462	53.6	79.5	11.6	1.54	4.32	6.07
Co	21.9	2.22	3.77	10.1	20.88	9.54	20.5
Ni	13.4	4.88	2.30	34.5	17.45	2.95	13.4
Cu	42.3	4.12	7.27	10.2	7.67	2.93	<1.9
Zn	284	10.5	48.8	3.7	2.74	4.29	23.7
Se	17.6	4.33	3.04	27.5	24.91	6.46	<3.1
Br	17.2	2.95	2.95	32.1	30.67	7.82	<4.2

Table VI. Results of the PIXE analysis of 35 control rabbit kidney slice samples. 7-10 μC was deposited during 5 minutes detector livetime. 25 μm Al and 44 μm mylar detector filters were used.

through the filter ranged from 0.95% for K K_α x-rays to 48.4% for Fe K_α, to 88.9% for Br K_α emissions, calculated by the GUPIX computer program (see **Figure 6**). Uncertainties in the filter transmission are magnified when the transmission of x-rays is low. The uncertainty in concentration was calculated from the average of the standard deviation of replicate samples, which were prepared from a single core sample, averaged over the 9 experiments. The detection limits reported were calculated from measurement of the background at the region of the spectrum under the analytical peak. The statistical errors were calculated from the counting statistics by the GUPIX computer program, and are approximately equal to the inverse of the square root of the counts in the spectral peak. Large uncertainties are expected for small peak areas, and the comparison of statistical error and average standard deviation gives a measure of the statistical error contribution to the overall uncertainty. Cobalt determined in the analysis is a result of the use of the cobalt-coated window, and is thought to be due to Compton scattering of the characteristic cobalt x-rays emanating from the window.

Preliminary results from the analysis of the metal-treated kidney slices showed significant inter-elemental effects between the various biological elements and toxicants when used in combination and provided information

on the rate at which toxic metals are taken up by kidney tissue[9].

Loss of mercury during the analysis. Loss of mercury from the samples that contained mercury was observed during consecutive analysis of the same sample. The loss of mercury is demonstrated in **Figure 17**, which plots the concentration of mercury versus the time the sample was exposed to the proton beam. The experiment was conducted under typical conditions used in the routine analysis of tissue slices. While the loss appears to follow an exponential curve, less than 10% of the mercury is lost if the sample is analyzed during the first five minutes of exposure to the beam. Iron was analyzed concurrently with mercury, and since the concentration of iron remained constant, shows that iron is not volatilized and that the loss of mercury is not due to changes in the sample or instrument. In order to minimize changes in the sample preparation, the analysis of mercury-containing samples was done during the first few minutes after the sample was placed in the beam. An alternative to simply reducing the analysis time to prevent loss of mercury is to convert the mercury to the sulfide, which is more stable under the influence of the proton beam, by treatment of the tissue slice with H_2S gas, but the extra sample preparation step would make the process more lengthy.

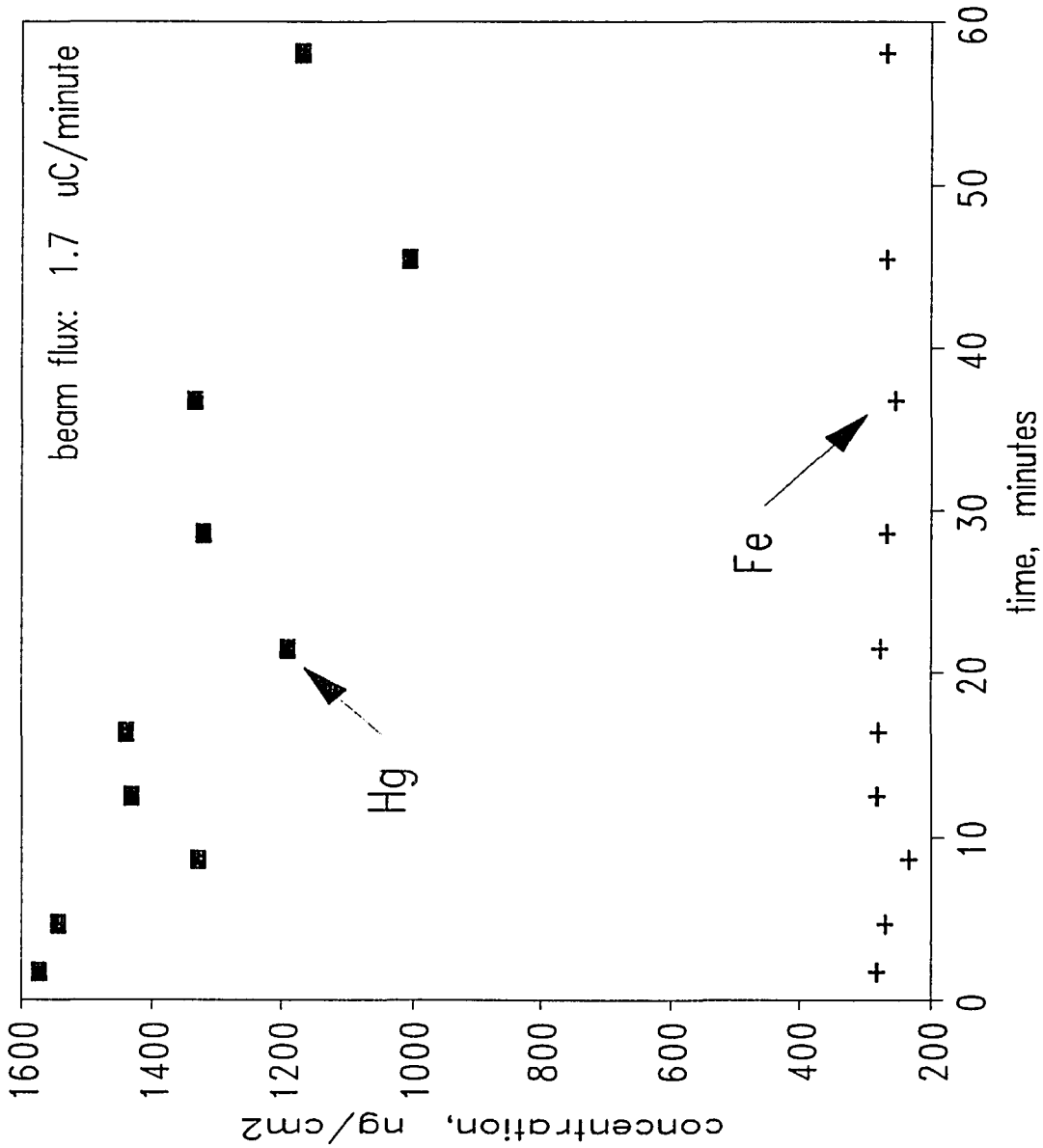

Figure 17. Results of the repetitive analysis of a mercury-treated kidney slice.

SUMMARY

PIXE analysis of biological specimens provides a means for obtaining major and trace element concentrations from a single analysis. This ability to quantitate a large number of elements in a single small sample with the high sensitivities typical of PIXE cannot be found in other techniques, although some methods for single element analysis can provide lower detection limits and/or higher accuracy. PIXE, however, is virtually the only method for multielemental analysis of a small unique sample which has insufficient material for other, more conventional analytical techniques.

PIXE has seen rapid growth in the analysis of biological specimens, and while the instrumentation and spectrum processing hardware and software have developed steadily since the early days of PIXE, sample preparation remains something of an art, requiring innovative techniques to prepare thin, reproducible targets. In practice, each sample type requires the development of a unique approach to sample preparation. The many publications concerning the analysis of diverse biological samples attest to the fact that PIXE is a successful technique in the analysis of biological systems. In studies on the uptake of toxic metals by rabbit kidney tissue at the University of Arizona, PIXE has provided results which have been pivotal in the

understanding of inter-element effects in these uptake studies. The high sensitivity and throughput of the University of Arizona instrument has provided data on over 4000 samples in the rabbit kidney project, and similar methods are being developed for the analysis of liver, brain, epitaxial cell, and blood samples.

APPENDIX A

Sample of the Output of the GUPIX Computer Program

```
***  GUPIX - Guelph Thin/Thick Target PIXE Program ***
                Version Date (y-m-d)  92-01-29

Time: 13:12:56                *** Results ***            Date (y-m-d): 92-06-02

File:g:as15d.484                    ID:                                Type:Ascii
Chi**2= 0.29432          Total # of counts:    8520.    %RMS sys error= 0.000
Total # of loops:   5                    Total fit time:   82.7 seconds.
Fit region has  991 chan (  10 to 1000).  File has 1024 chan with offset    1
Case: Thin PIXE      Aquisition date,time(80- 1- 0 @  0: 0) Duration:      0s.
    (Trace)     Average count rate(cps):     0.0   Average current(nA):   0.000
H: 7.764E-03                          Angle(Beam-Target normal) Alpha=  0
Charge: 3.410E+00                          (Detector- "    "  ) Theta= 45
Proton energy (keV):1700
Looking for 26 elmts:  Al K , Na K , Mg K , Si K , P  K , S  K , Cl K , Ar K ,
  K  K , Ca K , Sc K , Ti K , V  K , Cr K , Mn K , Fe K , Co K , Ni K , Cu K ,
  Zn K , Ga K , Ge K , As K , Se K , Br K , Hg L
Filters (Z,um):           (Mylar Z=100 etc.)  Fractional absorber error:0.000
 ( 13,   25.0)  (100,   44.0)
Detector efficiency correction of relative intensities: On
Det #,Be,Au,Si,Distance(cm):  1, 2.03E-03, 2.00E-06, 0.470,  4.50
Ag/At pars: 3.000  0.0000  0.0000  47914.  Deadtime(us): 25.0
1st is energy cutoff (if <0 then 2nd is Si dead layer thickness)
Det ID: XRF Det

        Peak and spectrum description:
Peak centroid = A1+A2*E+A3*E**2              A(1,2,3):    2.337   50.252 -0.0208
Peak width = SQRT(A4+A5*E)                     A(4,5):   6.8870   1.2010
With these values the fit region extends from   0.15 to  20.02 keV with FWHM
at center being  205.8 eV or 10.26 channels.  Excluding pile-up & escape the
elements have peaks ranging from   1.041 to  14.769 keV.

Background handled by digital filter (m-n-m): ( 5-10- 5)
Peak plateau: None.
Short step: None.
Peak tailing: None.
Matrix abs. edges: None.
Si escape peak energy in keV (if 0, then no escape used): 1.752
Pile-up [99(PU S )] peaks - #allowed: 50,  #used: 15

Stopping criteria: STEP:0.0010    LOOPS:  20
Total # of pars., fixed pars. & their IDs: (32,13)  7, 8, 9,10,11,13,17,18,26,
    27,29,31,32
################################################################################
 Note: ID/n,  n:(-2:filter, -1:surface, n:layer number)
 #    ID      FINAL VALUE   INIT. VALUE     ERROR      %ERROR LAST CHANGE  %CHANGE
 -    --      -----------   -----------     -----      ------ -----------  -------
 1              2.33691       3.00000     1.118E-02     0.48   1.686E-05     0.00
 2              50.2524       50.0000     1.992E-03     0.00  -1.174E-05     0.00
 3             -2.078333E-02  0.000000    2.472E-04    -1.19  -2.753E-06     0.01
 4              6.88698       8.00000     0.111         1.61  -6.939E-04    -0.01
 5              1.20104       1.00000     1.781E-02     1.48  -9.368E-05    -0.01
 6 Al K /-2     6.28310       10.0000     0.279         4.44  -3.878E-03    -0.06
 7 Na K / 0    0.000000       10.0000     0.618         0.00   0.000         0.00
 8 Mg K / 0    0.000000       10.0000     0.611         0.00   0.000         0.00
 9 Si K / 0    0.000000       10.0000     0.542         0.00   0.000         0.00
10 P  K / 0    0.000000       10.0000     0.631         0.00   0.000         0.00
11 S  K / 0    0.000000       10.0000     0.751         0.00   0.000         0.00
12 Cl K / 0     6.83807       10.0000     0.388         5.68   6.751E-03     0.10
```

13	Ar	K / 0	0.000000	10.0000	0.857	0.00	0.000	0.00
14	K	K / 0	160.072	411.000	1.13	0.71	1.109E-04	0.00
15	Ca	K / 0	179.399	172.000	1.23	0.69	1.488E-03	0.00
16	Sc	K / 0	3.97169	21.0000	0.547	13.78	8.249E-03	0.21
17	Ti	K / 0	0.000000	11.0000	0.652	0.00	0.000	0.00
18	V	K / 0	0.000000	10.0000	0.554	0.00	0.000	0.00
19	Cr	K / 0	2.34244	10.0000	0.258	11.02	-4.795E-03	-0.20
20	Mn	K / 0	6.85673	10.0000	0.319	4.65	-1.212E-04	0.00
21	Fe	K / 0	113.673	136.000	0.816	0.72	1.462E-04	0.00
22	Co	K / 0	8.65539	19.0000	0.431	4.97	2.394E-03	0.03
23	Ni	K / 0	2.75372	10.0000	0.172	6.24	5.377E-05	0.00
24	Cu	K / 0	4.89135	11.0000	0.180	3.68	-2.105E-04	0.00
25	Zn	K / 0	18.2208	39.0000	0.296	1.63	-1.074E-03	-0.01
26	Ga	K / 0	0.000000	10.0000	0.360	0.00	0.000	0.00
27	Ge	K / 0	0.000000	10.0000	0.360	0.00	0.000	0.00
28	As	K / 0	50.2900	27.0000	0.451	0.90	2.660E-03	0.01
29	Se	K / 0	0.000000	10.0000	0.361	0.00	0.000	0.00
30	Br	K / 0	2.00141	10.0000	0.182	9.10	-5.216E-03	-0.26
31	Hg	L / 0	0.000000	10.0000	0.476	0.00	0.000	0.00
32	PU	S / 0	0.000000	10.0000	1.00	0.00	0.000	0.00

##########

#	Element Z	Sym.	Peak Area	2-FWHM Area	% Fit Error	% Stat. Error	+1% Of Overlap	Limit of Detection
1:	13	Al K /-2	46.	46.	4.49	24.36	24.61	12.9
2:	11	Na K / 0	0.	0.	0.00	0.00	0.00	10.9
3:	12	Mg K / 0	0.	0.	0.00	0.00	0.00	7.2
4:	14	Si K / 0	0.	0.	0.00	0.00	0.00	12.7
5:	15	P K / 0	0.	0.	0.00	0.00	0.00	11.9
6:	16	S K / 0	0.	0.	0.00	0.00	0.00	11.2
7:	17	Cl K / 0	54.	60.	5.71	21.63	21.63	8.6
8:	18	Ar K / 0	0.	0.	0.00	0.00	0.00	23.6
9:	19	K K / 0	1323.	1327.	0.91	3.12	3.12	14.2
10:	20	Ca K / 0	1513.	1498.	0.89	3.36	3.59	50.2
11:	21	Sc K / 0	34.	33.	13.79	87.02	97.88	59.2
12:	22	Ti K / 0	0.	0.	0.00	0.00	0.00	25.0
13:	23	V K / 0	0.	0.	0.00	0.00	0.00	19.7
14:	24	Cr K / 0	21.	20.	11.03	58.67	58.67	16.0
15:	25	Mn K / 0	64.	63.	4.68	22.60	22.60	8.6
16:	26	Fe K / 0	1088.	1074.	0.90	3.40	3.40	17.1
17:	27	Co K / 0	85.	83.	5.00	22.87	24.46	28.0
18:	28	Ni K / 0	27.	36.	6.26	27.97	28.15	11.9
19:	29	Cu K / 0	50.	71.	3.72	16.24	16.24	8.1
20:	30	Zn K / 0	190.	282.	1.72	7.60	7.60	14.6
21:	31	Ga K / 0	0.	0.	0.00	0.00	0.00	5.5
22:	32	Ge K / 0	0.	0.	0.00	0.00	0.00	7.5
23:	33	As K / 0	557.	830.	1.06	3.87	3.87	13.9
24:	34	Se K / 0	0.	0.	0.00	0.00	0.00	7.1
25:	35	Br K / 0	23.	26.	9.12	50.88	53.89	19.0
26:	80	Hg L / 0	0.	0.	0.00	0.00	0.00	6.7

##########

File:g:as15d.484 Sec: 0. uC: 3.410 nA: 0.000 PUcor:1.0000

The last column is a decision on the presence of that element in the spectrum.
Y: present at level of quantization, N: not present at limit of detection
?: may be present at or near LOD levels (user must decide)

Element Z	Sym	Layer #	Area counts	H value (-5)	Yield /uC/ ng/cm2	Det. Eff. (-3)	Filter Trans. (-5)	Conc. (ng/cm2)	Error (ng/cm2)	% Error	LOD (ng/cm2)	
11	NaK	0	0	776	17435	113	0	0.0	0.0	0.00	999999.0	N

12	MgK	0	0	776	14300	280	0	0.0	0.0	0.00	106781.5	N
14	SiK	0	0	776	8641	613	0	0.0	0.0	0.00	999999.0	N
15	P K	0	0	776	6413	717	0	0.0	0.0	0.00	999999.0	N
16	S K	0	0	776	5019	752	0	0.0	0.0	0.00	36250.7	N
17	ClK	0	54	776	3642	802	15	4760.3	1029.5	21.63	996.5	Y
18	ArK	0	0	776	2571	838	174	0.0	0.0	0.00	313.9	N
19	K K	0	1323	776	2096	796	953	3145.7	98.1	3.12	44.3	Y
20	CaK	0	1513	776	1630	839	3149	1326.2	47.6	3.59	57.9	Y
21	ScK	0	34	776	1157	874	7421	17.2	16.8	97.88	39.2	N
22	TiK	0	0	776	862	901	13848	0.0	0.0	0.00	11.5	N
23	V K	0	0	776	641	921	21925	0.0	0.0	0.00	7.5	N
24	CrK	0	21	776	496	937	30842	5.7	3.3	58.67	5.5	?
25	MnK	0	64	776	369	949	39813	17.4	3.9	22.60	3.1	Y
26	FeK	0	1088	776	285	958	48352	310.6	10.6	3.40	6.4	Y
27	CoK	0	85	776	213	966	56097	27.7	6.8	24.46	12.1	?
28	NiK	0	27	776	111	972	62978	15.4	4.3	28.15	5.8	?
29	CuK	0	50	776	80	977	68852	35.1	5.7	16.24	5.0	Y
30	ZnK	0	190	776	61	980	73843	163.2	12.4	7.60	11.0	Y
31	GaK	0	0	776	44	984	78033	0.0	0.0	0.00	5.4	N
32	GeK	0	0	776	33	986	81555	0.0	0.0	0.00	9.3	N
33	AsK	0	557	776	25	988	84476	1005.4	38.9	3.87	22.2	Y
34	SeK	0	0	776	19	990	86905	0.0	0.0	0.00	14.9	N
35	BrK	0	23	776	14	977	88925	70.0	37.7	53.89	50.9	?
80	HgL	0	0	776	14	986	82050	0.0	0.0	0.00	27.1	N

##########

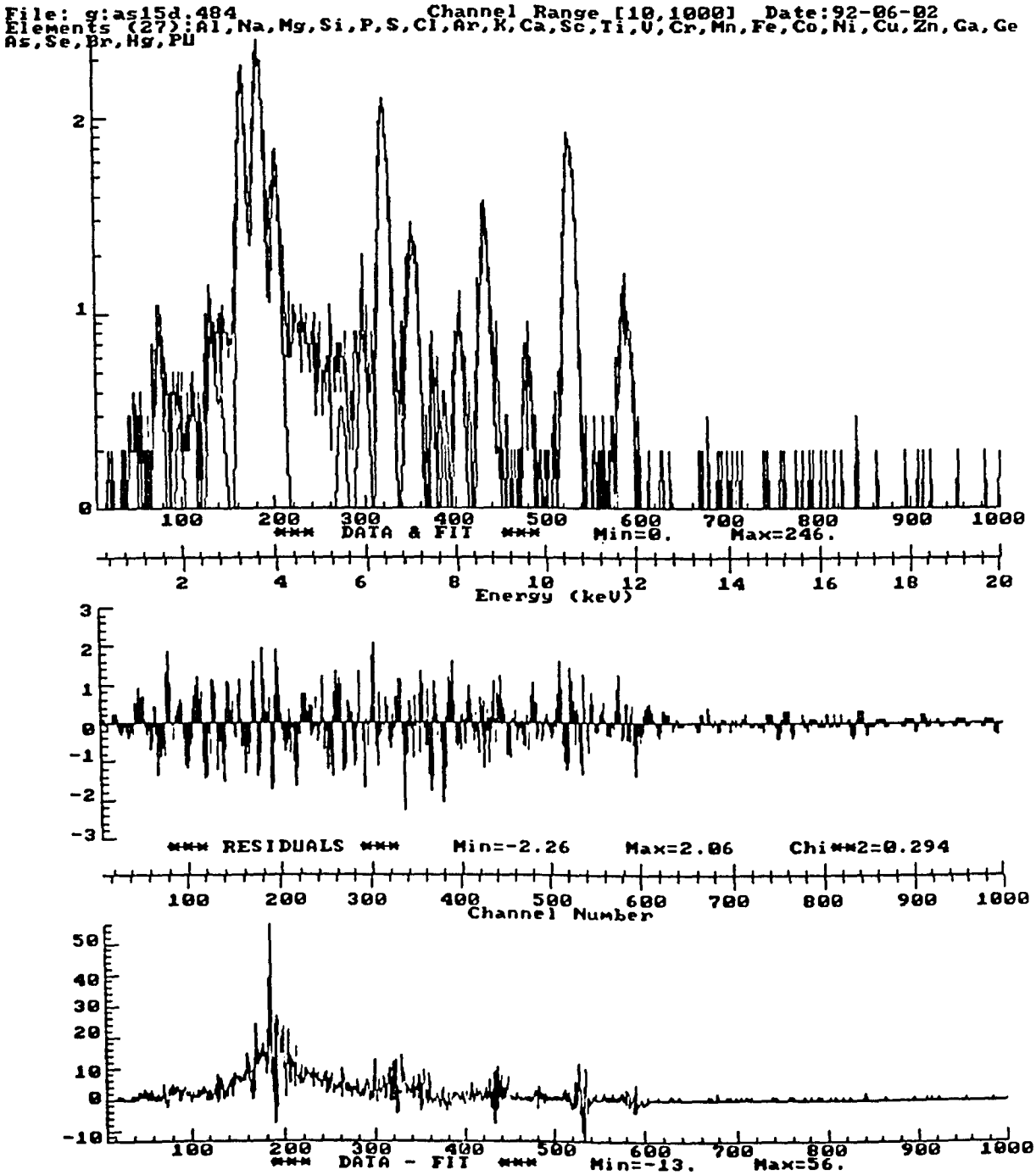
File: g:as15d.484 Channel Range [10,1000] Date:92-06-02
Elements (27):Al,Na,Mg,Si,P,S,Cl,Ar,K,Ca,Sc,Ti,V,Cr,Mn,Fe,Co,Ni,Cu,Zn,Ga,Ge
As,Se,Br,Hg,PU
*** DATA & FIT *** Min=0. Max=246.
Energy (keV)
*** RESIDUALS *** Min=-2.26 Max=2.06 Chi**2=0.294
Channel Number
*** DATA - FIT *** Min=-13. Max=56.

APPENDIX B

Experimental Comparison of PIXE and EDXRF

APPENDIX B

Experimental Comparison of PIXE and EDXRF

The use of the x-ray detection system from a commercial XRF instrument for PIXE analysis, while retaining the ability to use the XRF in its original configuration allows the direct comparison of the two techniques at the University of Arizona. The Mono-energetic (proton) excitation used in PIXE analysis allows the use of fundamental parameters of the system for quantitation, while quantitation in EDXRF is almost always carried out with the use of standard curves, because of the multiple-wavelength excitation and stability of the x-ray tube source. As explained in the body of this dissertation, PIXE is inherently a more sensitive analytical technique than XRF, with detection limits in the range of 10-100 times lower than those attained by EDXRF.

In the U. of Az. laboratory, the advantages of PIXE over XRF are somewhat offset by the longer detector-sample distance in the PIXE instrument; the repositioned sample wheel in the PIXE target chamber places the sample at 4.5 cm from the detector while the detector is only about 2 cm from the sample in the EDXRF configuration. The inverse square law dictates a ca. two-fold reduction in intensity for PIXE analyses in the present instrument, given the same sample x-

ray emission intensity. However, the reduction in x-ray intensity at the detector for PIXE compared to XRF is more than offset by the reduction in the intensity of the background in the PIXE analysis.

The ability of high-energy protons to excite all elements in the sample simultaneously gives PIXE the ability to quantitate all analytes in one run, while XRF must employ different source filters and multiple runs to optimize the entire range of detectable x-ray energies.

Table VII compares the results of the analysis of kidney slice samples that had been exposed to two different concentrations of chromium, mercury and arsenic, analyzed by PIXE and XRF. The samples were prepared by the mylar sandwich technique described in the body of this dissertation. Instrumental conditions in each system were designed to optimize the detection of most important elements in the samples.

The reported units for PIXE and XRF reflect the mode of quantitation for each technique. PIXE analysis uses a beam smaller than the sample diameter, along with an instrumental calibration standard calibrated in areal density (ng/cm^2), so an area smaller than the actual sample is analyzed. Quantitation for the EDXRF analysis used a calibration curve produced by standard addition of known amounts of each analyte to a separate tissue slice. While the PIXE analysis

SAMPLE	PIXE ng/cm2	XRF ug/sample	comments	PIXE/XRF ratio
hi Cr 12	5108	14.05		364
hi Cr 4	3074	12.16		253
lo Cr 12	1714	5.3		323
lo Cr 4	626.7	2.73		230
hi Hg 12	16629	26.92	above XRF cal. curve	618
hi Hg 4	33306	33.26	above XRF cal. curve	1001
lo Hg 12	2117	1.39		1523
lo Hg 4	788.2	0.56		1408
hi As 12	399	0.32		1247
hi As 4	407	0.37		1100
lo As 12	52.3	0.04	below XRF det. limits	1308
lo As 4	0	0.02	below XRF det. limits	0

Table VII. Results of the analysis of rabbit kidney slices by PIXE and EDXRF.

provided quantitative results for all the elements in the sample (above atomic number 20), calibration curves for only the three elements of interest were developed for the EDXRF analysis, due to the difficulties encountered in the preparation of multi-elemental tissue slice standards for the EDXRF analysis. Error for both analyses is estimated at 10%, based on previous analyses of tissue slices. The discrepancies in the ratio of PIXE to XRF results are due to differences in sample thickness and possibly an error in standard preparation.

The differences between PIXE and XRF can be seen qualitatively in **Figures 18 and 19.** The NIST standard reference material, bovine liver, was prepared for analysis by adhering a small amount of powder to a thin Kapton film stretched across a XRF sample cup with cellulose glue. The same sample was analyzed by each method, with EDXRF instrumental conditions optimized for the detection of the transition element K emission lines and L lines for heavy atomic number elements.

The PIXE spectrum shows a low background, with the range of peak heights over background including peaks of 140,000 to less than 10 counts in the same spectrum. The background appears at the low energy end of the spectrum (due to bremmstrahlung effects), and all peaks can be reasonably quantitated with the GUPIX spectrum processing

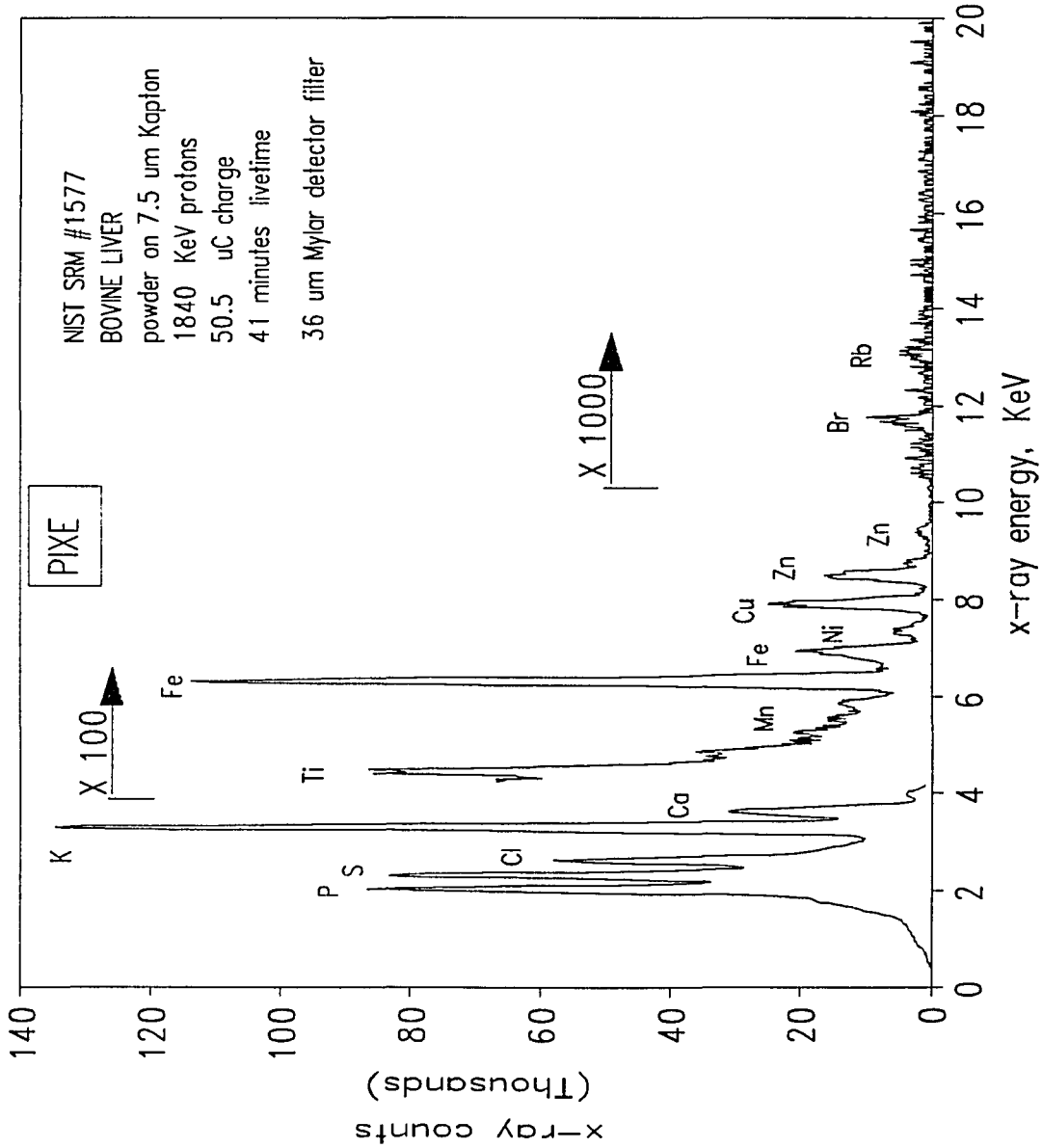

Figure 18. PIXE spectrum of bovine liver powder.

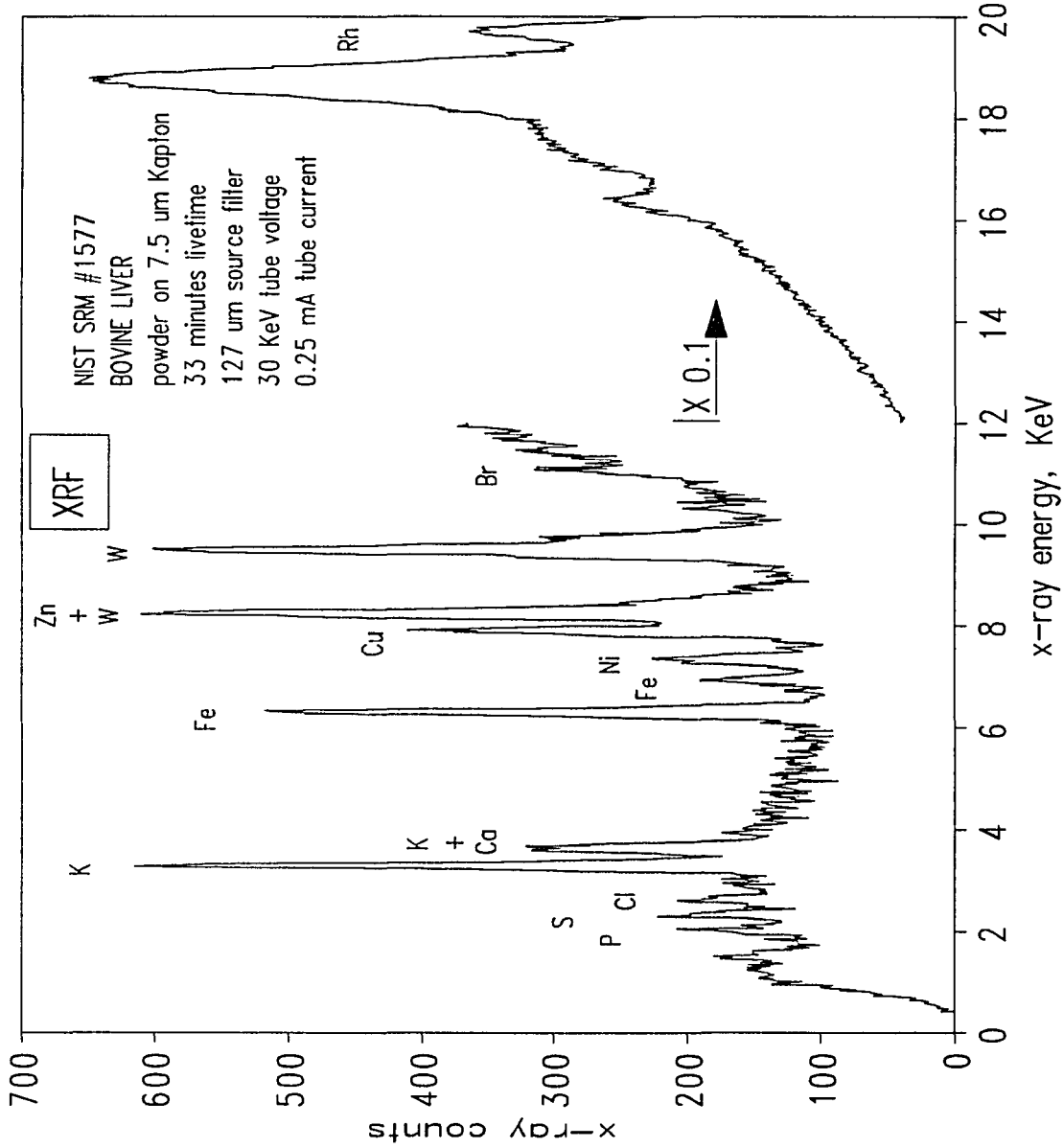

Figure 19. EDXRF spectrum of bovine liver powder.

software. In addition, trace elements are visible in the PIXE spectrum which are absent in the XRF spectrum.

The EDXRF spectrum shows a higher background at all energies than the PIXE spectrum due to the use of an x-ray tube source, with the background especially prominent at the high and low ends of the spectrum. Although the instrumental parameters were optimized for the detection of the transition elements, the signal-to-noise for some important trace elements (i.e. nickel) is only around two in this spectrum. Clearly, if the analysis of phosphorus, sulfur, chlorine, potassium or calcium was to be undertaken by EDXRF, another set of excitation and detection parameters would have to be employed, necessitating another run and more time expended in the analysis. Overlap of x-ray emission lines from the instrument, including tungsten (W) and rhodium from the electron source and target in the x-ray tube can be seen to interfere with elements in the sample. A the high energy end of the spectrum, spectral contributions from the rhodium target in the tube, along with Compton scattering of the rhodium x-ray line are the primary sources of irradiation for the sample.

The sample size was small (<2 mg of powder), and the sensitivity of the EDXRF analysis could be improved by the use of a thicker sample, but this observation only serves to

emphasize another advantage of PIXE over XRF; PIXE requires a much smaller sample size than XRF.

II. SEPARATION AND PURITY OF C_{60} AND C_{70}

SEPARATION AND PURITY OF C_{60} AND C_{70}

INTRODUCTION

Following the report of the first macroscopic synthesis of Buckminsterfullerenes ("fullerenes", including C_{60}, C_{70} and higher molecular weight fullerenes)[66], much attention has been given to their chemistry and physical properties, with comparatively little research devoted to the production, separation and purity determination of the various fullerenes. This section of the dissertation describes a process for production of several grades of fullerene products, and evaluates several analytical techniques commonly employed for the determination of the purity of a C_{60} or C_{70} fullerene sample.

Fullerene production considerations. In a typical production scheme graphitic soot is produced by vaporizing graphite rods by resistive heating, arcing or plasma, in an environment of low pressure inert gas. Yields of the various fullerenes from the soot vary widely with the method of soot production[67] and atmospheric conditions within the soot generator[68].

The soot is scraped from the walls of the generator and extracted into toluene or benzene, in which fullerenes are

soluble to the extent of ca. 3-5 mg per ml. The solvent is generally removed by use of a rotary evaporator[69], or by evaporation in a teflon-lined pan[70]. In most reports, no mention is made of the difficulties that may have been encountered in the recovery of the solids from solution, such as the solid fullerenes adhering to the glass walls of the rotary evaporator or contamination of the product during drying and scraping of teflon pans or vessels. The fullerenes also adsorb solvent so strongly that the last traces of the toluene can only be removed by heating in a vacuum oven[5]. It should be noted that the product also contains all extractable material present in the initial soot[66]. The large scale production of C_{60} and C_{70}, is seriously hampered by the highly adsorptive properties of the surface-active fullerenes, and by the presence of unwanted material in the product.

Due to similar chemical properties, the various species of fullerenes are difficult to separate. Small quantities of the pure materials have been produced by chromatographic separation by HPLC on phenylglycine-based "Pirkle" columns[71], alumina packed columns with hexane eluent[72], octadecylsilyl-bonded silica with mixed methanol-dichloromethane mobile phase[73], or by gel permeation chromatography[74]. None of these methods separate over 10 mg of material in a single run, and many injections must be

made in order to recover a weighable quantity of purified product. Another chromatographic separation method uses a carbon stationary phase and toluene eluent, and offers higher throughput, although the C_{70} obtained is contaminated with C_{60}[75]. A methodical survey of the separation of fullerenes on ten different modified chromatographic stationary phases provides retention data and should prove useful in the development of a large-scale preparative separation scheme[76]. In an extraction scheme, utilizing various solvents, the higher fullerenes are separated from C_{60} and C_{70}, but the latter two are not separated[67,77]. Higher fullerenes have also been separated by chromatography and their UV-Vis spectra taken[78]. A method of utilizing Soxhlet extraction to run a chromatographic separation of large amounts (ca. 0.4 g.) of C_{60} and C_{70} has been reported[79,80], but shortcomings of this method involve the use of large quantities of alumina, which is not recovered, long separation times (12-20 hours) and products which are mixtures of the two fullerenes due to the inability to analytically separate the two fullerene bands on the column; C_{60} is highly adsorbed onto to the alumina and tailing of the C_{60} band contaminates the C_{70} band. The use of a precipitated alumina/fullerene mixture as the charge on the column is also a limiting factor in the separation since any solid fullerene must first dissolve before separation can

occur. In addition, the separation of the higher fullerenes, which are retained on the column as a dark brown zone (attributed by Hare, et al.[81] to be decomposition products of C_{70}), is not afforded by the soxhlet/alumina method.

A new separation method. A three-step process for the large scale production of C_{60} and C_{70}, that circumvents the difficulties that have been described above, has been developed. The ability of researchers who can use lower grades of fullerenes (which contain a degree of C_{70} or higher fullerene contamination) will be facilitated by the first step of the process. The second and third steps provide products which have the higher degree of purity that is required for more intensive studies. The stepwise process is as follows:

I. The benzene extract that contains the fullerenes is frozen and the fullerenes are freed from the solvent, benzene, by sublimation of the benzene under reduced pressure. Benzene has been found to be the ideal solvent for this purpose because it has a low boiling point (80.1° C) and a high freezing point (5.5° C) and fullerenes are soluble in it to the extent of ca. 5 mg/L. The solid fullerene mixture that is freed from the solvent, benzene, is a finely divided amorphous powder which does not adhere

to the walls of the container and contains only traces of adsorbed solvent.

II. The solid fullerene mixture redissolved in benzene (or a benzene extract of graphitic soot can be used directly) is subjected to successive freeze-thaw cycles. Crystalline C_{60} with a purity in excess of 95% is produced by this method, together with a C_{70}-enriched solution of benzene which is used in step III for the separation of C_{70}.

III. In the final step, higher fullerenes are removed from the C_{70}-enriched extract in a pretreatment step, then pure C_{70} is separated from the C_{60} by solid phase extraction on a Bondesil SCX (strong cation exchange) column with a hexanes eluent.

The methods of selective precipitation of C_{60} by freeze-thaw cycles, and chromatographic separation of C_{60} and C_{70} constitute a stepwise approach to the large-scale separation of the fullerenes, C_{60} and C_{70}. The product of the sublimation of a benzene extract of graphitic soot yields a friable solid product which contains chiefly C_{60}, with all benzene-extractable materials. The freeze-thaw technique yields crystals of nearly pure C_{60}. The left-over extract is a solution enriched in C_{70} from which macroscopic quantities of C_{70} are obtained by the elution chromatographic method. In addition, the higher fullerenes are separated in the course of the process during the pre-

column treatment of the extract. Each step of the separation process will be described in detail below.

Purity assessment of C_{60} and C_{70}. Purity of samples of the fullerenes, C_{60} or C_{70}, has typically been determined by several methods, including mass spectroscopy[82], NMR spectroscopy[83], infrared and Raman spectroscopy[84], high performance liquid chromatography (HPLC) and UV-Visible spectroscopy[83]. The authors report either the ratio of C_{60}:C_{70} signal or simply note the lack of the C_{60} or C_{70} signal, thereby implying the purity of their sample. Quantitative determinations of purity of C_{60}/C_{70} mixtures which contain small concentrations of one fullerene in the other, is nontrivial, due to instrumental limitations and the difficulty in separation of the two fullerenes.

Mass spectroscopic determinations can provide high sensitivity if the instrument is equipped with a high temperature sample inlet probe. However, accurate quantitation requires knowledge of various parameters, such as ionization profiles, volatization rates of C_{60} and C_{70}, sampling timing and fragmentation, before it can reliably quantitate fullerene mixtures. In short, the use of standards is required. **NMR spectroscopy**, especially ^{13}C-NMR, is a relatively insensitive technique, and requires knowledge of relaxation lifetimes which are solvent-

dependent. **Vibrational (infrared) spectroscopy** shows several C_{60} and C_{70} infrared bands in the region of 1500-400 cm^{-1}, but the analytically useful bands are weak, resulting in low signal-to-noise ratios. **HPLC** determinations require high detector and integrator sensitivity, and can be competitive with UV-VIS sensitivities, but the path length of most HPLC detector cells is much less than the standard 1 cm path length of typical UV-VIS cells and the inability of UV-Vis detectors to optimize both C_{60} and C_{70} detection wavelengths for fullerenes simultaneously creates a bias in the analysis (without knowledge of molar absorptivities for standard fullerene solutions). **UV-Vis spectroscopy** offers a method for determination of fullerene purity with the advantages of easy sample preparation, high molar absorptivities for the fullerenes, and spectra which differ significantly. If the molar absorptivities of C_{60} and C_{70} are well known, every point in the spectrum of a fullerene mixture can be compared with standard spectra and a mathematical solution can be generated to calculate the contribution of each fullerene component, thereby establishing the composition of the mixture.

Some analytical methods are better than others in the detection of impurities other than fullerenes, but every method requires the use of high-purity fullerene standards for instrument calibration.

In this dissertation, a method of production of various grades of purified fullerene products, including purified C_{60} and C_{70} suitable for standardization purposes, is outlined. In addition, the molar absorptivities of C_{60} and C_{70}, determined with standards prepared by the separation method outlined above are reported. The strengths and weaknesses of the analytical methods named above for the determination of the purity C_{60} and C_{70} samples will be addressed.

PRODUCTION AND SEPARATION OF THE FULLERENES

Recovery of fullerenes from a benzene extract of graphitic soot.

Removal of the solvent from fullerene solutions presents special problems, including the tendency of the solute to coat the walls of the container in which the concentration is carried out, difficulty in removal of the last traces of solvent from the precipitated solid and contamination from scraping the product from the surface of vessels. It was discovered in this laboratory that all the above obstacles can be avoided if the solvent is sublimed from the extract.

The extract is degassed by several freeze-thaw cycles, then the solvent is removed by sublimation and condensation into a collection vessel. The frozen extract pulls away from the walls of the sublimation vessel due to preferential sublimation of solvent closest to the vessel wall, where heat transfer is greatest. The product collects as a dark red-brown, friable powder in small clumps at the bottom of the sublimation vessel and is easily recovered. The low density of the product produced by the sublimation method makes for easier handling of small quantities. However, the time involved in sublimation of large quantities of solvent

can be lengthy, and preconcentration of the extract is often desirable.

Production and extraction of graphitic soot. Fullerene-rich graphitic soot was obtained by maintaining a DC arc with 170-180 amps between two 10 cm long graphite rods, 6 mm in diameter, kept 2 mm apart in an inert partial atmosphere of helium at a pressure of 150-200 torr. The soot that was formed in the inert helium atmosphere was deposited on the surface of a water-cooled copper cylinder that enveloped the arc. The graphitic soot was scraped off the surface of the copper cylinder with a Teflon coated scraper. No special precautions were taken to prevent the soot from coming in contact with air[85]. This method of producing fullerene-rich soot is essentially the same as the method that has been used by previous investigators[66,69]. When a sufficient quantity of soot was collected in this manner, the fullerenes, (primarily C_{60} and C_{70}) were separated from the soot by extraction with benzene in a Soxhlet extractor.

Approximately 100 g of graphitic soot was placed in a large Soxhlet extractor equipped with a 80 X 220 mm extraction thimble and 3 L boiling flask. Approximately 2500 mL of benzene was placed in the boiling flask with a few carborundum boiling chips. The soot was extracted for 24 hours, the rate of solvent turnover was approximately

once every 20 minutes. Depending on the amount of fullerenes present in the soot, another 100 g batch of soot was extracted into the same volume of solvent. The benzene extract was vacuum filtered through a 7 cm glass microfiber filter (GF/A, Whatman Ltd, England) in a buchner funnel. The extract contained about 80% C_{60}, the remaining 20% was C_{70}, with small amounts of other fullerenes. Yields of fullerene solids from the graphitic soot were 2-8%, depending on the conditions under which the soot was formed.

Separation of solid fullerenes from the benzene extract. The fullerene-saturated benzene extract was completely freed from dissolved gases by several freeze-thaw cycles, and finally frozen in an acetone-dry ice bath. The benzene was then removed by sublimation under reduced pressure ($\approx 10^{-3}$ mm Hg) and recovered by condensation in a dry-ice/acetone cooled trap. During the sublimation process, the solidified benzene extract that was in contact with the walls of the container sublimed first. This caused the solid fullerene mixture to collapse into small clumps and collect at the bottom of the container in the form of a dark brown powder. It should be noted that this powdery material did not adhere to the walls of the container and it was not necessary to resort to scraping the container walls to recover the

fullerenes. This simple expedient of freezing the benzene extract and sublimation of the benzene under reduced pressure facilitated the separation of the fullerenes from the solvent and overcame the serious difficulties that were encountered in recovering the fullerenes by evaporation of the solvent.

Figure 20 is a schematic representation of the system that was used in the sublimation process. The fullerene saturated benzene extract was introduced into the round bottom sublimation flask which was connected to another round bottom receiver flask which in turn was connected to two guard tubes immersed in liquid nitrogen to trap any uncondensed benzene. The pressure in the system, which was less than 10^{-3} mm Hg, was maintained by a vacuum pump and measured with a thermocouple-based manometer connected to the sublimation flask. The dissolved air in the benzene extract was removed by alternately freezing the extract in the acetone-dry ice bath and then allowing it to thaw under vacuum. After two or three degassing cycles, the benzene extract was frozen and the benzene sublimed under reduced pressure. After all the benzene had sublimed, the dark brown amorphous solid left in the bottom of the sublimation flask was recovered readily. This solid was mostly C_{60}, with an admixture of a small amount of C_{70}, traces of a brown material which was likely to contain higher fullerenes

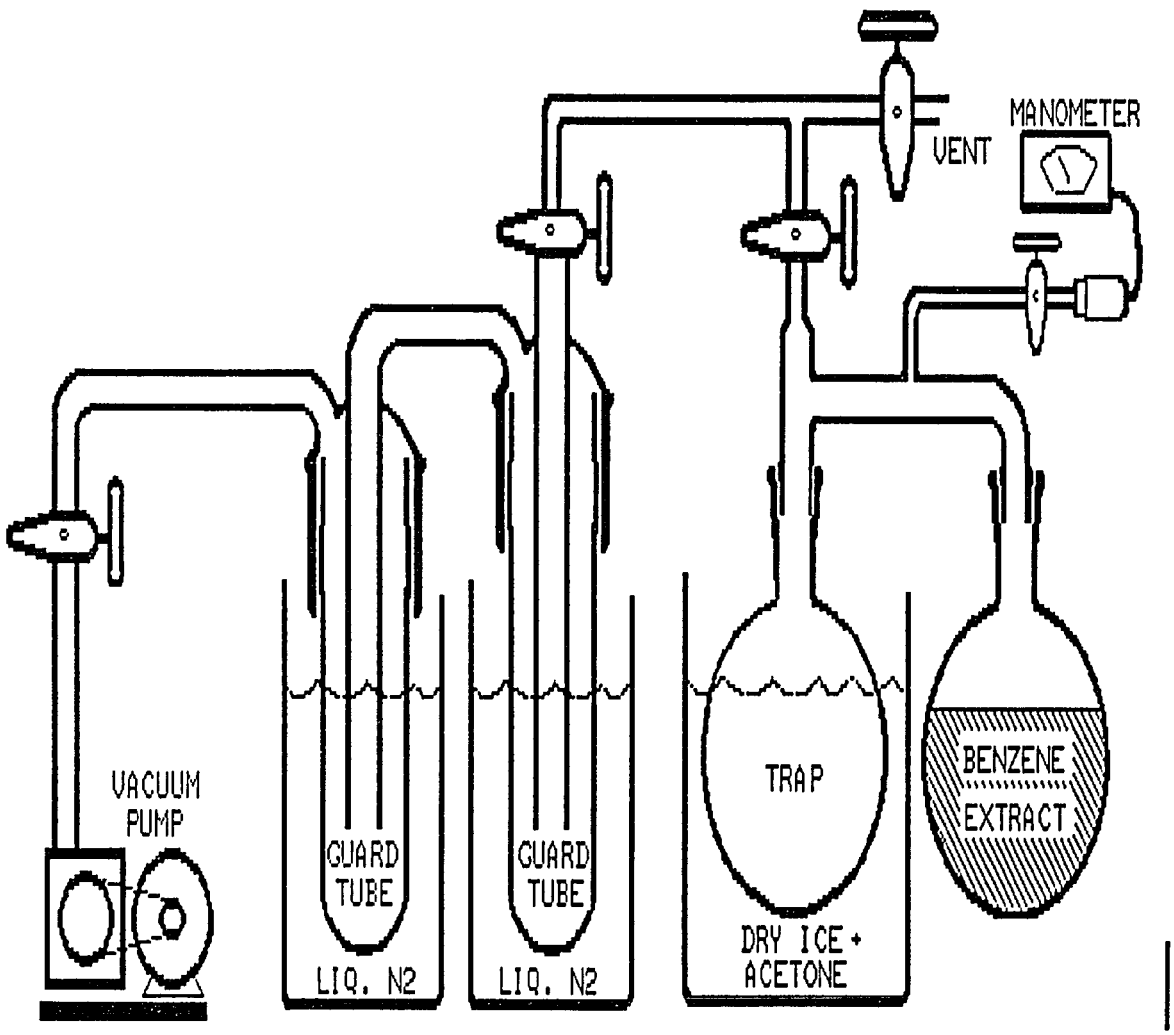

Figure 20. Apparatus for the sublimation of a frozen extract of graphitic soot.

and traces of other contaminants.

Trace impurities in the dark brown C_{60}-C_{70} mixture. There are three types of contaminants in the solid fullerene mixture that is produced by the single step vacuum sublimation of benzene from the frozen benzene extract: (I) Organic impurities that arise from the binders in the graphite, the impurities originally present in the organic solvent or extracted by the organic solvent from the plasticware or stopcock grease. (II) Metal impurities that are carried over from the graphitic soot to the benzene extract, and (III) solvent impurities such as water or benzene that are trapped in the solid fullerene matrix or strongly adsorbed on the fullerene surfaces.

The organic contaminants in the solid fullerene mixture can be selectively extracted with a solvent such as petroleum ether or ethyl ether in which C_{60} and C_{70} are insoluble. The extracted organic contaminants were identified with the aid of a Hewlett Packard GC-MS system and a high temperature inlet probe; trioctyl phthalate, a plasticizer, and silicone vacuum grease were identified as the major contaminants. The presence of the latter was confirmed by X-ray fluorescence analysis of the non-volatile residue that is left behind after the thermogravimetric analysis (TGA) of the fullerenes; the residue gave a strong

unmistakable Si K_α peak at 1.739 eV. Both the infrared spectra (**Fig. 21**) and TGA (**Fig. 22**) confirmed the removal of the silicone vacuum grease by extraction with ether. The contamination of the solid fullerenes with these organic compounds could be avoided by using Teflon stopcocks and Teflon joint sleeves in the vacuum sublimation system (**Fig. 19**), and by preventing the organic solvents, especially benzene, from coming in contact with any plasticware.

Trace metal impurities in the solid fullerene mixture were identified by X-ray fluorescence analysis with a Tracor 5000 energy dispersive system equipped with a 50 kV rhodium target X-ray source and a Si(Li) detector cooled in liquid nitrogen. Samples of the carbon rod used in the manufacture of graphitic soot and several samples of fullerene products were powdered and analyzed. The principal metal impurities in the products were Fe, Ni, Cu and Zn; no attempt was made to determine these elements quantitatively in the carbon matrix. From a knowledge of instrument response to metals in similar powder samples, however, it was estimated that the principal contaminant was Fe ($\approx$ 10 ppm), and the Ni, Cu and Zn contaminants were present at concentrations of less than 6 ppm. It is not surprising that these metal impurities , which are strongly adsorbed on the fullerene surfaces, are carried into the benzene extract and remain adsorbed when the fullerenes are recovered after vacuum

sublimation of the benzene. Although these metal impurities are found in the low ppm levels, their presence may cause difficulties during investigations of the properties of the fullerenes.

The most common impurities that are found in the solid C_{60}-C_{70} mixture are adsorbed solvents. Fortunately, these solvents, which have low boiling points, are readily removed by heating the fullerenes in an oven (<150°C) without any obvious detrimental effects. The simplest method of determination of the amount of solvent adsorbed by the fullerenes is by thermogravimetry. A Perkin Elmer model TGS-2 system with a total capacity of 10 mg and a sensitivity of 0.001 mg was used in this work. Plots of % weight loss vs temperature yield information on the amount of solvent that is lost and the type of solvent that is lost, from the temperature at which the weight loss occurs. In addition, any non-volatile residues, e.g. metal oxides and SiO_2 that are left after complete combustion of the carbon in an oxygen atmosphere yield quantitative information on the extent of contamination. The results of infrared and thermogravimetric analysis of the product in air, before and after treatment with three aliquots of ethyl ether and drying at 110° C overnight are shown in **Figures 21 and 22**. It can be seen that the solvent and vacuum grease contaminants have been substantially removed from the sample

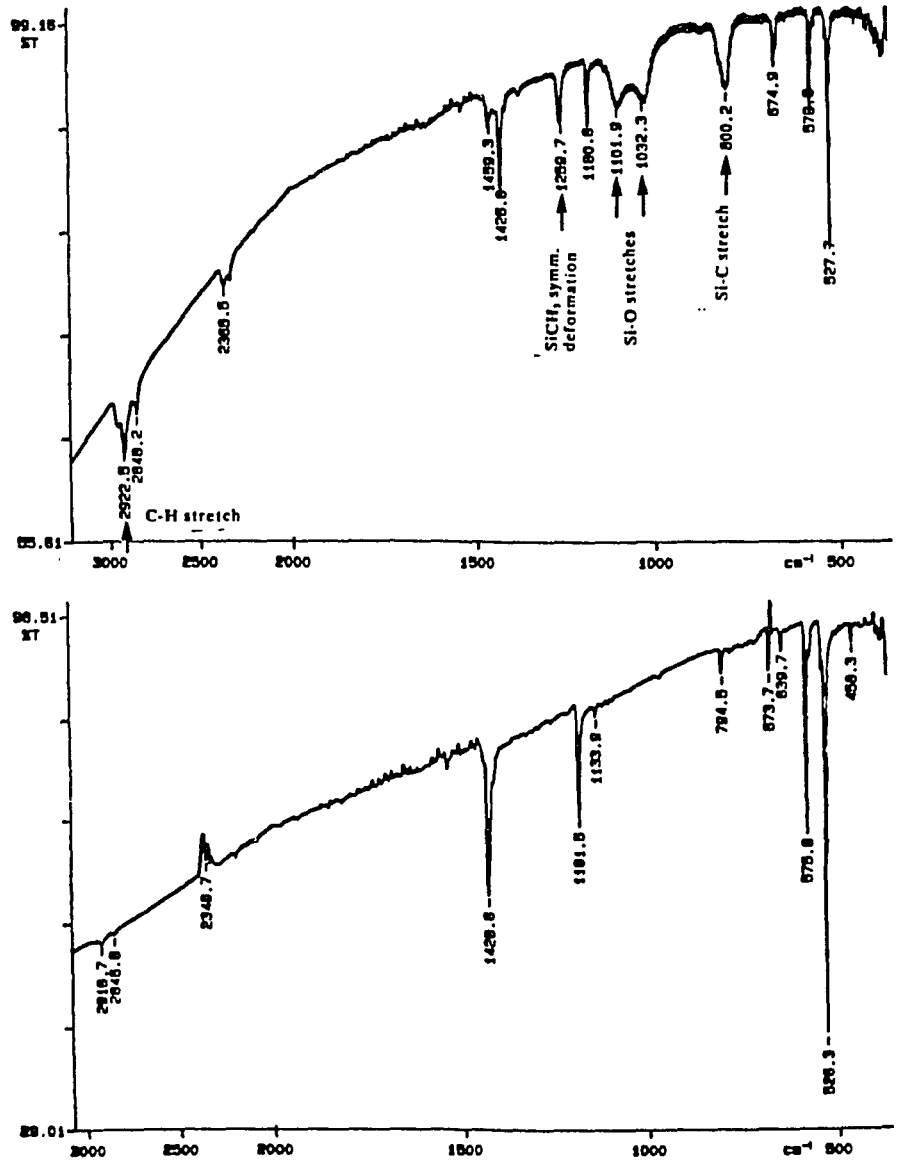

Figure 21. Infrared spectra of the product of the sublimation of a benzene extract of graphitic soot before and after treatment with ethyl ether and drying at 110° C.

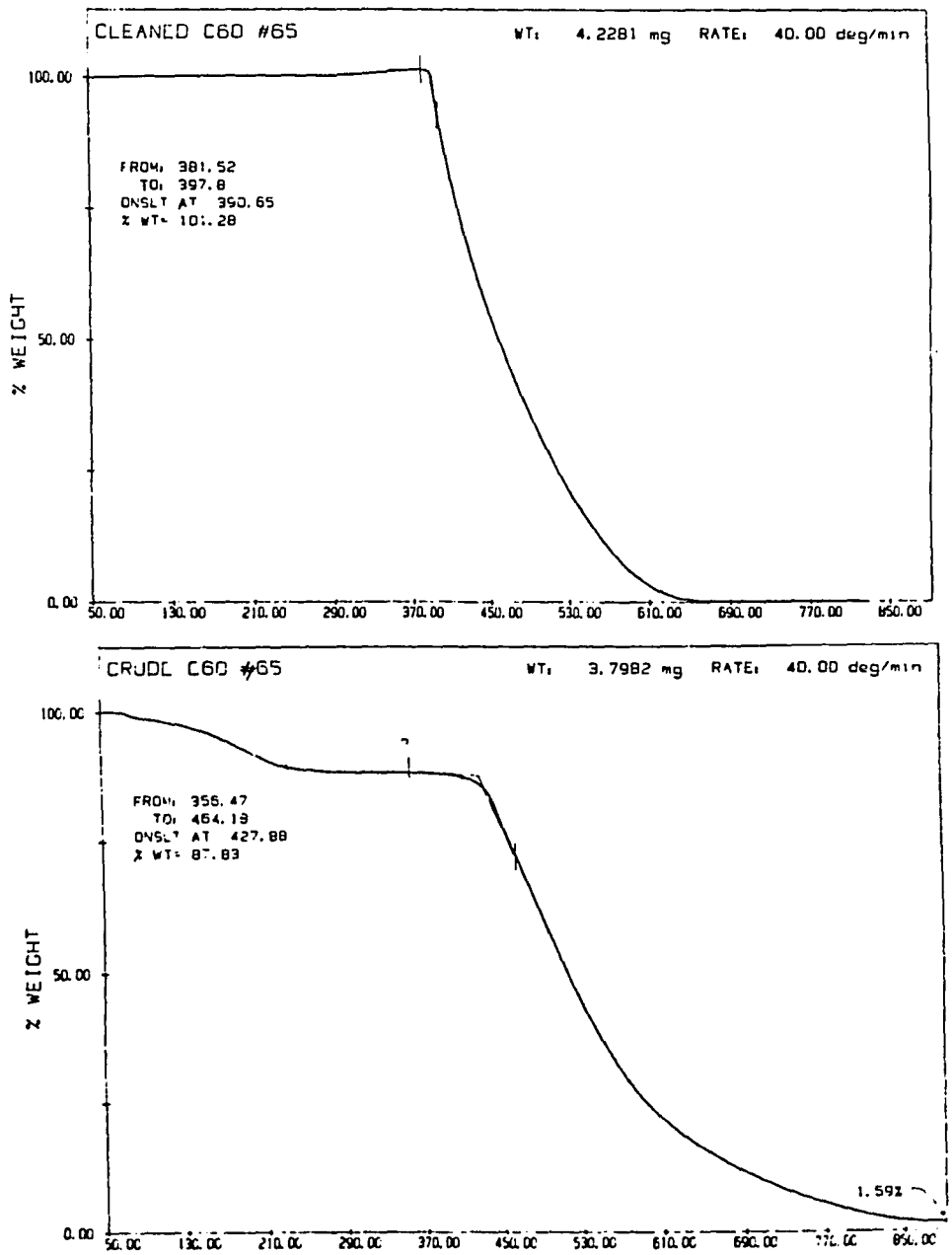

Figure 22. Thermogravimetric plots of the product of the sublimation of a benzene extract of graphitic soot before and after treatment with ethyl ether.

by this process.

Freeze-thaw selective precipitation of C_{60}. In a separation scheme discovered serendipitously while degassing the fullerene extract in benzene, fractional precipitation of C_{60} is achieved by **slowly** freezing a benzene solution of fullerenes, which results in crystallization of pure solvent first, followed by crystallization of nearly pure C_{60}. Thawing the solid mixture allows separation of crystalline C_{60}, leaving the supernatant solution enriched in C_{70}. The separation of C_{60} is incomplete by this "freeze-thaw" method, but repetitive freeze-thaw cycles results in crystals of over 95% pure C_{60}, and the resulting C_{70}-enriched solution is ideal for separation by chromatographic methods.

To precipitate C_{60} selectively, the benzene soot extract was placed in 1 L separatory funnels. The extract was slowly frozen in a freezer at 2 ± 1°C; the freezing process took approximately 16 hours. The frozen extract was thawed at room temperature for approximately 4 hours, and the crystalline fullerene solids were removed to a small beaker by briefly opening the stopcock at the bottom of the separatory funnel. The excess solution was removed from the slurry by decantation. The precipitate was air-dried. Purity of the first precipitate (1X) was approximately 87% C_{60}. The extract was subjected to two more freeze-thaw

cycles, each cycle yielded less solid fullerenes, thereby precipitating the bulk of the C_{60} present in the extract. The remaining supernatant was enriched in C_{70}, and was reserved for the chromatographic separation of C_{60} and C_{70}.

The precipitated fullerenes (1X) were redissolved in boiling benzene; the optimal concentration for redissolution was found to be approximately 0.5 g fullerenes per liter of benzene. It was found that less concentrated solutions did not produce a higher purity product, and higher fullerene/benzene ratios did not allow all the solids to redissolve (see below about solubility behavior). Two freeze-thaw cycles produced twice-precipitated (2X) fullerene crystals which were approximately 94% C_{60}, with a recovery of 75%. A third freeze-thaw cycle in this second round of freeze-thaw cycles was often not included, due to the small yield and the presence of higher amounts of C_{70} in the product. Instead, the third freeze-thaw cycle was not included and the supernatant was reduced in volume, and was subjected to two freeze-thaw cycles.

The product contained substantial amounts of C_{70}, and was therefore treated as a first (1X) precipitate. The supernatant was reserved for the chromatographic separation process.

In order to produce 98+% C_{60}, three or four precipitations were required. The final precipitate was

washed with petroleum ether and was dried overnight at 80° C. **Figure 23** diagrams the steps of the process.

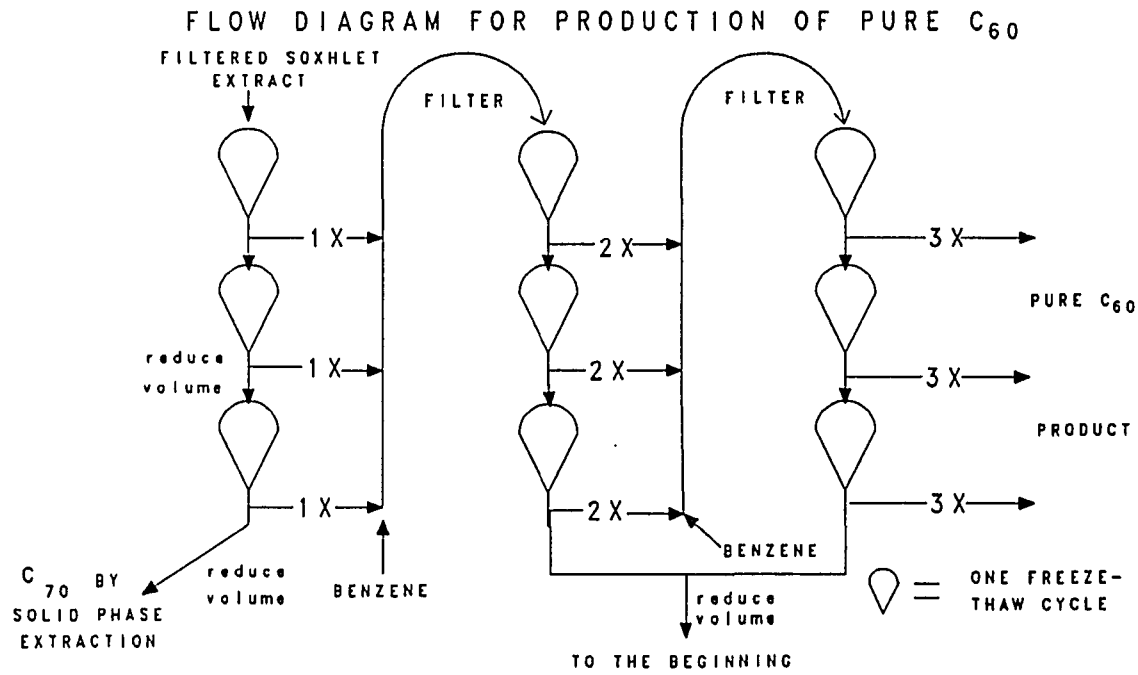

Figure 23. Flow diagram for the freeze-thaw process for the production of purified C_{60}.

Similar to a well-known phenomenon used in the desalting of brines[86,87,88,89] in which purified water is separated from saline solution, the slow freezing of a benzene solution of fullerenes causes separation of solvent and solution, and the solvent freezes in a pure crystalline form. In the selective precipitation of C_{60}, crystals of the solvent are first formed on the walls of the separatory funnel; this matrix of intertwined crystals that are formed on the walls confines the concentrated fullerene solution to the center of the vessel, allowing crystals of nearly pure C_{60} to form. It is important to emphasize that these freeze-thaw cycles yield a precipitated product, containing little solvent or contaminants present in the initial soot extract, as demonstrated by thermogravimetric analysis, which indicated the product was 99.9% pure (**Figure 24**).

Another observation of the selective precipitation of C_{60} was made by Coustel, et al.[90], who found that 95% pure C60 precipitated from a hot, saturated soot extract in toluene as the extract cooled. The crystals appeared to contain a "core" of very pure C_{60} surrounded by a layer of material which contained a higher concentration of C_{70}. They attribute the purification mechanism to higher affinity of C_{70} for the toluene solvent. Since the C_{60} crystals produced by the freeze-thaw process are formed in a similar manner, it is therefore possible that they also contain a

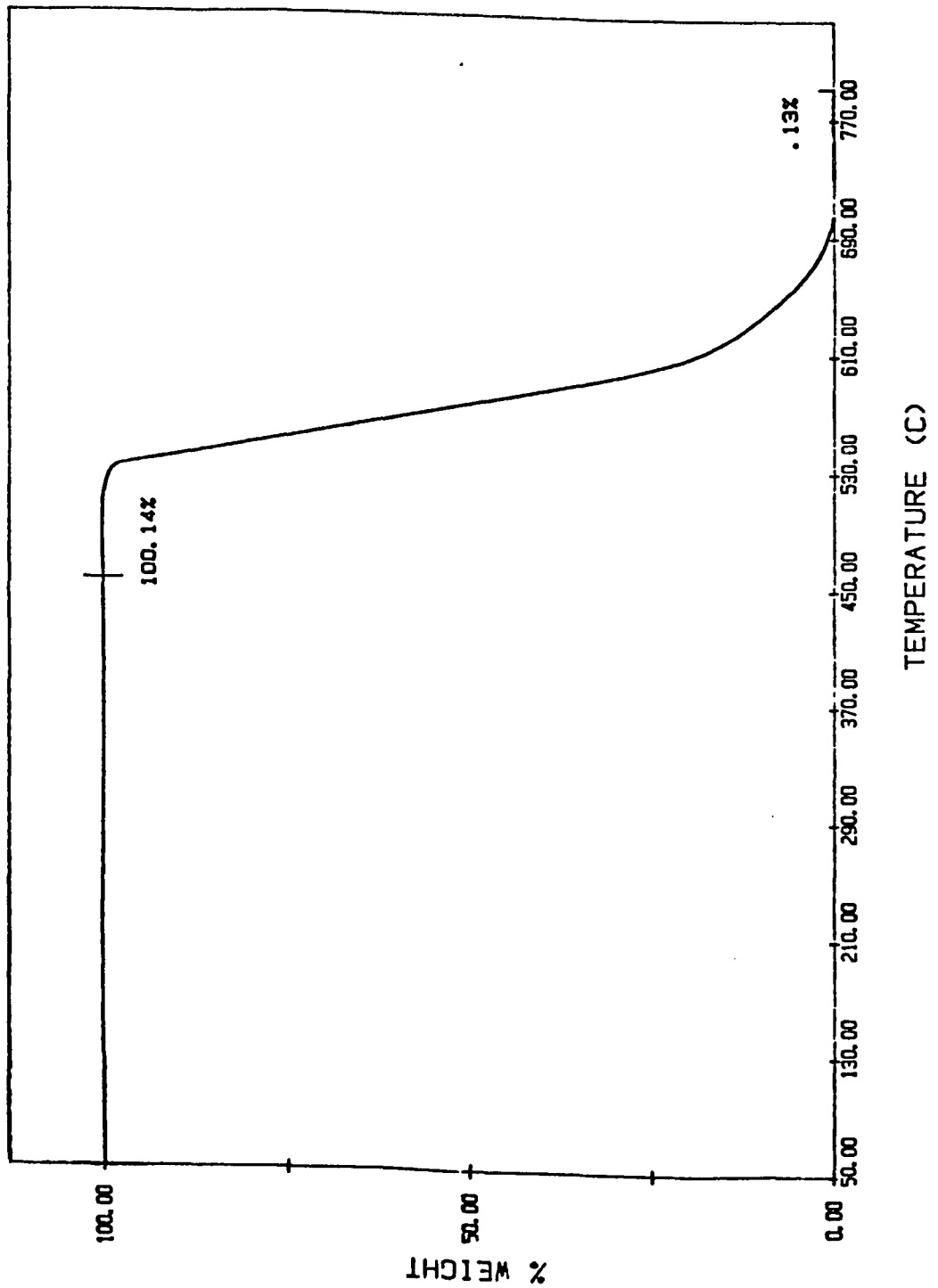

Figure 24. TGA of the product of the freeze-thaw process for the production of C_{60}.

"core" of purified C_{60} surrounded by less pure material.

The freeze-thaw process for purification of C_{60} is a high throughput technique. In our laboratory scale operation, over 2 g of high purity C_{60} was produced weekly. Over 80% of the benzene used was recovered from the process by use of a rotary evaporator to reduce the volume of the solutions, followed by distillation of the recovered benzene. It is important to use benzene of reasonably high purity because the freeze-thaw technique requires separation of the solvent in a pure, solid form. As the purity of the C_{60} increased with each reprecipitation step, the crystals formed were progressively larger and displayed better facets, although x-ray crystallographic analysis showed them to lack long-range order, possibly due to inclusion of small quantities of solvent in the crystal lattice which evaporated on drying the crystals. The finished product was shiny black needles, about 2 mm long, sometimes with a red-brown tint.

Although it has been shown that the solubility of fullerenes in benzene is around 5 g/L[83], It was found that no more than about 0.5 g of the precipitated fullerenes would dissolve in 1 L of boiling benzene, even after several hours, unless more than 1 L of benzene was used, and the volume subsequently reduced. The material which would not readily redissolve was red-brown, and was found to contain a

much higher C_{60}/C_{70} ratio than the supernatant solution. Dissolution in benzene and freeze-thawing of this brown-yellow material invariably produced 95-98% pure C_{60} crystals after only one freeze-thaw cycle. These observations indicate that either C_{70} is more soluble in benzene than C_{60} or some sparingly soluble C_{60} compound, such as $C_{60}O$, which decomposes to C_{60} in an excess of boiling benzene, is formed in the freeze thaw process (the red-brown solid was absent in the original soot extract). If a C_{60} compound is not formed, then the solubility behavior of the fullerenes in benzene appears to exhibit hysteresis, allowing higher concentrations of fullerenes to be solubilized without precipitation only if the solution is evaporated from a large to a smaller volume. Another explanation could be that the highly ordered molecules in the crystal lattice resist solvation by benzene. These observations of the limited solubility of the precipitated C_{60} product and the increase of purity of the insoluble material were also reported by Coustel, et al.[90], who surmised that C_{70} is more soluble in toluene than C_{60}, and Hare, et al.[81], who presumed that improved molecular packing in the crystalline solid is responsible for the slow rate of solvation. This selective solubility phenomenon may form the basis for an as yet undeveloped separation scheme, or for the production of $C_{60}O$.

Separation of pure C_{60} and C_{70} by chromatography. The chromatographic separation of fullerenes produces pure products, in well separated fractions. Any mixed fractions collected can be re-run to eliminate loss of material. The fullerenes, which are both polarizable species, are thought to be separated by hydrophobic interaction with the water which is associated with the immobilized sulfonic acid group on the Bondesil SCX. This conclusion is supported by the fact that the separation is mediated by the use of THF (a relatively "wet" solvent) in the mobile phase; omission of the THF causes the degradation of the separation over several runs. Whatever the mechanism, the surface of the modified adsorbent provides a unique combination of polar and non-polar interactions with the fullerenes[91].

Preliminary experiments showed Bondesil to be effective in the separation of C_{60} and C_{70}. Initially, a solution of water-saturated dichloromethane in heptane were tried as eluent, and although good separations were achieved for the first one or two runs, the separation progressively degraded with each subsequent run, due to "tailing' of the C_{60} band. After several attempts with other eluents and modifiers to maintain the separation, it was found that the use of a small percentage of THF in eluent is important in retaining the characteristics of the solid phase and, in addition, it was found to mediate the interaction of the fullerene-solid

phase interaction. If higher THF:hexanes ratios are used, the elution of fullerenes occurs faster with corresponding degradation of the separation. Loadings of ca. 4 mg fullerenes/10 g. Bondesil, and eluent composition of ca. 2% THF in hexanes were found to be in a good range for optimum separation of fullerenes, and nearly 100 mg of fullerenes on a large Bondesil column were separated in one run under these conditions. It is unknown whether this separation scheme affords any separation of larger fullerenes; The composition of the dark brown material removed in the pre-treatment step is believed to include the higher fullerenes, and is being investigated.

The chromatographic separation of C_{60} and C_{70} described here is a robust method. Over 30 runs were conducted on a single column without renewal of the solid phase with no degradation of the separation.

Pretreatment. The C_{70} enriched benzene solution produced by the freeze-thaw production of purified C_{60} contained a brown material which was thought to be larger fullerenes, derivatized fullerenes[81] and/or tars from the soot production process. These materials are highly retained on Bondesil, and were found to contaminate the column during separation, so were removed by pretreatment. The pretreatment step was as follows: 100 mL of the

concentrated C_{70}-enriched solution was mixed with 10 g of Bondesil and the mixture was air-dried with gentle heating in a fume hood to free it from benzene. The powdered mixture was placed in a small column and 1.5 L of a mixture of dichloromethane (DCM) in heptane (20/80 v/v) was used to elute the C_{60} and C_{70}, leaving behind the dark brown material which would have contaminated the separation column. The dark brown material could be removed from the Bondesil by elution with 100% THF. The heptane/DCM solvent was removed from the C_{60}/C_{70} solution in a rotary evaporator, and the solids were redissolved in heptane for use in the separation scheme. After this pretreatment, no brown contamination remained on the column after the separation run.

Separation. For the large-scale separation of C_{60} and C_{70}, a bed of 400 g Bondesil SCX was prepared in a 600x65 mm column, which was equipped with a medium porosity glass frit at the bottom and a teflon stopcock to control the flow of eluent. The final bed height was 13.5 cm and the single volume displacement was approximately 280 mL. The bed was conditioned with 1 L of the running solvent, 2.5% THF in hexanes. The top of the bed was stirred gently and allowed to settle to form a flat profile. The conditioning solution was allowed to drain to within 1 cm of the top of the bed to dampen the effects of the fullerene solution addition. A

300 mL aliquot of the fullerene solution in heptane, with a 0.32 g/L concentration of dissolved solids, was slowly added through a 15 cm diameter #1 Whatman filter paper to remove any particulate material from the fullerene-saturated heptane solution. After the fullerenes had been deposited onto the bed, isocratic elution of the fullerenes was accomplished with the 2.5% THF in hexanes running solution. The flow rate was controlled by gravity at about 25 mL/minute. Two well separated bands, first purple, then brown, were observed travelling down the bed. The progress of the separation was monitored by taking the UV-Vis spectrum of the effluent periodically. Each separation run required approximately 3 L of eluent, and required approximately 2 hours to elute both separated fractions. Two fractions containing the separated fullerenes were collected, and the solvent was removed using a rotary evaporator. The solids were redissolved in a minimal amount of benzene, and the solutions were poured into a large excess of petroleum ether, thereby precipitating the fullerenes. Ageing the precipitate by gentle heating in a water bath for several minutes coagulated the solids, and the solvent was decanted. The products were dried overnight at 80° C, yielding a black or dark brown powder. Alternatively, the fullerenes were dissolved in benzene to

remove them from the evaporation vessel, then the benzene was sublimed as described above.

PURITY ASSESSMENT OF FULLERENE SAMPLES

UV-Visible Spectroscopic Determination of Purity. Because of their high molar absorptivities and pronounced differences in their spectra, C_{60} and C_{70} are readily determined by UV-Vis spectroscopy. The ease of preparation and analysis of solutions of the two fullerenes also makes the UV-Vis method for purity determination of fullerene samples an attractive alternative to HPLC or mass spectroscopy. Precision and accuracy of quantitative UV-Vis analyses typically fall in the range of ±1% precision and ±0.5 to ±2% accuracy[92].

A graphical approach. The purity of a fullerene sample and uncertainty in the purity assessment can be obtained using a graphical approach derived as follows:
given the Beer-Lambert law for 1 cm path length, at any single wavelength, the absorbance of a solution of pure C_{60} or C_{70} is,

$$A_{60_{pure}} = \varepsilon_{60_{pure}} [C_{60}]_{pure}$$

$$A_{70_{pure}} = \varepsilon_{70_{pure}} [C_{70}]_{pure}$$

The absorbance of an unknown solution of mixed fullerenes is described as,

$$A_{mix}=\varepsilon_{60}[C_{60}]_{mix}+\varepsilon_{70}[C_{70}]_{mix}$$

substitution and rearrangement yields an equation for a straight line,

$$\frac{A_{mix}}{A_{70_{pure}}}=\frac{A_{60_{pure}}}{A_{70_{pure}}}\cdot\frac{[C_{60}]_{mix}}{[C_{60}]_{pure}}+\frac{[C_{70}]_{mix}}{[C_{70}]_{pure}}$$

If the absorbances, at a fixed wavelength, of pure and mixed fullerene solutions are substituted into this equation, and the concentration of the pure standards is known, the slope and intercept of the calculated line will yield the concentrations of C_{60} and C_{70} in the mixture. The correlation coefficient for the line confirms the purity of the original standards. The concentration of the mixed fullerene solution need not be known, and the concentration of each component can be derived from the above equation. Many instrument manufacturers offer computer software which expands the above one-dimensional approach of quantitation to the use of matrix algebra to extract concentrations of solutes in mixed solutions, allowing five or more standard spectra of different concentrations to be used in the two dimensional matrix.

Plots of the linear equations are shown in **Figure 25.** In these experiments, the value of R^2 was 0.999+ for the linear fit. The standard solutions were made from weighed pure fullerene samples prepared by the chromatographic

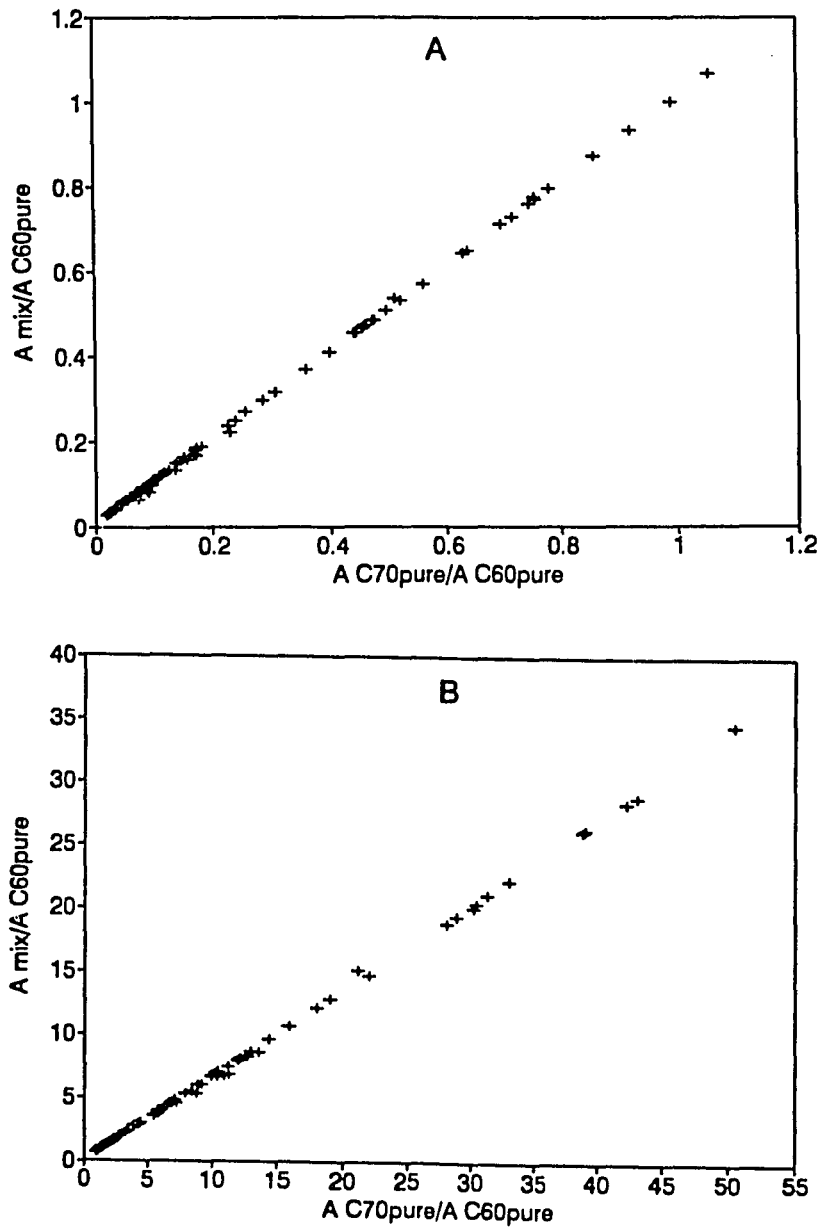

Figure 25. Linear fit derived from the UV-Vis spectra of fullerene solutions. A; solution prepared to contain 1.10% C_{70} in C_{60}. B; solution prepared to contain 0.9% C_{60} in C_{70}.

technique and were dissolved in known volumes of spectral grade heptane. Results were 0.95% w/w C_{70} found in the solution prepared to contain 1.10% C_{70} in C_{60}, and 3.0% C_{60} found in the solution prepared to contain 0.9% C_{60} in C_{70}.

Molar absorptivities. To demonstrate the high molar absorptivities of C_{60} and C_{70}, spectra of several known concentrations of each fullerene in spectral grade (Aldrich, Milwaukee, WI) heptane at 20° C were taken on a Perkin-Elmer model 552 diode-array instrument (Norwalk, CT) with instrumental parameters under microprocessor control. Results of the analysis are shown in **Figure 26** with comparisons of selected values to other work in **Table VIII.** Uncertainties in the measurements were determined by the standard deviation of the results from four separately prepared solution for each fullerene.

Infrared Determination of Purity. In an attempt to assess the ability of IR spectroscopy to quantitate small amounts of C_{60} in a sample of C_{70} or vice versa, The absorptivities of the two fullerenes were assessed, using pure samples prepared by chromatography.

Quantitative infrared analysis of solids in KBr pellets requires knowledge of the absorptivities of each fullerene, along with geometric parameters of the pellet. Beer-

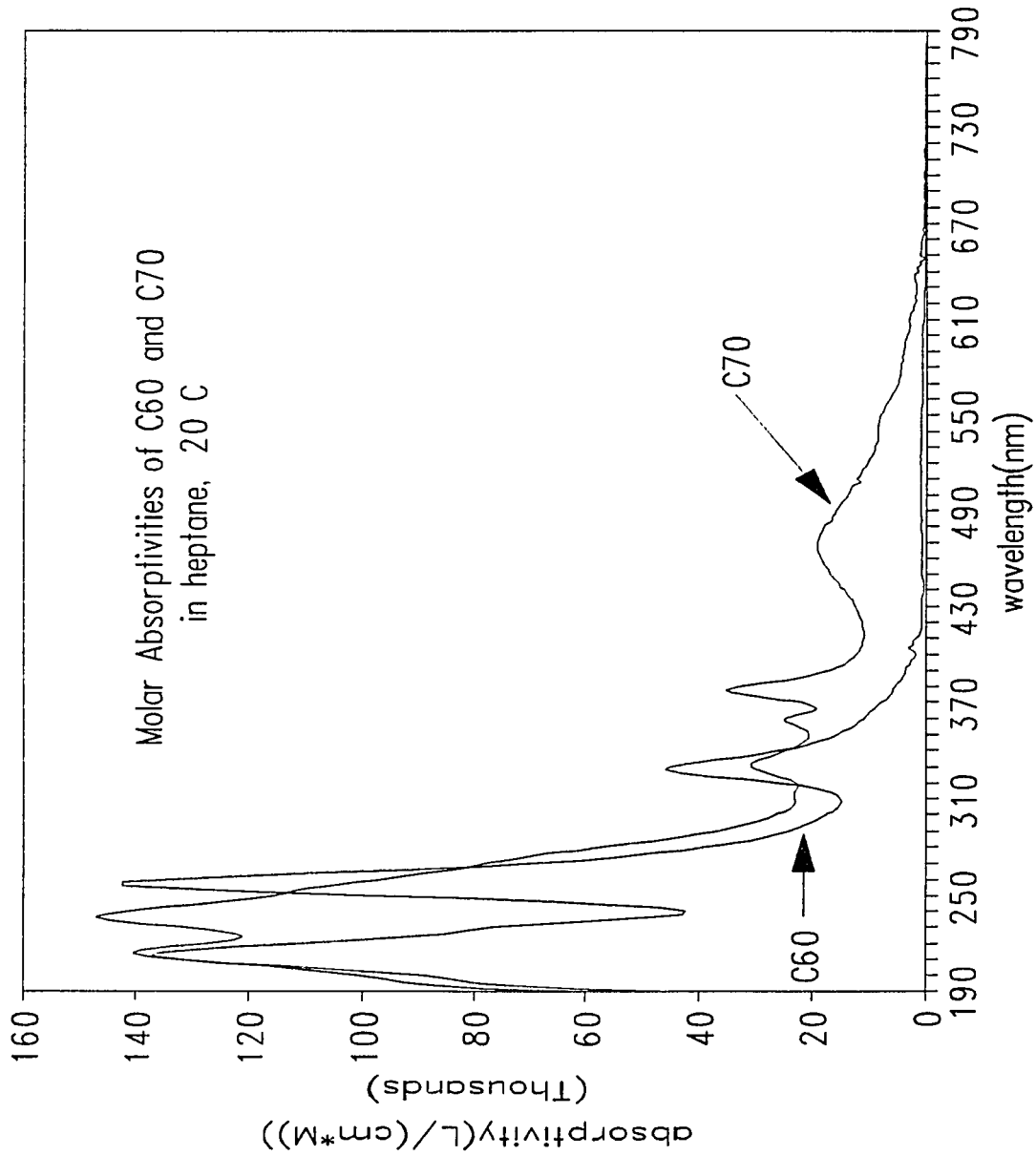

Figure 26. Molar absorptivities of C_{60} and C_{70} in heptane.

wave-length nm	molar absorptivity (this work)	molar absorptivity (Hare, et al.)[a]
C_{60}		
213	136000 ± 5500	135000
257	142200 ± 4800	175000
329	46100 ± 5600	51000
C_{70}		
214	140000 ± 1300	
236	147000 ± 1400	
331	30900 ± 390	
361	24800 ± 310	
378	35200 ± 450	
468	19200 ± 300	

Table VIII. Molar absorptivities of C_{60} and C_{70} at selected wavelengths. a: see reference 81.

Lambert's law is then assumed to be valid in this application, although considerable light scattering occurs in solid KBr pellets. The limitations of the technique are attributed to the low absorptivity of the fullerenes in general, resulting in a low signal to noise ratio, overlap of absorption bands of C_{60} by bands in the C_{70} spectrum, errors in pellet measurement, inhomogeneity in the fullerene/KBr mixture and low instrumental throughput. These shortcomings limit the ability of IR spectroscopy to determine the purity of highly purified fullerenes.

Spectra of pure C_{60} and C_{70} are shown in **Figure 27.** The fullerene samples have IR bands in the region from about 450 to 1500 cm^{-1}. C_{60} shows four characteristic bands at 527, 576, 1183 and 1429 cm^{-1}. C_{70} has a more complex spectrum, including bands at 578 and 1430 cm^{-1} which overlap the C_{60} bands at those wavelengths. The overlap of two out of four C_{60} bands by C_{70} bands, the low intensity of the spectrum and corresponding low signal-to-noise ratios makes the infrared determination of purity of fullerene samples a relatively insensitive method.

In a demonstration of the IR quantitation technique, pure standards were prepared by the chromatographic separation method described here. KBr pellets of known concentration were prepared from the purified fullerenes as follows. 0.6±.07 mg of each fullerene was weighed to the

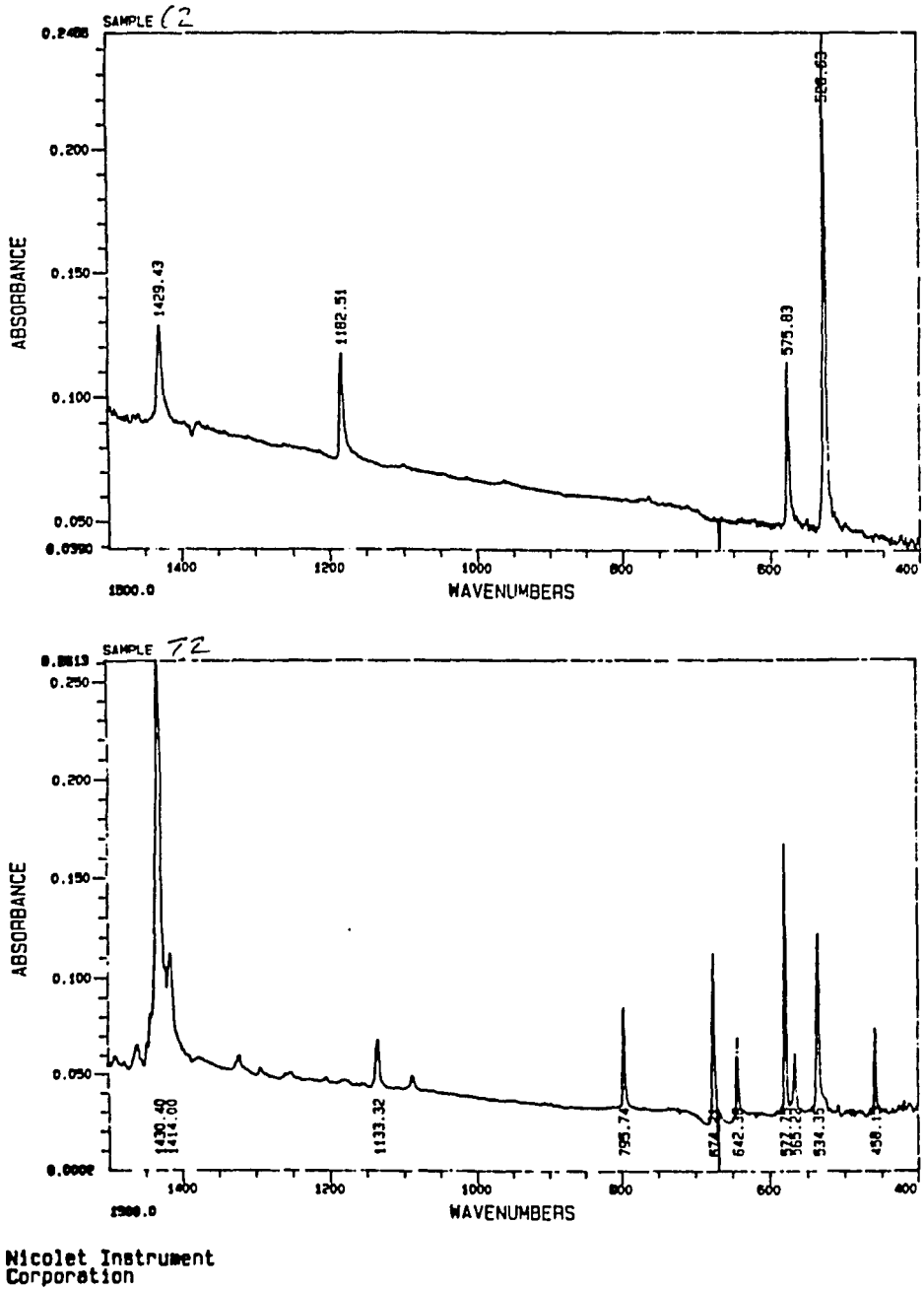

Figure 27.and 27a. Infrared adsorption spectra of purified C_{60} and C_{70}.

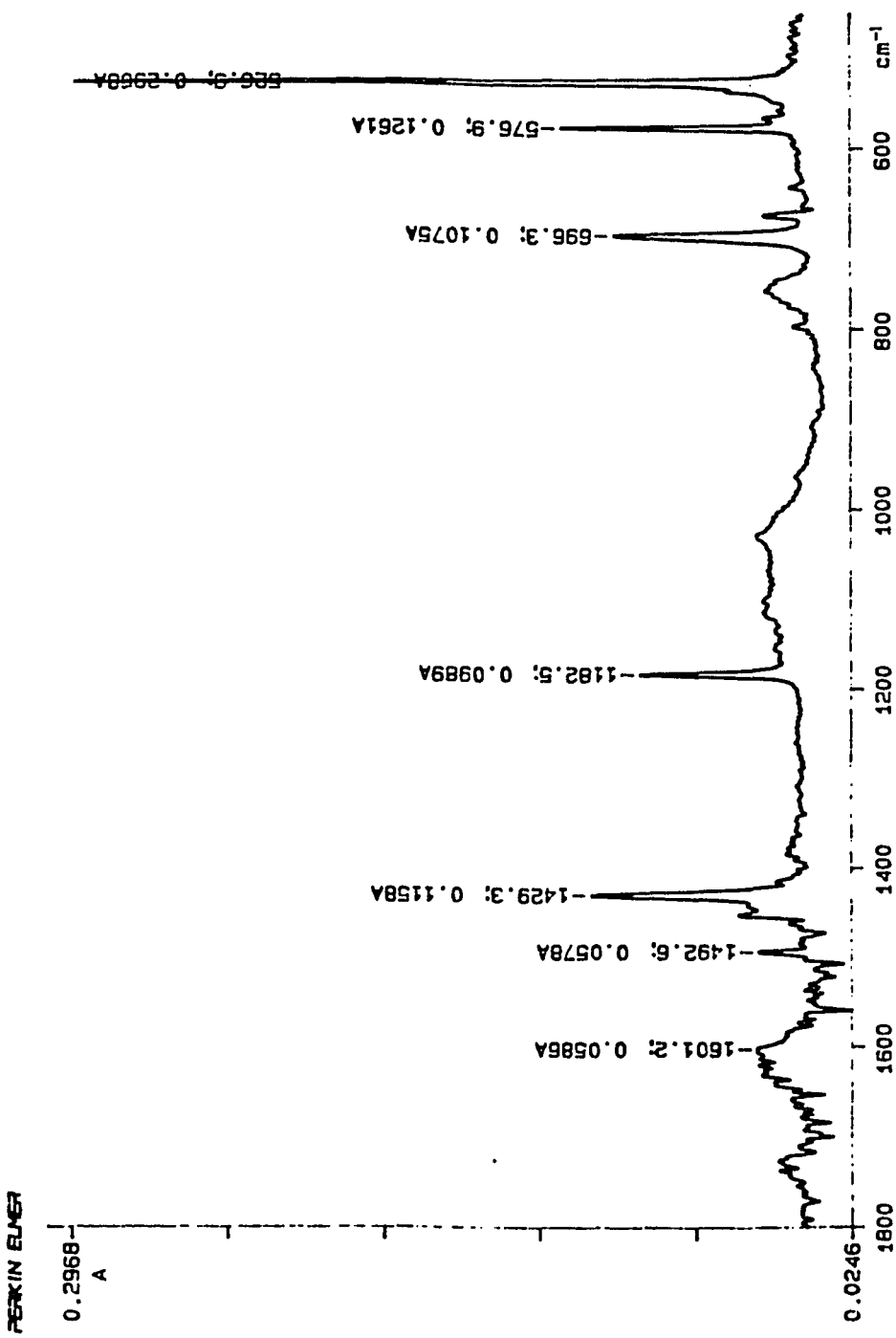

Figure 28. Infrared absorption spectrum of a sample that contains ca. 8% C_{70} in C_{60}.

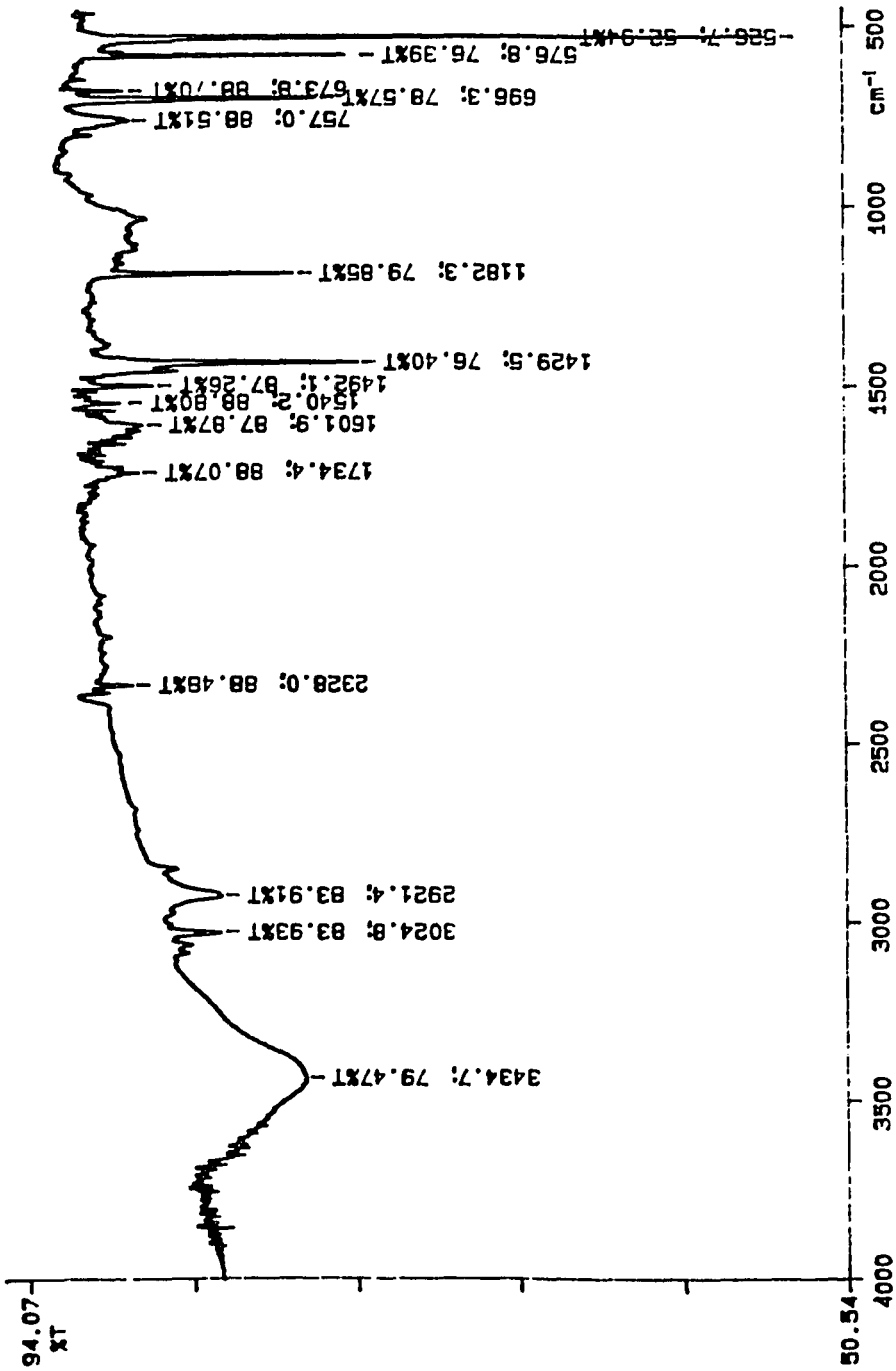

Figure 29. Infrared transmission spectrum of the 8% C_{70} sample, showing contamination by water, toluene and polystyrene.

C_{60} concentration:	0.004324 mol/L KBr 0.001685 mol/Kg KBr		
wavelength cm^{-1}	absorbance	ϵ (molar)	ϵ (molal)
1429	0.0683	209	536
1183	0.0702	215	550
577	0.1058	323	830
527	0.3374	1031	2645

C_{70} concentration:	0.004766 mol/L KBr 0.001858 mol/Kg KBr		
wavelength	absorbance	ϵ (molar)	ϵ (molal)
1430	0.332	976	2504
1134	0.037	109	279
1087	0.0115	34	87
796	0.0775	228	585
674	0.1287	378	971
642	0.0608	179	459
578	0.2085	613	1573
565	0.0477	140	360
535	0.1499	441	1131
458	0.0643	189	485

Table IX. Infrared absorptivities of C_{60} and C_{70} in KBr pellets.

nearest 0.0005 mg on a CAHN electrobalance and was ground with 0.5±.001 g of IR grade KBr (Aldrich) weighed to the nearest 0.0002 g in a Wig-L-Bug grinder (Spex Industries). 0.25±.0005 g of the mixture was weighed into a 1.3 cm diameter die and KBr pellets were produced at 20000-22000 psi under vacuum. Spectra were taken of each pellet versus a blank prepared in the same manner as the samples on a Nicolet model 510P instrument with 32 scans and a resolution of 2 cm^{-1}. **Table IX** shows the results of the study. The absorbance measurements were corrected for baseline displacement and the Beer-Lambert law is assumed to be accurate for the purpose of this demonstration[93]. Both molar (moles/L KBr) and molal (moles/Kg KBr) concentrations were calculated from the dimensions of each pellet and the weights of fullerenes and KBr used in the sample preparation. The low infrared absorptivities found in this study demonstrate the relative insensitivity of the technique.

This conclusion can be seen intuitively in **Figure 28**, which shows an IR spectrum of a C_{60} sample known to contain about 8% C_{70}. In addition to the presence of bands due to the contamination of the sample by polystyrene from the grinding process (bands at 696 and 757 cm^{-1}), the baseline is noisy. The C_{70} bands appear as shoulders on C_{60} bands or

as weak bands. Quantitation of the C_{70} content of this sample would be difficult, even at the 8% level.

Despite the shortcomings of the method in determination of purity of a purified fullerene sample, infrared absorption spectroscopy is useful in the identification of other contaminants in a fullerene sample. For example, from the IR spectrum shown in **Figure 29**, which is from the same sample as in **Figure 28**, water, toluene and polystyrene can be identified as contaminants.

HPLC Determination of Purity. High performance liquid chromatography (HPLC) of the fullerenes is a rapid and sensitive method for the determination of purity of a fullerene sample, and has been used extensively in purity determinations in the literature[83,94,95]. HPLC is usually carried out by reverse-phase techniques on analytical columns (see introduction), and is generally not used for preparative purposes, due to the severe limitations of column loading and sample recovery[76].

HPLC offers an alternative to the UV-Vis determination of purity described above, with the advantage of the detection of impurities which might otherwise interfere with the UV-Vis analysis. The necessary use of detectors with small sample volumes and short optical pathlengths, and the

limitations of low column loadings, however, limit the sensitivity of HPLC analysis.

Calculation of the detection limit for HPLC analysis. The detection limit for quantitation of a fullerene by HPLC can be calculated, within an order of magnitude, with the use of instrumental parameters. With data from chromatograms obtained during the preliminary work on the separation of C_{60} and C_{70}, manufacturer's published instrumental specifications and assumptions required for the calculation, an estimate of the precision available by HPLC determination of fullerene purity can be obtained. **Table X** lists the instrumental parameters, assumptions and sources used in the following calculations.

For quantitative analysis, it is generally accepted that the signal to noise ratio (S/N) must at least 2. From a systematic treatment of instrumental sources of noise, Crouch, et. al determined that the precision in a UV-Vis absorbance measurement, in which the sample cell is fixed and the absorbance is low, is on the order of ±0.001 under optimum conditions[96]. So, for the purposes of this discussion, the minimum absorbance for determination of purity is 0.002 AU. The minimum concentration for quantitation (given by the Beer-Lambert law) is:

Column[a]: Octyl (C-8) modified silica, 10 μm diameter, 25 cm X 4.6 mm

Detector precision:[b]
± 0.001

Flow Cell: Rainin.
Type: analytical
Path: 1.0 mm
Volume: 10 μL

Chromatographic data:
Injection volume: 20 μL
Flow rate[a]: 1 mL/min
Retention time[a]:
C_{60} ≈ 10 minutes
C_{70} ≈ 11.5 minutes
Peak width[a]: $w_{1/2}$ ≈0.24 min
w ≈1.1 min

Fullerene absorptivities
Wavelength: 212 nm
Molar Absorptivities: (simplified for comparison)
C_{60} 140000
C_{70} 140000

Fullerene solubility: 5 g/ liter (≈ 0.007 M)

Table X. Parameters used in the calculation of HPLC detection limits. a: data from our experiments; b: see reference 96.

$$C = \frac{A}{\epsilon b} = \frac{0.002}{(1.4X10^5)(0.1\ cm)} = 1.4X10^{-7}\ M$$

which defines the lower limit of concentration detectable by the HPLC detector for an idealized case where the absorptivities of C_{60} and C_{70} are the same (1.4 X 10^5 at 212 nm).

With an injection volume of 20 μL and the consideration that benzene or toluene represent the solvents in which fullerenes are most soluble ($\approx$ 5 g/L), the maximum weight of fullerene sample that can be injected is $\approx$ 10 mg. This assumption does not include the likelihood of overloading the column.

From the experiments conducted in the course of our investigations[91], the peak width (w) of a fullerene sample is $\approx$ 1.1 minute at a flow rate of 1 mL/minute and since over 96% of the fullerene is eluted in this time, the assumption that $\tau = \sigma = 4w$ is assumed to be valid. Therefore, the variance of the chromatographic peak is σ = 0.275. An example of the HPLC chromatograph obtained in our experiment is shown in **Figure 30**[91].

By trial-and-error mathematical fitting of a Gaussian peak with the above variance, it was found that the maximum concentration in the chromatographic peak was 1.4 X 10^{-7} M when the peak was adjusted for an absorbance maximum of 0.002 AU (= 2 times the noise); the total concentration of

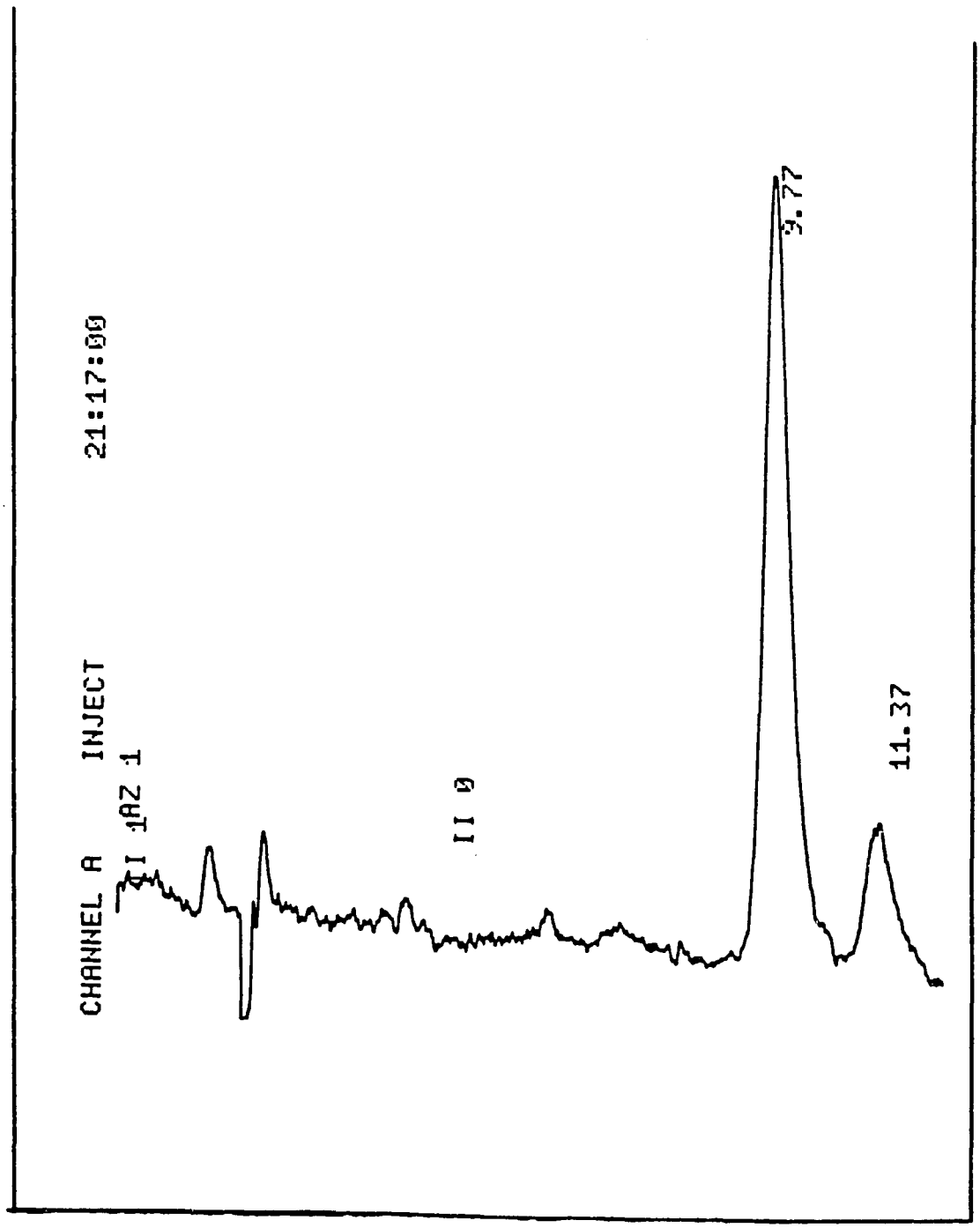

Figure 30. HPLC chromatogram of a mixture of C_{60} and C_{70}.

fullerene in the peak was 1.1 X 10^{-7} M in the 1.1 mL peak volume (= 1.0 X 10^{-7} g).

In order to achieve a concentration of 1.1 X 10^{-7} M of C_{70} in the original 20 μL injection volume, in which 0.0001 g of fullerenes are soluble (from solubility and injection volume data), 1.0 X 10^{-7} g of C_{70} must be injected, so the minimum percentage of C_{70} detectable in a sample of C_{60} is 0.01 %.

The above calculations are generous in the assumptions of molar absorptivities and that the column will not be overloaded under these hypothetical conditions. In addition, UV detectors are not very sensitive at 212 mn, and the precision of the absorbance measurement is likely to lower than that which was used in the calculation; the noise level in **Figure 29** is seen to be high and shows drift. HPLC is therefore capable of determining a limit of 0.01 % of one fullerene in another, but practical applications will likely show the limit to be higher than calculated here.

SUMMARY

The fast-developing field of fullerene production and separation has produced many viable techniques for obtaining purified fullerenes. The separation scheme presented in this work is unique in that the production of a purified C_{60} material in a crystalline form by the freeze-thaw process provides large quantities of material that is essentially recrystallized, thereby eliminating many by-products of the soot production and extraction process. The supernatant produced during the freeze-thaw process is highly enriched in C_{70}, with C_{60}/C_{70} ratios of about 3:1. This solution is therefore a good source for the production of C_{70}. The chromatographic separation of C_{60} and C_{70} described here has the advantages over other chromatographic methods of being robust (many runs can be completed without exhausting the stationary phase), with high capacity (30 mg/run) and pure C_{70} is obtained without contamination by C_{60}, a problem often encountered in other chromatographic separations due to tailing of the C_{60} peak.

Purity assessment of a purified fullerene sample has been accomplished by many analytical methods in the literature. Each method must be evaluated for its ability to detect small amounts of one fullernene in another, its ease of use and its ability to detect contaminants other

than fullerenes in the sample. Because of the ease of sample preparation and analysis, UV-Visible spectroscopy is attractive in purity determinations, and since the fullerenes have high molar absorptivities and unique spectral features, UV-Vis has high sensitivity. High performance liquid chromatography (HPLC) analysis takes longer to complete, but can detect other contaminating materials in the fullerene sample. Both UV-Vis and HPLC with UV detection have the ability to detect 0.02 g of C_{70} fullerene in a 1 g sample of C_{60}, or vice versa. From data outlined in the literature, it can be inferred that mass spectrometry offers high sensitivity, and can detect contaminants, but the analysis requires a high temperature sample probe, and fragmentation and sample volatilization inconsistencies can cause problems. Infrared and especially NMR spectroscopy are facile methods of analysis but are not sensitive enough to determine small amounts of one fullerene in another. Whichever method is used, it is imperative to have high-purity standards for instrumental calibration.

REFERENCES FOR PART I.

1. S.J. Kirchner, H. Oona, S.J. Perron, Q. Fernando, J. Jong-Hae Lee, H. Zeitlin. Proton induced x-ray emission analysis of deep-sea ferromanganese nodules. Anal. Chem. **52:** 2195-2201 (1980).

2. T.B. Johansson, R. Akselsson, S.A.E. Johansson; X-Ray analysis: elemental trace analysis at the 10^{-12} g level. Nucl. Instr. Meth. **84:** 141-143 (1970).

3. S.A.E. Johansson, T.B. Johansson; Proton induced x-ray analysis of trace elements in tissue sections. Nucl. Instr. Meth. **137:** 473-516 (1976).

4. S.A.E. Johansson, J.L. Campbell; PIXE: A Novel Technique for Elemental Analysis. John Wiley and Sons, New York, 1988.

5. PIXE: A Novel Technique for Elemental Analysis. p. 5.

6. G.W. Grime, F. Watt; Nuclear microscopy - elemental mapping using high-energy ion beam techniques. Nucl. Instr. Meth. **B50:** 197-207 (1990).

7. S.A. MacLaren, F.D. Correll, J.R. Huddle, J. Vanhoy, W.D. Kulp,III; A simple external-beam milliprobe system for in-air PIXE. Nucl. Instr. Meth. Phys. Res. **B56/57:** 708-711 (1991).

8. PIXE: A Novel Technique for Elemental Analysis. pp. 116-117.

9. T. Lowe, Q. Chen, Q. Fernando, R. Kieth, A.J. Gandolfi; Analysis of Renal Slices by Proton Induced X-Ray Emission. Enviro. Health. Perspect., Aug. (1993) (in press)

10. W. Maenhaut; Multielement analysis of biological materials by particle-induced x-ray emission (PIXE). Scann. Microscopy. **4:** 43-64 (1990).

11. S.B. Török, R.E. Van Grieken; Fundamental Reviews. Anal. Chem. **64**, 184R-185R (1992).

12. K.G. Malmqvist; Quantitative PIXE analysis of biomedical material-sample preparation, irradiation and quality control. Nucl. Instr. Meth. **B49:** 183-190 (1990).

13. J. Chadwick. The γ rays excited by the ß rays of radium. Phil. Mag. **24**: 594-600 (1912).

14. L.S. Birks, R.E. Seebold, A.P Batt, J.S. Grosso; Excitation of characteristic x-rays by protons, electrons, and primary x-rays. J. Appl. Phys. **35**: 2578-2581 (1964).

15. N.A. Bailey, J.W. Mayer; A P-N junction semiconductor radiation detector for use with beta- and gamma-ray-emitting isotopes. Radiology **76**: 116-117 (1961).

16. F.W. Kunz; Energy dispersive x-ray fluorescence analysis of research materials. Spectroscopy. **3**: 16-23 (1988).

17. J.L. Campbell; X-ray spectrometers for PIXE. Nucl. Instr. Meth. Phys. Res. **B49**: 115-125 (1990).

18. As calculated by the TRIM program in the Van de Graaff lab at the University of Arizona.

19. J.A Leavitt, L.C. McIntyre Jr., M.D. Ashbaugh, J.G Oden, Z. Lin, B. Deyfomly-Arjomandy; Cross sections for 170.5° backscattering of ^{4}He from oxygen for ^{4}He energies between 1.8 and 5.0 MeV. Nucl. Instr. Meth. **B44**: 260-265 (1990).

20. G.I. Johansson, J. Pallon, K.G. Malmqvist, K.R. Akselsson. Calibration and long-term stability of a PIXE set-up. Nucl. Instr. Meth. **181**: 81-88 (1981).

21. L.J. Cabri, J.L. Campbell, J.H.G Laflamme, R.G Leigh, J.A. Maxwell, J.D. Scott; Proton-microprobe analysis of trace elements in sulfides from some massive sulfide deposits. Can. Mineralogist. **23**: 133-148 (1985).

22. H. Oona, S.J. Kirchner, P.L. Kresan, Q. Fernando, Q. Thin carbon foils for the elimination of charging effects in proton induced x-ray emission spectrometry. Anal. Chem. **51**: 302-303 (1979).

23. M. Ahlberg, G. Johansson, K. Malmqvist; Elimination of charging in the proton-induced x-ray emission analysis of insulating samples. Nucl. Instr. Meth. **131**: 377-379 (1975).

24. PIXE: A Novel Technique for Elemental Analysis. p. 47.

25. J.R. Chen; An application of PIXE in medicine: Legionnaires's Disease. Nucl. Instr. Meth. **181**: 337-343 (1981).

26. I.V. Mitchell, K.M. Barfoot, H.L. Eschbach; Ion beam monitoring using self-supporting reference foils. Nucl. Instr. Meth. **168**: 233-240 (1980).

27. R. Jenkins, R. Gould, D. Gedcke; Quantitative X-Ray Spectrometry. Marcel Dekker, New York, 1981.

28. PIXE: A Novel Technique for Elemental Analysis. p. 134.

29. H. Thibeau, J. Stadel, W. Cline, T.A. Cahill; On-demand beam pulsing for an accelerator. Nucl. Instr. Meth. **111**: 615-617 (1973).

30. K.G. Malmqvist, E. Karlsson, K.R. Akselsson; Performance of an on-demand beam excitation system for PIXE analysis. Nucl. Instr. Meth. **192**: 523-532 (1982).

31. PIXE: A Novel Technique for Elemental Analysis. p. 139.

32. W. Bambynek, B. Crasemann, R.W. Fink, H.U. Freund, H. Mark, C.D. Swift, R.E. Price, P. Venugopalo Rao; X-Ray fluorescence yields, auger, and Coster-Kronig transition probabilities. Revs. Mod. Phys. **44**: 716-813 (1972).

33. J.H. Scofield; Exchange corrections of K x-ray emission rates. Phys. Rev. **A9**: 1041-1049 (1974).

34. PIXE: A Novel Technique for Elemental Analysis, p. 124

35. PIXE: A Novel Technique for Elemental Analysis. p. 8.

36. P.R. Bevington, Data Reduction and Error Analysis for the Physical Sciences, McGraw-Hill, New York (1969) pp. 204-246

37. F. H. Schamber; X-Ray Fluorescence Analysis of Environmental Samples, T. G. Dzubay, Ed., Ann Arbor Science Publishers (1977).

38. A number of references for relative intensities of x-ray emission lines are used in the GUPIX program, most importantly those calculated by J. H. Scofield, Phys. Rev., **A9** 1041 (1974). For a more complete description of the references used, see S. A. E Johansson, J. L. Campbell, PIXE: A Novel Technique for Elemental Analysis, John Wiley and Sons, Chirchester, UK, (1988) Chapter 1.

39. G.I. Johansson, X-Ray Spectrom., **11**, (1982) 194.

40. R.K. Jolly, H.B. White Jr.; Preparation of thin film deposits from biological and other matter. Nucl. Instr.Meth. **97**: 103-105 (1971).

41. R.M. Baum, R.D. Willis, R.L. Walter, W.F. Gutknecht, A.R. Stiles; X-Ray Fluorescence Analysis of Environmental Samples. (T.G.Dzubay, Ed.), Ann Arbor Sci., Ann Arbor, Mich. (1977).

42. H.P.M. Kivits, F.A.J De Rooij, G.P.J Wijnhoven; A fast method for PIXE and XRF target preparation of aqueous samples. Nucl. Instr. Meth. **164**: 225-229 (1979).

43. N.F. Mangelson, M.W. HilL; Particle induced x-ray emisssion elemental analysis: sample preparation for a versatile instrumental method. Scanning Microscopy. **4**: 63-72 (1990).

44. R.L. Walter, R.D. Willis, W.F. Gutknecht, J.M. Joyce; Analysis of biological, clinical, and environmental samples using proton-induced x-ray emission. Anal. Chem. **46**: 843-855 (1974).

45. N.F. Mangelson, M.W Hill, K.K. Nielson, J.F. Ryder, Proton induced x-ray emission analysis of Pima indian autopsy tissues. Nucl. Instr. Meth. **142**: 133-142 (1977).

46. L.E. Carlsson, K.R. Akselsson; Applicability of XRF and PIXE to fast drill core analysis in air. Adv. X-Ray Anal. **24**: 313-321 (1981).

47. M.A. Chaudhri, A. Craford; The influence of trace elements on fluoride uptake by teeth. Nucl. Instr. Meth. **181**: 327-331 (1981).

48. M.J. Renan, C.F. Albrecht, D.T.L. Jones; Multi-elemental x-ray analysis of normal and malignant mammalian tissue by proton excitation of thick samples in air. Nucl. Instr. Meth. **181**: 297-300 (1981).

49. J.L. Campbell; Specimen preparation in PIXE analysis. Nucl. Inst. Meth. **142**: 263-273 (1977).

50. N.F. Mangelson, M.W. Hill, K.K. Nielson, D.J. Eatough, J.J. Christensen, R.M. Izatt, D.O. Richards; Proton induced x-ray emission analysis of Pima indian autopsy Tissues. Anal. Chem. **51**: 1187-1194 (1979).

51. T. Pinheiro, H. Duflou, W. Maenhaut; Applicability of microwave acid digestion to sample preparation of biological materials for analysis by particle-induced x-ray emission

(PIXE). In: Biol. Trace Elem. Res. (G.N. Schrauzer, Ed.), Humana Press, Inc, 1990, pp. 589-597.

52. R.L. Walter, R.D. Willis, W.F. Gutknecht, J.M. Joyce; Analysis of biological, clinical, and environmental samples using proton-induced x-ray emission. Anal. Chem. **46**: 843-855 (1974).

53. F.A. Rickey, P.C. Simms, K.A. Mueller; PIXE analysis of water with detection limits in the ppb range. IEEE Trans. Nucl. Sci, **NS-26**, 1347-1351 (1979).

54. T.T. Gorsuch: The Destruction of Organic Matter. Pergamon Press, Oxford, 1970.

55. K.R Akelsson, S.A.E Johansson. PIXE analysis research in Lund. IEEE Trans. Nucl. Sci., **NS-26**, 1358-1362 (1979).

56. Lochmüller, C.H., Galbraith, J.W., and Walter, R.L. Trace metal analysis in water by proton-induced x-ray emission analysis of ion exchange membranes. Anal. Chem. **46**: 440-442 (1974).

57. C.L. Luke; Determination of trace elements in inorganic and organic materials by x-ray fluorescence spectroscopy. Anal. Chim. Acta. **41**: 237-250 (1968).

58. F.C. Jundt, K.H. Purser, H. Kubo, E.A. Schenk; Proton induced x-ray analysis of trace elements in tissue sections. J. Histochem. Cytochem. **22**: 1-6 (1974).

59. J.L. Campbell. Specimen preparation in PIXE analysis. Nucl. Inst. Meth. **142**: 263-273 (1977).

60. S.B. Russell, C.W. Schulte, S. Faiq, J.L. Campbell; Specimen backings for proton-induced x-ray emission analysis. Anal. Chem. **53**: 571-574 (1981).

61. J.L. Campbell, B.H. Orr, A.W. Herman, L.A. McNelles, Thomson, J.A., and Cook, W.B. Trace element analysis of fluids by proton-induced x-ray fluorescence spectrometry. Anal. Chem. **47**: 1542-1553 (1975).

62. J.L Campbell, S.B Russell, S. Faiq, C.W. Schulte, R.W. Ollerhead, R.R. Gingerich; Optimization of PIXE Sensitivity for Biomedical Applications. Nucl. Inst. Meth., 181, 285-292 (1981).

63. W.R. Smythe; Trace element analysis by the observation of characteristic x-rays. Bull. Am. Phys. Soc. **17**: 504 (1972).

64. Li M., Tan M., Chin J., Shen K., Chen Z., Chang J., Zhu W., Li W., Xia Z., and Kuang A. PIXE analysis of human serum. Nucl. Inst. Meth. **181**: 309-313 (1981).

65. F.C. Young, M.L. Roush, P.G. Bergman; Trace element analysis by proton-induced x-ray excitation. Int. J. Appl. Rad. Iso. **24**: 153-163 (1973).

REFERENCES FOR PART II.

66. W. Kratschmer, L.D. Lamb, K. Fostiropoulos, D.R. Huffman; Solid C_{60}: A New Form of Carbon. Nature (London), 347, 354, (1990)

67. D.H. Parker, P. Wurz, K. Chatterjee, K.R. Lykke, J.E. Hunt, M.J. Pellin, J.C. Hemminger, D.M. Gruen, L.M. Stock; High Yield Synthesis, Extraction and Mass Spectrometric Characterization of Fullerenes C_{60} to C_{266}. J. Am. Chem. Soc., 113, 7499-7503 (1991).

68. R.E. Smalley, in a talk at the University of Arizona, September, 1991.

69. R.E. Haufler, J. Conceicao, P.F. Chibante, Y. Chai, N.E. Byrne, S. Flanagan, M.M. Haley, S.C. O'Brien, C. Pan, Z. Xiao, W.E. Billups, M.A. Ciufolini, R.H. Hauge, J.L. Margrave, L.J. Wilson, R.F. Curl, and R.E. Smally; Efficient Production of C_{60} (Buckminsterfullerene), $C_{60}H_{36}$, and the Solvated Buckide Ion. J. Phys. Chem., 94, 8634, (1990).

70. Private Communication, MER Corporation, Tucson, AZ.

71. J.M. Hawkins, T.A. Lewis, S.D. Loren, A. Mayer, J.R. Heath, Y. Shibato, R.J. Saykally; Organic Chemistry of C_{60} (Buckminsterfullerene): Chromatography and Osmylation. J. Org. Chem., **55**, 6250-6252 (1990).

72. R. Taylor, J.P. Hare, A.K. Abdul-Sada, H.W. Kroto; Isolation, Separation and Characterization of the Fullerenes C_{60} and C_{70}: The Third Form of Carbon. J. Chem. Soc., Chem. Comm., 1423-1425 (1990).

73. J.B. Howard, T. McKinnon, Y. Makarovsky, A.L. Lafluer, M.E. Johnson; Fullerenes C_{60} and C_{70} in Flames. Nature, 352, 139-141 (1991).

74. M.S. Meier, J.P. Selegue; Efficient Preparative Separation of C_{60} and C_{70}. Gel Permeation Chromatography of Fullerenes Using 100% Toluene as Mobile Phase. J. Org Chem., 57, 1924-1926 (1992).

75. W.A. Scrivens, P.V. Bedworth, J.M. Tour; Purification of Gram Quantities of C_{60}. A New Inexpensive and Facile Method. J. Am. Chem. Soc., 114 7917-7919 (1992).

76. C.J. Welch, W.H. Pirkle; Progress in the Design of Selectors for Buckminsterfullerene. J. Chrom., 609, 89-101 (1992).

77. C. Smart, B. Eldrich, W. Reuter, J.A. Zimmerman, W.R. Creasy, N.Rivera, R.S. Ruoff; Extraction of Giant Fullerene Molecules, and their Subsequent Solvation in Low Boiling Point Solvents. Chem. Phys. Lett., 188, 171-176 (1992).

78. K. Kikuchi, N. Nakahara, T. Wakabayashi, M. Honda, H. Matsumiya, T. Moriwaki, S. Suzuki, H. Shiromaru, K. Saito, K.Yamauchi, I. Ikemoto, Y. Achiba; Isolation and Identification of Fullerene Family: C_{76}, C_{78}, C_{82}, C_{84}, C_{90}, and C_{96}. Chem. Phys. Lett., 188, 177-180 (1992).

79. K. Chatterjee, D.H. Parker, P. Wurz, K.R. Lykke, D.M. Gruen, L.M. Stock; Fast One-Step Separation and Purification of Buckminsterfullerene, C_{60} from Carbon Soot. J. Org. Chem., 57, 3253-3254 (1992).

80. K.C. Khemani, M. Prato, F. Wudl; A Simple Soxhlet Chromatographic Method for the Isolation of Pure C_{60} and C_{70}. J. Org. Chem., 57, 3254-3256 (1992).

81. J.P. Hare, H.W. Kroto, R. Taylor; Preparation and UV/Visible Spectra of Fullerenes C_{60} and C_{70}. Chem. Phys Lett., 177, 394-398 (1991).

82. D.R. Luffer, K.H. Schram; Electron Ionization Mass Spectrometry of Synthetic C_{60}. Rap. Comm. Mass Spectr., 4, 552-556 (1990).

83. H. Ajie, M.M Alvarez, S.J. Anz, R.D. Beck, F. Diederich, K. Fostiropoulos, D.R. Huffman, W. Kratschmer, Y. Rubin, K.E. Shriver, D. Sensharma, R.L. Whetten; Characterization of the Soluble All-Carbon Molecules C_{60} and C_{70}. J. Phys. Chem., 94, 8630-8633 (1990).

84. D.S. Bethune, G. Meijer, W.C. Tang, H.J. Rosen, W.G. Golden, H. Seki, C.A. Brown, M.S. de Vries; Vibrational Raman and

Infrared Spectra of Chromatographically Separated C_{60} and C_{70} Fullerene Clusters. Chem. Phys. Lett., 179, 181-186 (1991).

85. Private Communication, MER Corporation, Tucson, AZ.

86. G. Margolis, T.K. Sherwood, P.L. Thibaut Brian, A.F. Sarofim. The Performance of a Well Stirred Ice Crystallizer. In. Eng. Chem. Fundam., 10, 439-452 (1971).

87. E.F. Janzow, B.T. Chao; Induced Crystallization of Large Free Ice Crystals in Slowly Flowing Brine. Desalination, 12, 163-175 (1973).

88. A.J. Barduhn; The State of the Crystallization Process for Desalting Saline Waters. Desalination, 5, 173-184 (1968)

89. H.F. Wiegandt, A. Madani, P. Harriott; Ice Crystallization Developments for the Butane Direct-Contact Process. Desalination, 67, 107-126 (1987).

90. N. Coustel, P. Bernier, R. Aznar, A. Zahab, J. Lambert, P. Lyard; Purification of C_{60} by a Simple Crystallization Procedure. J. Chem. Soc., Chem. Commun., 1402-3 (1992).

91. D.D. Johnson, The Role of Structure, Orientation and Composition of Chemically Tailored Surfaces on Differential Migration Techniques; Dissertation at the University of Arizona, 1992.

92. H.A. Strobel, W.R Heinman; Chemical Instrumentation: A Systematic Approach, 3rd Ed. John Wiley and Sons, New York (1989) Ch. 16.

93. H.H. Baur, G.D. Christian, J.E.O'Reilly; Instrumental Analysis. Allyn and Bacon, Inc., Boston (1979) p. 222-223

94. G. Zhennan, Q. Jiuxin, Z. Xihuang, W. Yongquing, Z. Xing, F. Sunqi, G. Zizhao; Buckminsterfullerene C_{60}: Synthesis, Spectroscopic Characterization, and Structure Analysis. J. Phys. Chem., 95, 9615-9618 (1991).

95. M. Diack, R.L. Hettich, R.N. Compton, G. Guiochon; Contribution to the Isolation and Characterization of Buckminsterfullerenes. Anal. Chem., 64, 2143-2148 (1992).

96. L.D. Rothman, S.R. Crouch; Theoretical and experimental investigation of factors affecting precision in molecular absorption spectroscopy. Anal. Chem., **47:** 1226-1233 (1975).